



Federal Ministry
of Education
and Research



Ministry of
Science & Technology

German-Israeli Cooperation in Water Technology Research



Proceedings of the Status Conference 2019
September 24 – 25, 2019
Dresden, Germany

Contact

Federal Ministry of Education and Research (BMBF), Germany

Dr. Christian Alecke

Email: christian.alecke@bmbf.bund.de

Ministry of Science and Technology (MOST), Israel

On scientific matters:

Dr. Moshe Ben Sasson

Email: mosheBS@most.gov.il

On administrative matters:

Ms. Shani Edri

Email: shani@most.gov.il

Project Management Agency Karlsruhe (PTKA), Germany

Dr. Leif Wolf

Email: leif.wolf@kit.edu

Dr. Anne Gunkel

Email: anne.gunkel@kit.edu

Further information on the German-Israeli cooperation is available at
www.cogeril.de

Content

The German-Israeli Cooperation in Water Technology Research 2

Conference Papers

Project Group 2018

EfflueNF: Wastewater Reuse by High Recovery Feedseeded NF and ISD.....	4
LIG-Feedspacer: Laser-Induced Graphene Spacers for Low Energy Desalination	10
TertNF: Optimized Nanofiltration for Tertiary Desalination	16
Rhizosphere: Root and Rhizosphere Hydraulic Properties.....	22

Project Group 2017

SATPlanner: Improved Degradation and Enhanced Infiltration Rates in SAT by Hydraulic Manipulation	28
SmartPipe: Development of a Textile Reinforced Pipe System with Integrated Monitoring Function.....	34
NFCDI: Nanomembranes for Cost-Effective Hybrid Desalination-Filtration of Wastewater	40
CLUWAL: Closing the Urban Water Loop – Integrated Urban Water and Wastewater Management for Increased Sustainability.....	46
AnMBRA: Industrial Wastewater and Reuse Process with Near Complete Recovery of Effluent, Nutrients and Energy	52

Project Group 2016

MAR-DSW: Aquifer Recharge as Sustainable Storage Solution for Desalinated Water	59
TREES: Tracking Effects of Environmental Organic Micro-Pollutants in the Subsurface.....	67
AdsFilt: Removal of Inorganic Contaminants from Aqueous Solutions by Novel Hybrid Adsorption/Filtration Processes	73

Overview of New Projects Started in 2019..... 79



The German-Israeli Cooperation in Water Technology Research

The bilateral cooperation in water technology was established already in 1974. Since then, more than 150 projects with Israeli and German partners have led to trusted relations between Israeli and German researchers.

The objectives of the German-Israeli Water Technology Cooperation Program are:

- To improve the water situation in Israel, its direct neighborhood and/or Germany
- To facilitate access to new markets for Israeli and German enterprises in the water and environmental sector
- To support and strengthen bilateral and multilateral cooperation in the water sector as well as facilitate cooperation between science and industry

Innovative water technology solutions from Germany and Israel are well recognized around the globe. Israeli exports in the area of water technology are rapidly growing with more than 300 companies and more than 100 start-ups engaged today. And in water technology, Germany is among the top countries with the highest export market share worldwide, predicted to grow further.

Focal themes of the 2019 status conference are:

- Aquifer management, groundwater recharge and remediation
- Organic micro-pollutants and pathogens
- Wastewater: recycling, reduction and reuse
- Brine production of desalination processes
- Sustainable Urban Water Management
- Water technologies to reduce agricultural water demand
- Novel sensors and data management for water resources systems

In future, even stronger efforts are required to respond to the growing pressure on the global water resources. Vital ecosystems have vanished or are at risk. Efficient water technology and its appropriate use are key to reach the Sustainable Development Goal 6 (Ensure availability and sustainable management of water and sanitation for all) of the United Nations. The German-Israeli water technology research cooperation aims to contribute to the SDGs by securing the required innovation.



Project Group 2018

Wastewater Reuse by High Recovery Hybrid Process Integrating Feed-Seeded Nanofiltration and Interstage de-Supersaturation

Johannes KAMP¹, Deniz RALL^{1,2}, Chidiebere S. NNEBUO³, Omer IZRAEL³, Jack GILRON³, Ora KEDEM⁴ Matthias WESSLING^{1,2}, Oded NIR^{3*}

¹ RWTH Aachen University, AVT.CVT - Aachener Verfahrenstechnik, Chemical Process Engineering, Forckenbeckstrasse 51, 52074 Aachen, Germany

² DWI - Leibniz Institute for Interactive Materials, Forckenbeckstrasse 50, 52074 Aachen, Germany

³ Ben-Gurion University, Blaustein Institutes for Desert Research, Zuckerberg Institute for Water Research, Sede Boqer Campus 8499000, Midreshet Ben-Gurion, Israel

⁴ Weizmann Institute of Science, Life Sciences, Biological Chemistry, Rehovot 76100, Israel

*Corresponding Author: odni@bgu.ac.il

ABSTRACT

In this collaboration project, we work to develop and optimize a new treatment process to utilize effluent from wastewater treatment aimed at achieving the salinity and nutrients removal required for various reuse or discharge alternatives, with reduced energy demand and minimal liquid discharge. To achieve this goal, we are developing novel tailor-made hollow fiber polyelectrolyte multilayer membranes (HF-PEMM's) with tunable solute rejection. This is accompanied by data-driven approach for relating membrane synthesis conditions to their properties. Since high recovery is limited mainly by inorganic scaling, we study two strategies to address this issue. The first (feed seeding) operates the high-recovery nanofiltration stage with salt crystals in the feed channel, acting as nucleation seeds and preventing precipitation on the membrane surface. The second is an inter-stage de-supersaturation (ISDS) technique, in which we filter supersaturated streams through a fixed bed, enabling rapid and effective precipitation. The results we obtained thus far show the membranes to be highly flexible, tunable and robust. Moreover, using the data-driven approach we could predict their salt rejection and water permeability. Preliminary results with synthetic effluent show 55% increase in retentate concentration factor when applying feed-seeding, while several successful ISDS trials demonstrated the feasibility of our approach.

KEYWORDS

Domestic wastewater reuse, scaling prevention, minimal liquid discharge, polyelectrolyte nanofiltration membranes, Neural Network modeling.

INTRODUCTION

Wastewaters effluent is an important water source for water scarce countries and could be reused in different manners including crop irrigation, restoration / conservation of aquatic environments and more, while in water abundant countries, effluent quality must usually meet the requirements for unlimited discharge to rivers. Nanofiltration offers a wide range of solute rejection properties and selectivity and can thus provide an economically attractive route for meeting a variety of water reuse quality requirements. Nevertheless, the practical recovery ratio (i.e. the amount of permeate extracted from a unit volume of feed) is limited to 70-80% due to inorganic chemical scaling. The main goal of this project is thus to develop NF membranes, process configurations and operational strategies for meeting water quality required by several reuse alternatives, with minimal liquid discharge and reduced energy demand.

We are working towards achieving these goals by combining two complimentary novel approaches, within the general process scheme shown in Fig. 1. The **first approach** utilizes nanofiltration (NF) membranes with tuneable ion-rejection capabilities (Menne et al. 2016), synthesized via layer-by-layer deposition of polyelectrolytes on porous hollow-fibers. HF-PEMM's (hollow fiber polyelectrolyte multilayer membranes) remain stable during mechanical (backwash) and chemical (strong acid/base) cleaning procedures, which can reverse inorganic salt scaling and fouling by colloidal matter. This robustness allows to apply feed-seeding (Pevrov 2015), i.e. adding seed crystals onto which salt precipitation occurs preferentially over precipitation on the membrane surface.

In case of any membrane surface precipitation, the new HF-PEMMs can be easily regenerated by acid cleaning (Nir et al. 2018), colloidal fouling is more easily controlled due to the spacer-free feed channel, as well as the option for controlled backwashing.

The **second approach** utilizes an inter-stage de-supersaturation step aimed at decreasing the concentration of potentially scale-forming ions and mineral colloids entering the membrane module. Previously, inter-stage de-supersaturation was suggested (Rautenbach et al. 2000, Halevy et al.

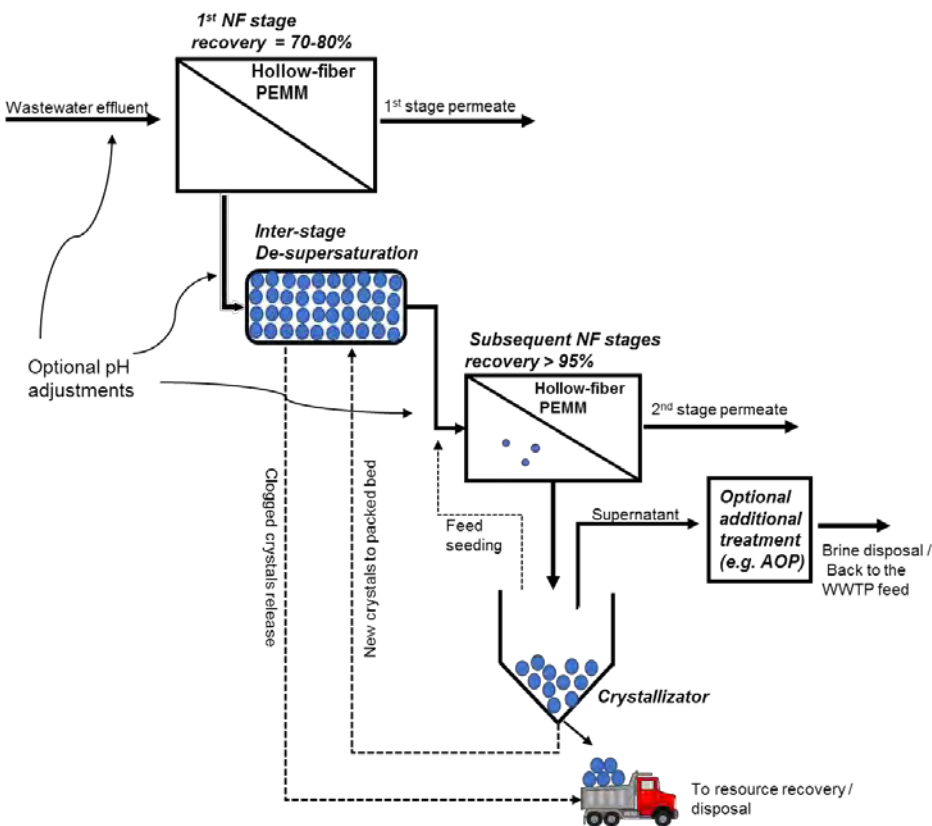


Figure 1: General process scheme of the high-recovery effluent nanofiltration for the reuse of wastewater effluent. The proposed process combines feed-seeded nanofiltration with an interstage de-supersaturation step. The membranes to be used are new tailor-made hollow fiber polyelectrolyte multilayer membranes.

2013), however the technical solution suffered from slow precipitation kinetics and high solid content in the supernatant. In our approach, the supersaturated (inter-stage) feed stream percolates through a packed bed column or a fibrous cloth filter hosting Ca-P or CaCO₃ crystals inducing rapid desaturation. This approach offers two major benefits over the use of current crystallization approaches: (1) High liquid-solid contact area resulting in accelerated precipitations and reduced hydraulic retention times; (2) Lower effluent suspended crystal concentrations resulting from the filtering effect of the porous interior of the ISDS module.

METHODS

Membrane Preparation. The NF membranes were prepared from hollow fiber UF membranes by dynamic layer-by-layer deposition of PDADMAC and PSS polyelectrolytes. More details can be found in (Menne et al. 2016)

Preparation of PEM on silicon wafers. Silicon wafers were coated by dip coating with symmetric salt concentrations of 0.1 and 0.5 mol/l and with asymmetric 0.1 mol/l in the polycation (PDADMAC) and 0.5 mol/l in the polyanion (PSS) solution. Up to 20 layers were coated and the

layer thickness was measured with ellipsometry. The cauchy model for thin polymer films was used for thickness modelling.

Salt retention. To characterize the PEMM's, salt solutions containing 5 mmol/l of a single salt were filtrated in crossflow filtration setup at a retentate pressure of 3.5 bar and a crossflow volume flow of 60 l/module, resulting in a Reynolds number of 2300. To get a detailed overview on the charge characteristics of the produced membranes monovalent (NaCl), divalent (MgSO_4) and asymmetric salts (Na_2SO_4 , MgCl_2) were used.

Seeded nanofiltration. We filtered synthetic effluent solutions containing 1 mM sodium phosphate and 3 mM calcium chloride with and without HAp seeds. We gradually concentrated the solutes in the retentate stream by recirculating it through a 0.5m long module with 10 fibers, while extracting permeate (feed&bleed mode with no bleed). We maintained the volume in the feed tank constant by feeding the system with raw water at a flow rate equal to that of the permeate.

RESULTS AND DISCUSSION

Membrane characterization

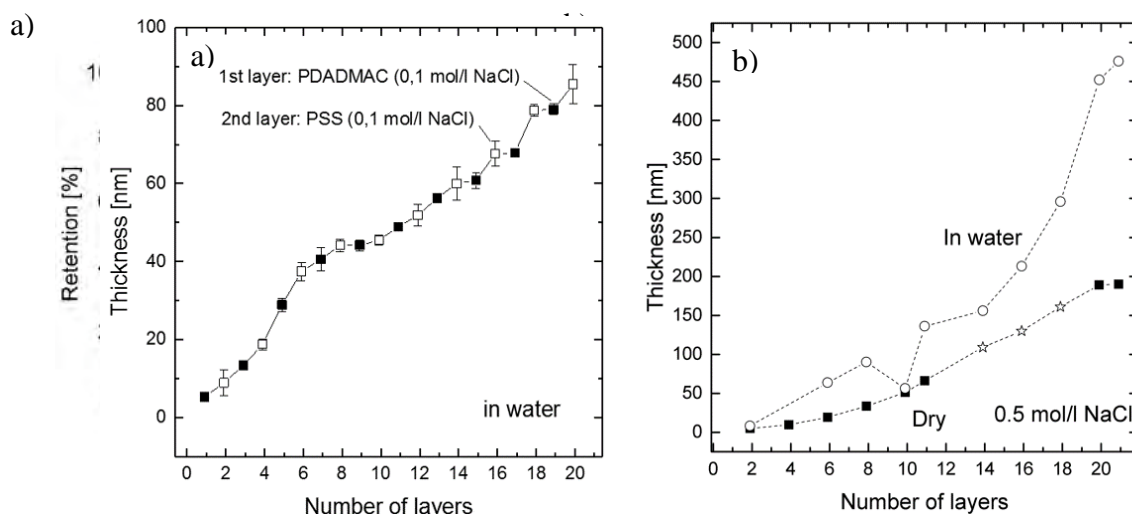


Figure 2: Retentions for MgSO_4 , Na_2SO_4 , MgCl_2 and NaCl over the number of bilayers for a) 0.1 mol/l NaCl in PE solutions and b) from 0.5 mol/l in PE solutions

Figure 3: Thickness of the layer structure a) from 0.1 mol/l NaCl b) 0.5 mol/l NaCl in both PE solutions

We tested the effect of the number of polyelectrolyte bilayers coated on the membrane and the ionic strength of the polyelectrolyte solution on the retention of four salts (Fig. 2). For both the Na_2SO_4 retentions is at about 90% from the first bilayer, since the retentions for the other salts is still low. By applying more bilayers the retention of MgSO_4 and MgCl_2 is increasing to over 90% for the set from 0.1 mol/l NaCl at 3, for the set from 0.5 mol/l from 2 bilayers. The thicker layer-buildup is recognizable from the 0.5 mol/l compared to the 0.1 mol/l PE solution. Both PE systems lead to monovalent ion retention for NaCl of about 60%. Interestingly the Na_2SO_4 retention is declining over the number of bilayers from over 90% to about 50%. For the set from 0.1 mol/l NaCl it is briefly recognizable with a drop from 90% to about 80% retention at 5 bilayers, but clearly by the decrease to about 40% at 10 bilayers. The decrease of retention for Na_2SO_4 is stronger for the membranes applied from 0.5 mol/l NaCl , which decrease to about 70% at 3 bilayers and after 6 bilayers drop to about 50%. These effects can be explained by the interdiffusion of the linear shaped polycation PDADMAC, which overcompensates the charges of the polyanion PSS. This leads to a stronger positive charge of the membrane, which results in a high donnan repulsion of the divalent cation Mg^{2+} and to lower rejections of the divalent anion SO_4^{2-} .

Layer growth on silicon wavers

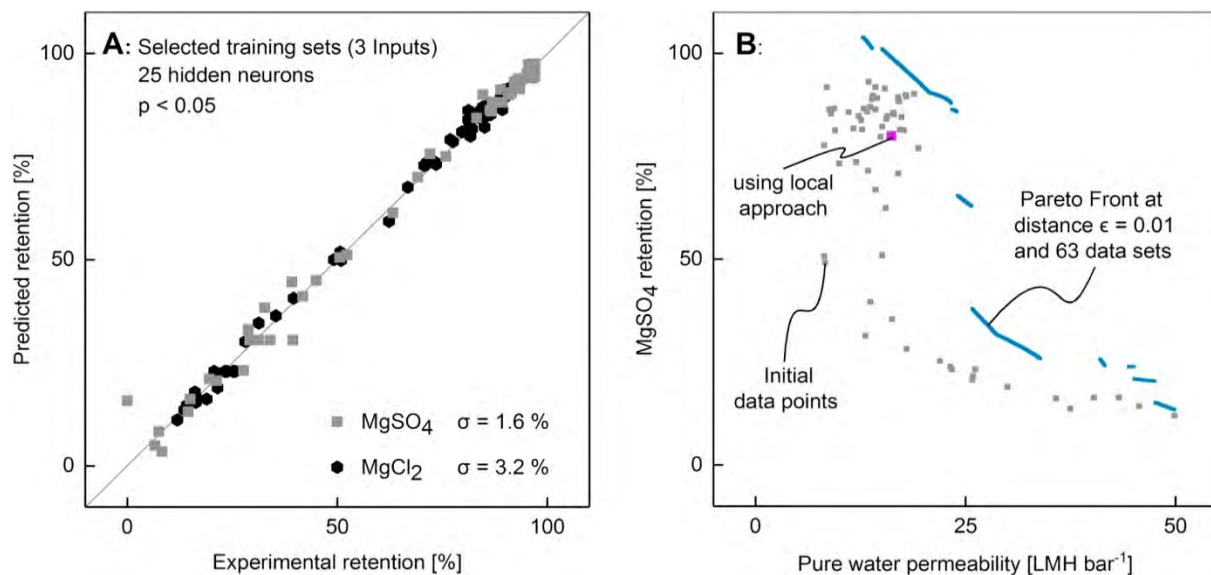


Figure 4: Pareto front optimization using an ANN embedded global deterministic multi-objective optimization framework. A) Regression of the reduced ANN training with three inputs showing the predicted versus the experimental retention of MgSO₄ and MgCl₂. B) Developed Pareto front for the retention of MgSO₄ versus the pure water permeability with comparison of the membrane found by local solver optimization. (Source (Rall et al. 2019)

The measurement of the thickness by ellipsometry is given in Figure 3. Here the different layer growth from 0.1 and 0.5 mol/l NaCl in the PE solution is clearly recognizable. Resulting in a layer thickness of about 85 nm from 0.1 mol/l NaCl (a) compared to about 450 nm from 0.5 mol/l NaCl (b) for 20 layers. The exponential layer growth of the layers from 0.5 mol/l is due to interdiffusion and overcompensation of the polycation PDADMAC during the coating process into the already adsorbed polyelectrolyte multilayer (Ghoštine et al. 2013). The overcompensation of the polycation PDADMAC leads to a overall positive membrane charge, which is observed by the drop in retention for Na₂SO₄ in Figure 2Figure

Data driven membrane development

In a recently published paper demonstrated for the first time that a neural network model could predict, and tailor ion separation properties and flux of a membrane based on production parameters of layer-by-layer (LBL) nanofiltration membranes (Rall et al. 2019). Here, the mass transport properties were linked to synthesize influencing factors in membrane production. The resulting trade-off (Pareto front) between two objectives, permeability and retention, provides valuable insight into the fabrication process and can be used for the planning newly tailored membranes. The optimization framework was subjected to an easily scalable convective coating method for layer-by-layer nanofiltration membranes (Menne et al. 2016).

Seeded Nanofiltration

When operating the NF unit without seeds (Fig. 2A), the water permeance was initially $6.75 \text{ Lm}^{-2}\text{h}^{-1}\text{bar}^{-1}$ (pure water permeance was $7 \text{ Lm}^{-2}\text{h}^{-1}\text{bar}^{-1}$) and decreased slowly as the osmotic pressure difference increased. After approx. 5 hrs of smooth operation we recorded a sharp decline of ~40% in the permeance. At the same time, the initially transparent solution changed its color to white, indicating of mineral precipitation. We then performed three additional filtration experiments at the same conditions, but this time we added seed crystals to the recirculating retentate stream. We compared the permeance in the case of seeded and unseeded NF (Fig. 2B) based on the feed concentration factor (CF). At $\text{CF} < 2$, the permeance was practically identical for both seeded and unseeded NF. Yet, in the seeded NF a significantly higher CF was reached before a sharp decline in permeance was recorded.

In the seeded NF, the critical CF was ~51% higher, which translates to 35% reduction in the volume of the concentrate (Fig. 3A). Moreover, P concentration in the permeate of the seeded NF was more than three times lower (Fig. 3B). This is highly beneficial, as nutrient removal is an important goal of advanced effluent filtration, especially when the water is discharged to the environment. The higher observable P rejection is due to the lower P concentration in the retentate during the seeded filtration, due to fast, heterogeneous precipitation on the surface of the seeds. This opens a route to recover most of the P available in the effluent as calcium-phosphate, a critical raw material for the fertilizer industry. Lastly, the concentration of calcium ions in the permeate was only 20% lower for the seeded NF (Fig. 2C). This was also expected considering both the higher permeability of Ca^{2+} and cake-enhanced concentration-polarization. High calcium concentration generally improves the water quality for environmental, agriculture and potable uses, as well as reduces corrosion in transport systems. In addition, lower calcium concentration in the retentate enables higher recovery of both permeate and phosphorus by reducing the CaCO_3 precipitation potential.

Interstage desupersaturation

To test the concept of ISDS through fixed bed filtration, we filtered synthetic solutions supersaturated with $\text{CaCO}_{3(s)}$ through a 30 cm column bed of calcite particles having a diameter of 1-2 mm. At hydraulic retention times of ca. 10 minutes and 5 minutes, (based on empty bed volume) the precipitation potential of CaCO_3 decreased by 83% and 61% respectively. demonstrating the feasibility of the suggested approach. We will use these and future results to derive kinetic parameters. Moreover, we will try to cut-down retention times by working with

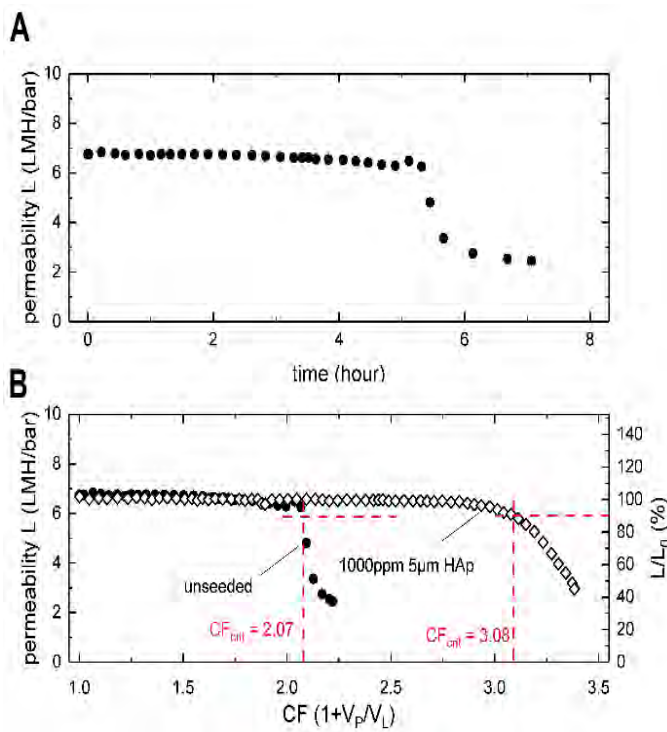


Figure 5: Permeance plots of seeded and unseeded filtration with 6 bar TMP, pH = 7, 1 m/s crossflow, 0.01m^2 membrane surface and full retentate recycling.

A) Unseeded filtration permeance vs time.

B) Unseeded and seeded filtration permeance as a function of the concentration factor. 90% original permeance is marked by the red line as the critical CF.

Each experiment was repeated three times with excellent reproducibility.

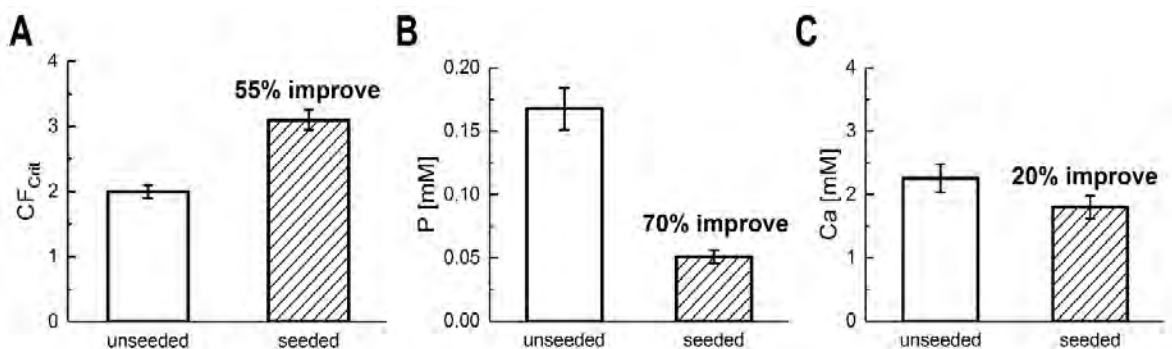


Figure 6: Comparison between seeded vs unseeded (conventional) nanofiltration. A) Critical concentration factor, which is related to the achievable recovery ratio and to final volume of the concentrate. B) Phosphorous concentrations in the permeate, related to P removal efficiency. C) Calcium concentrations in the permeate.

smaller calcite particles. This will result in increased pressure drop; however, what we measured so far was only in the order of milibars and could be further increased. Moreover, work on ISDS by filtration through filter-cakes containing calcite microparticles is underway.

REFERENCES

- Halevy S., Korin E. and Gilron J. (2013). Kinetics of gypsum precipitation for designing interstage crystallizers for concentrate in high recovery reverse osmosis, Industrial and Engineering Chemistry Research 52.
- Menne D., Kamp J., Wong Erik J. and Wessling M. (2016). precise tuning of salt retention of backwashable polyelectrolyte multilayer hollow fiber nanofiltration membranes, Journal of Membrane Science. 499, 396–405.
- Nir O., Sengpiel R. and Wessling M. (2018). Closing the cycle: Phosphorus removal and recovery from diluted effluents using acid resistive membranes. Chemical Engineering Journal 346, 640-648.
- Pervov A.G. (2015). Precipitation of calcium carbonate in reverse osmosis retentate flow by means of seeded techniques - A tool to increase recovery, Desalination 368.
- Rahman S.M., Eckelman M.J., Onnis-Hayden A. and Gu A.Z. (2016). Life-Cycle Assessment of Advanced Nutrient Removal Technologies for Wastewater Treatment, Environmental Science & Technology 50, 3020–3030.
- Rautenbach R., Linn T. and Eilers L. (2000). Treatment of severely contaminated waste water by a combination of RO, high-pressure RO and NF - Potential and limits of the process, Journal of Membrane Science 174, 231–241.
- Rall, D., Menne, D., Schweidtmann, A. M., Kamp, J., von Kolzenberg, L., Mitsos, A., & Wessling, M. (2019). Rational design of ion separation membranes. Journal of Membrane Science, 569, 209

Biofouling Control in RO/NF Desalination with Novel Laser-Induced Graphene Coated Polymeric Spacers

Emily MANDERFELD¹, Mauricio NUNES KLEINBERG², Jana SCHWARZE¹, Chidambaram THAMARAISELVAN², Yoram OREN², Axel. ROSENHAHN^{1*}, Christopher. J. ARNUSCH^{2*}

¹ Ruhr University Bochum, Faculty for Chemistry and Biochemistry, 44780 Bochum, Germany

² Department of Desalination and Water Treatment, Zuckerberg Institute for Water Research, The Jacob Blaustein Institutes for Desert Research, Ben-Gurion University of the Negev, Sede-Boqer Campus 8499000, Israel

*Corresponding author's e-mail: arnusch@bgu.ac.il; axel.rosenhahn@rub.de

ABSTRACT

Membrane based desalination worldwide consist of more than 17000 operating desalination plants that produce over 3.3 million cubic meters of water per hour. Membrane fouling is a major challenge that decreases water production and increases the costs. Especially membrane spacers facilitate biofouling, thus new spacer technology is needed including new materials and electrochemically based strategies. Laser-induced graphene (LIG) was previously shown to resist bacterial fouling, and when configured as electrodes could reduce bacterial viability in solution. Toward the incorporation of LIG into spacer technology, we fabricated LIG on poly(ether)sulfone (PES) with optimized electrical conductivity and varied the surface wetting properties using atmospheric plasma and chemical modification. The superhydrophilic and superhydrophobic LIG surfaces were challenged with diatom *Navicula perminuta* solutions in a microfluidic testing chamber, which showed that superhydrophobic LIG coatings resisted diatom accumulation 2x better than the superhydrophilic LIG coatings. However, all of LIG coating types collected up to 30x more diatoms than the control coatings, which included dodecanethiol- and PES-coated glass probably because of the differences in roughness. A new microfluidic testing device for real-time analysis of diatom attachment on feed spacers was established and optical tracking was performed using a control feed spacer. Optimization of material properties and designs will shed light on mechanistic aspects of fouling and guide future spacer design strategies.

KEYWORDS

Antifouling, laser-induced graphene, microbial tracking, biofilm

INTRODUCTION

New materials that prevent or inhibit biofilm formation on surfaces will lead to important innovations in water technology, including membrane technology. Graphene is currently a material that is being applied to surfaces for the inhibition of bacteria, although the mechanism of action is still not fully understood. Recently, laser induction was found to be a robust and rapid method for preparing thin graphene coatings on polyimide films, showing potential in many research directions including environmental applications [SIN17]. This so-called laser-induced graphene (LIG) can now be generated on many types of polymer and other carbon containing surfaces [CHY18, SIN18]. The potential of the material has been shown in environmental applications to resist surface biofilm growth, and to actively eliminate bacterial viability in solution if low potentials are applied to the surface. We previously developed methods for LIG formation on other polymers such as poly(ether)sulfones and investigated the antimicrobial and antibiofilm properties of the LIG [SIN18]. We observed that under an electric potential, a combination of chemical and electrical effects could prevent biofilm growth. Such a strategy might be applicable in membrane spacer technology because membrane spacers are subject to fouling. In this present paper, we aim to develop novel methods for preventing bacterial or diatom adhesion and the consequent biofilm

proliferation on RO, NF and UF membranes used for desalination and water treatment by development and refinement of robust laser-induced graphene (LIG) surfaces on polymeric materials, which might be incorporated into membrane spacer technology.

Developing novel polymeric surfaces that include LIG as well as understanding their antimicrobial and electrochemical properties might lead to their application in membrane module construction for desalination technology. This will be highly significant in designing new spiral wound as well as for other membrane modules, which are the heart of modern desalination technology. New approaches in fouling control as those proposed here might reduce energy demand and other operational costs of desalination and water treatment plants around the world.

METHODS

LIG Preparation

General LIG and PES substrate preparation methods have been described [SIN18]. Briefly, LIG was irradiated on the surface of PES sheet using a 10.6 μm carbon dioxide (CO_2) laser cutting system (Universal VLS 3.50 Laser cutter platform). Settings of power (5-9 % of full power 50 W), image density (1000 pulse per inch), and scan rate (25 %) were used under ambient conditions. For LIG in microfluidic testing, the PES substrate was glued onto a glass slide with Hybrifix super 7 glue (Den Braven Sealants bv, The Netherlands), and then LIG was made. Plasma treatment on LIG samples were performed with O_2 plasma (Atomflo 400, Surfex Technologies) for 60s at 100 W. Superhydrophobic LIG surfaces were made by silane treatment as follows. The LIG samples were first exposed with atmospheric plasma for 60s and then treated with trichloro(1H,1H,2H,2H-perfluoroctyl) silane for 30 min. under vacuum atmosphere and dried at room temperature.

SAM Preparation as Control Monolayers

To allow the SAMs to assemble on a gold-coated glass slide (Georg Albert, PVD, Silz, Germany) the slides were kept in 1 mM thiol solution following previously published protocols [THO14]. DDT was purchased from ProChimia Surfaces (Gdansk, Poland) and dissolved in ethanol p.a. (Roth, Germany). The gold-coated glass slides were cleaned under an ozone-generating UV lamp for 1 h. The slides were ultrasonicated in ethanol p.a., rinsed with ethanol p.a. and dried under nitrogen flow. The slides were immersed in DDT solution for 24 h and cleaned as before. For characterisation, contact angle geometry as well as spectroscopic ellipsometry were used.

Bacterial culture

Cobetia marina was cultured from a dry culture from Deutsche Sammlung von Mikroorganismen und Zellkulturen (DSMZ, Braunschweig, Germany). An aliquot from the bacterial culture was spread out with a sterile inoculating loop onto a marine agar plate (sterile marine bouillon medium with 2 % Bacto Agar, Difco, Augsburg, Germany). The culture was allowed to grow over night at 18°C and then for 6 days at 4°C. Individual bacterial colonies from the plate were inoculated into 7.5 ml sterile and filtered MB medium and cultured on an orbital shaker at 18°C over night. A morning culture was prepared by filtering the overnight culture through a 5 μm filter (Merck Millipore, Burlington, Massachusetts, USA) and diluting it 1:100 in MB medium. After letting it incubate for 4 hours at 18°C on an orbital shaker until an OD_{600} of 0.1 was reached, the bacterial culture was centrifuged (Hettich Zentrifugen, Lauenau, Germany) for 3 min at 3000 rpm. The collected pellet was resuspended in nutrient free artificial sea water (ASW) at pH 8.0. The bacterial concentration was adjusted to 7.5×10^6 per ml.

Dynamic microfluidic *Navicula perminuta* attachment assay

The accumulation of *N. perminuta* was performed using a previously established dynamic microfluidic attachment diatom assay [NOL18]. For the assay, a suspension with a concentration of 2 mio/ml of *N. perminuta* was prepared from the same culture in sterile filtered artificial seawater. The accumulation was then performed for 90 min with a shear stress of 0,16 Pa using IBIDI sticky slides (IBIDI, Germany). To remove the access diatoms, which did not stick to the surface, a washing step with artificial seawater was performed for 10 minutes. The number of diatoms were counted via fluorescence microscopy over 30 fields of view per sample (Nikon Eclipse TE2000-U, 10x

phase contrast objective (Nikon CFI Plan Fluor DLL 10x NA 0.3 by Nikon, Tokyo, Japan, BV-2A fluorescence filter). For analysis, the observed differences were tested by an ANOVA analysis for statistical significance. To confirm the results, UV-Vis was used to evaluate the optical density of the outlet solution.

RESULTS AND DISCUSSION

We optimized the laser settings in order to generate LIG with the lowest electrical resistance. For that purpose, LIG squares ($1\text{ cm} \times 1\text{ cm}$) were fabricated on the polyethersulfone (PES) films with variable laser duty cycle (5 to 9%) (Figure 1a) and the electrical resistance of each LIG square was measured using a multimeter. The lowest average resistance was measured for the LIG fabricated with laser duty cycles of 6%, and all following samples were prepared with this protocol (Figure 1b). The lowest resistance gave an indication of a better quality of the graphene. Raman spectroscopy was used to characterize the sample of PES-LIG, which presented the characteristic peaks for graphene, D ($\sim 1350\text{ cm}^{-1}$), G ($\sim 1580\text{ cm}^{-1}$) and 2D ($\sim 2700\text{ cm}^{-1}$) peaks (Figure 1c). The D peak is induced by defects in sp^2 carbon bonds and the G peak is the first-order allowed peak for graphite and confirmed the presence of the sp^2 carbon bond. The 2D peak originates from second-order zone-boundary phonons and confirmed the presence of single layer graphene. In order to increase the hydrophilicity of the LIG, the surface was treated with an atmospheric plasma, which oxidizes the surface. The water contact angle was reduced from $37^\circ \pm 1^\circ$ for the LIG surface to $10^\circ \pm 0.1^\circ$ for the plasma treated LIG surface (LIG-Plasma). Superhydrophobic LIG surfaces (LIG-S-Hyd) were generated by coating with a fluorinated silane compound and increased the water contact angle to $145^\circ \pm 2$. Reasons for the surface wetting changes can be attributed to changes in surface chemistry, as XPS showed an increased content of oxygen on the LIG-plasma surfaces and for LIG-S-Hyd, a high amount of fluorine was observed (Figure 1d).

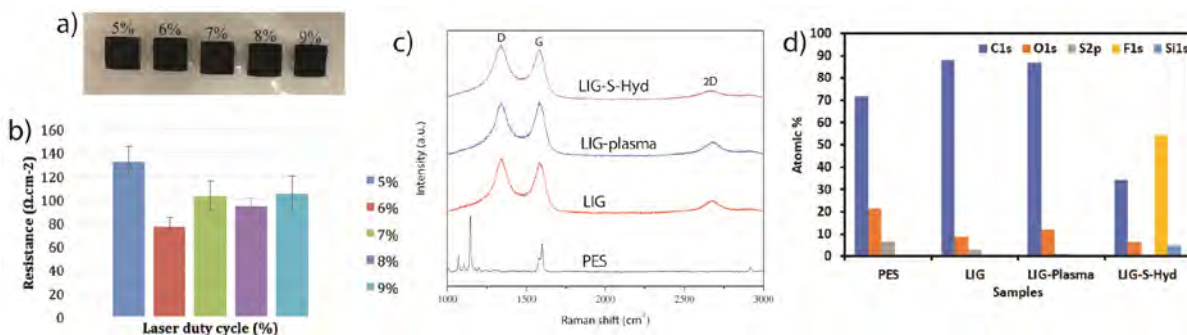


Figure 1: Fabrication and characterization of LIG, plasma treated LIG (LIG-plasma), and perfluorosilane coated superhydrophobic LIG (LIG-S-Hyd). a) Image of LIG made with 5-9% laser power. b) Resistance of LIG made with laser power 5-9%. c) Raman spectra of LIG series made with 6% laser power. d) XPS of LIG series made at 6% laser power.

Quantitative analysis of the attachment of marine biofilm formers

The LIG, LIG-plasma and LIG-S-Hyd coatings were tested against a second class of marine biofouling microorganisms, the diatom *Navicula perminuta* (Figure 2). Microfluidic attachment assays showed an increase of the diatom density of *N. perminuta* on the LIG surface. Compared to LIG, the superhydrophobic LIG showed less diatom adhesion, however, the LIG-Plasma surface showed increased diatom adhesion. Nevertheless, LIG-S-Hyd showed a diatom adhesion 30x higher than the control surfaces (DDT and PES). In previous reports however, *N. perminuta* was shown to adhere better to hydrophobic surfaces. The enhanced diatom density on the LIG surfaces might be due to the rough surface, which might cause the diatoms to be trapped and accumulate. The algae were present in very large agglomerates on the test surfaces after the assay. Taken together, in contrast to previous observations, superhydrophobic LIG had the least amount of diatom attachment and might be more favourable in spacer design considerations.

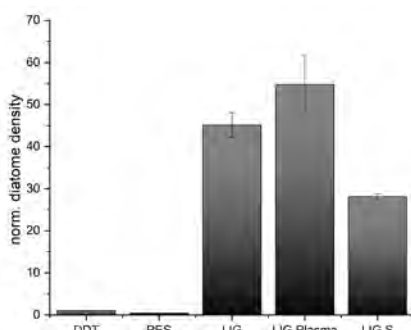


Figure 2: Attachment of the marine diatom *N. perminuta* under dynamic conditions to the tested surfaces. PES are the nonmodified Polyethersulfone (PES) polymers, LIG are the LIG modified PES surfaces, LIG Plasma the hydrophilized counterparts and LIG S the superhydrophobic LIGs. Dodecanethiol (DDT) SAMs were included as hydrophobic controls. Average of 3 repeats is shown.

Micro-flow cell real-time analysis of feedspacers under flow conditions

In order to evaluate feed spacers in real time, a novel micro-flow cell method for analysis of diatom attachment on feed spacers was established. A pump was connected to a flow system, which was connected to a reservoir of the diatom suspension. The flow system consisted of a glass slide (bottom of the system), feed spacer and a top (with inlet and outlet for the diatom suspension). An O-ring was incorporated into the top-part to prevent leakages and the channel system was held together by a metal bracket consisting of two frames (Figure 3a-c). The system mimics the feed spacer channel in a reverse osmosis membrane module.

The diatoms were observed with a 10x phase contrast objective. The focus of the microscope was placed at a crossing of the bars of the feedspacer to follow the movement of the diatoms. It was possible to observe the diatoms flowing over the lower bar of the feedspacer first and then underneath the perpendicular upper bar (video is provided in the supplemental material). Figure 3d shows the movement of one diatom. This method is suitable to analyze the microbial attachment mechanism on the LIG feedspacers. Also it could be used to optimize the cleaning processes by real-time analysis of the cleaning step in order to optimize flow speed, duration and the potential application of pulsed flows. Figure 3e shows the trajectory of some diatoms, which was obtained by stacking all images over each other followed by the subtraction of the background.

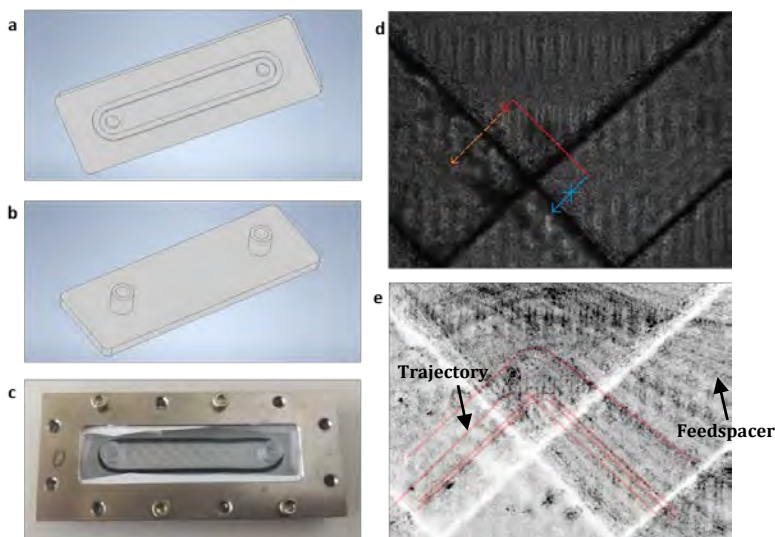


Figure 3: Microscope image of a part of the feedspacer and the trajectory of a single diatom through the cross-bar feedspacer. In red the observed diatom motion across the first bar of the feedspacer. The orange part demonstrates how the diatoms are dragged below the upper bar. Diatoms are following the flow direction and do not follow the blue line.

Microfluidic attachment assay for the marine bacterium *Cobetia marina*

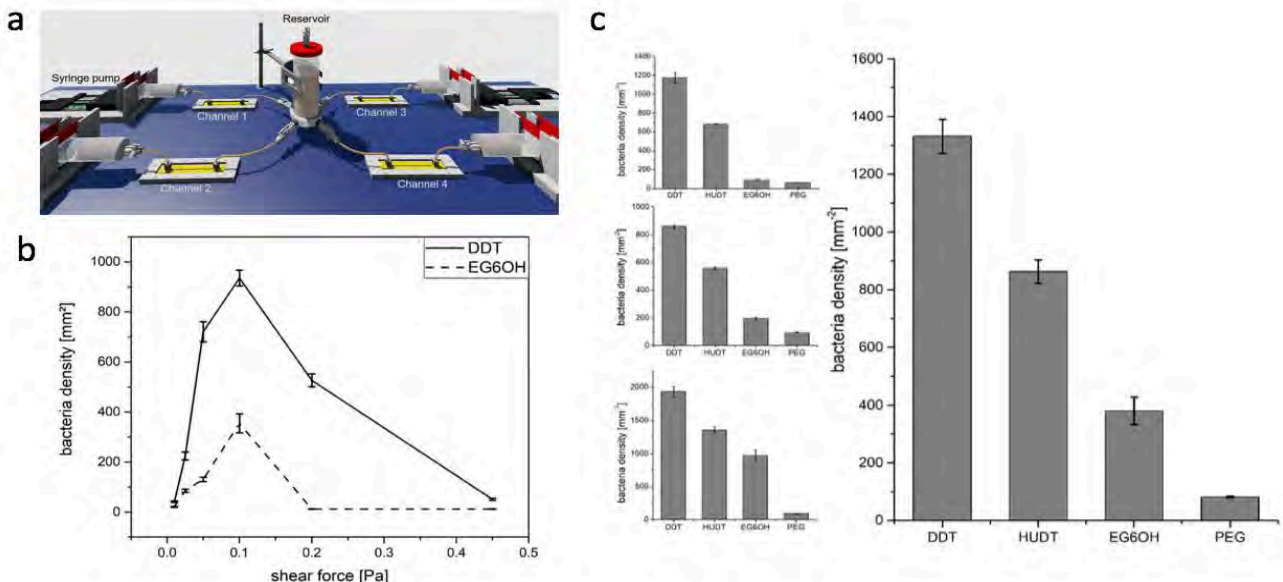


Figure 4: Quantitative assay to study the attachment strength of the marine bacterium *Cobetia marina*.

In particular in the Mediterranean Sea, bacterial biofilm formers are frequently affecting the performance of spiral wound reverse osmosis modules. In order to optimize feedspacers, quantitative techniques to measure the settlement of bacteria under shear are required. Recent studies have shown the excellent antifouling properties of the LIG modified surfaces. Thus, we extended our established microfluidic assay [NOL17,NOL18] towards bacteria. As a constant shear force is used, the attachment is continuously challenged and the measured numbers of biofilm forming organisms reflect their attachment strength to the surfaces. In Figure 4a, the microfluidic setup is shown [NOL18]. In figure 4b, the shear force during a 30 min accumulation experiment was varied and the number of bacteria on the surface was measured. High shear forces hamper bacteria attachment and low shear forces cause the bacteria to stick in the tubings and sediment before they can reach the surfaces. The optimal shear force for the tests was observed to be approximately 0.1 Pa. At this shear force, resistant surfaces such as polyethylene glycols (PEG, EG6OH) can easily be distinguished from “sticky” aliphatic surfaces such as DDT (self-assembled monolayer of dodecanethiol) (Figure 4c). In our future work, we will apply this bacterial growth assay in addition to the diatom biofilm assay to test the fouling properties of the LIG materials.

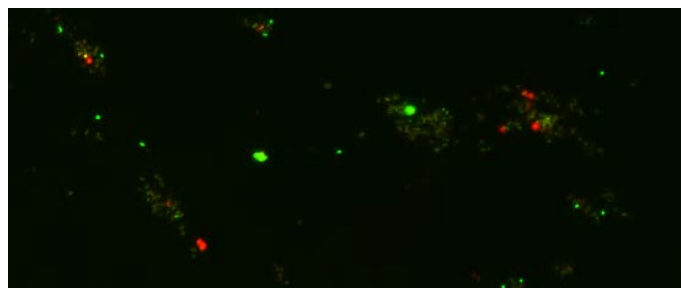


Figure 5: Fluorescence microscopy image of the stained bacteria on the DDT surface. Red: dead bacteria; green: living bacteria.

As the LIG modified feedspacers showed biocidal properties, we additionally established a live/dead staining assay for marine bacteria. For staining, a combination of Syto 9 (red, dead bacteria) and PI (green, living bacteria) is used. As shown in Figure 5, the fraction of dead and living bacteria can directly be calculated from the occurrence of the two fluorescence colors. The staining protocol will be applied within the project to LIG modified PES and feedspacers in order to detect the physiological state of the marine bacteria after attachment in the microfluidic environment.

CONCLUSIONS

Surface wetting properties and surface roughness played a role in fouling of LIG surfaces. The superhydrophobic LIG surfaces fouled less with diatoms in comparison to other LIG surfaces but fouled more than the self-assembled monolayer surfaces probably due to the roughness. These parameters will be taken into consideration when designing spacer and membrane technology with LIG. Methods and apparatus have been built to test spacer fouling and future experiments that include electrically charged surfaces will be performed.

ACKNOWLEDGEMENT

The work was funded by the project BMBF 02WIL1487.

REFERENCES

- [CHY18] Chyan, Y.; Ye, R.; Li, Y.; Singh, S. P.; Arnusch, C. J.* Tour, J. M.* Laser-Induced Graphene by Multiple Lasing: Towards Electronics on Cloth, Paper and Food. *ACS Nano* **12** (3), 2176-2183, (2018).
- [THO14] Thome, I. *et al.* Conditioning of self-assembled monolayers at two static immersion test sites along the east coast of Florida and its effect on early fouling development. *Biofouling* (2014). doi:10.1080/08927014.2014.957195
- [NOL18] Nolte, K. A. *et al.* Parallelized microfluidic diatom accumulation assay to test fouling-release coatings Parallelized microfluidic diatom accumulation assay to test fouling-release coatings. *Biointerphases* **13**, 041007-1-041007-8 (2018).
- [NOL17] Nolte, K. A.; Schwarze, J.; Rosenhahn, A. Microfluidic accumulation assay probes attachment of biofilm forming diatom cells. *Biointerphases*, doi:10.1080/08927014.2017.1328058 (2017).
- [SIN17] Singh, S. P.; Li, Y.; Be'er A.; Oren, Y.; Tour, J. M.; Arnusch, C. J. Laser-Induced Graphene Layers and Electrodes Prevents Microbial Fouling and Exerts Antimicrobial Action *ACS Applied Materials and Interfaces* **9** (21), 18238-18247, (2017).
- [SIN18] Singh, S. P.; Li, Y.; Zhang, J.; Tour, J. M.; Arnusch, C. J. Sulfur-doped laser-induced porous graphene derived from polysulfone-class polymers and membranes *ACS Nano* **12** (1), 289–297 (2018).

Toward Optimized Nanofiltration for Tertiary Desalination

Michael ZELNER¹, Philipp JAHN², Mathias ULBRICHT^{2,*} and Viatcheslav FREGER^{1,*}

¹ Wolfson Department of Chemical Engineering, Technion - Israel Institute of Technology, Technion City, 32000, Haifa

² Lehrstuhl für Technische Chemie II, Universität Duisburg-Essen, 45117 Essen, Germany

*Corresponding author's e-mail: mathias.ulbricht@uni-essen.de; vfreger@technion.ac.il

ABSTRACT

Standard treatment for wastewater nowadays is secondary treatment, which cannot remove salinity and some organic micropollutants. An attractive solution to this problem is nanofiltration (NF), but as currently available NF membranes strongly reject multivalent ions, the process suffers from high energy consumption and severe calcium phosphate scaling. As a potential solution, in this project we aim to develop currently unavailable NF membranes that would reject NaCl to about 30-50%, yet with reduced rejection of desired calcium, magnesium, sulfate and phosphate ions. The investigated approaches are: (a) a NF membrane obtained by grafting a negatively charged polymer on a suitable ultrafiltration membrane, operating through the combination of sieving and Donnan effects and (b) a mosaic membrane composed of a polymeric matrix with oppositely charged submicron particles. In this report our results obtained during the first year are presented.

KEYWORDS

Mosaic nanofiltration membranes; tertiary treatment; wastewater desalination.

INTRODUCTION

Freshwater constitute only 3% from the Earth's water sources, and from which, almost 70 percent is locked up in glaciers or ice at the North and South poles. Due to constant growth in the world's population, problems such as water scarcity and energy consumption are expected to grow worse in the coming decades. Worldwide, agriculture accounts for 70% of all water consumption, compared to 22% for industry and 8% for domestic use. In most of the developing countries, clean water is either hard to come by or it is a commodity that requires significant currency to obtain. This problem can be solved by using energy to clean the water and pump it to vast distances.

Nowadays, the main water treatment for domestic waste consists of a primary treatment which removes gross suspended solids and a secondary treatment that removes dissolved organic compounds. Thus obtained secondary effluents can be used in agriculture, yet when its quality doesn't meet required standards, tertiary treatment can be an optional extra stage. For example, a solution widely used in Israel is a secondary water injection into the ground for recharge of a regional aquifer. The recharged water undergoes additional purification and storage before it is pumped for irrigation (Elkayam, 2015). However, at present, no treatment provides a solution for the removal of salts. Excess salinity of the treated water leads to salt accumulation in soil and suppressed plant growth when reclaimed water is used for irrigation (Raveh, 2016).

Membrane desalination processes such as Reverse Osmosis (RO) and Nanofiltration (NF) can reduce the salinity level of water through nearly total (RO) or partial (NF) removal of excess salt, as well as some recalcitrant organic contaminants (e.g. drugs, pesticides, and endocrine disrupting compounds). RO-based desalination technology is used mostly for drinking water and industrial supplies in countries that have reached the limits of renewable water resources (such as Israel itself). Little desalination is used for agriculture (1%), but its use for high-value crops in greenhouses is gradually increasing. The cost of RO desalination of secondary effluents is lower

than the cost of seawater desalination due to its lower salinity. The cost may be reduced further, when only a partial desalination is needed and NF may be used. NF is preferred over RO for partially removing excess salinity since the higher permeability of NF membranes provides significant energy savings with enough salt removal.

Unfortunately, all available NF and RO membranes remove not only undesired salt (i.e., monovalent ions Na^+ and Cl^-) and recalcitrant organics from water, but also totally retain multivalent ions, such as calcium (Ca^{2+}), magnesium (Mg^{2+}), phosphate (PO_4^{3-}) and sulphate (SO_4^{2-}), that are essential for plants, animals and for corrosion prevention. As a result, NF or RO treatment leads to a drastic depletion of the product water of these multivalent ions thus remineralization of the desalinated product is required. More importantly, the large content of multivalent ions in secondary effluent, typical in municipal waste streams, causes severe scaling, may limit the water recovery to 80% and even 50%.

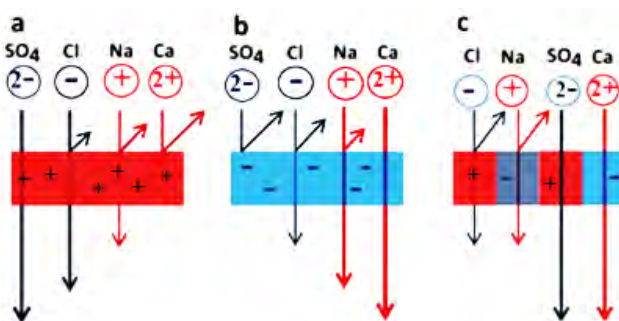


Figure 1: (a) A positively charged membrane with low-rejection for negative ions; (b) a negatively charged membrane with low-rejection for positive ions; (c) a charge-mosaic membrane with low-rejection for divalent ions.

The problem of scaling and need for remineralization may be eliminated, if the rejection pattern for mono- and multivalent ions is reverse, i.e., NaCl is rejected more or just as multivalent ions. To address this challenge, in this study we explore two main solution:

- Preparation of novel energy-saving NF membranes which may show the desired reversed selectivity. Such novel NF membranes, tailored to the specific needs of tertiary treatment, would minimize energy consumption, maximize water recovery, lower operational costs, and enable significant savings on chemicals and fertilizers essential for treatment and irritations. The proposed membrane will utilize the principle of the mosaic structure, based on alternating positive and negative domains. The principle is described in Figure . Such a structure will be formed using a positively charged cross-linked polyamine matrix with embedded negatively charged submicron particles made of well-defined materials such as MOFs or cross-linked polymers.
- Preparation of a NF membrane obtained by grafting a negatively charged polymer on a suitable ultrafiltration membrane, which provides a partial solution to tertiary treatment through reduced rejection of divalent cations;

METHODS

The largest challenge in preparing mosaics is to obtain stable and highly charged domains well-separated at the nanoscale. Here our approach was to use solid inorganic or cross-linked polymeric nanoparticles (NP) as a negative phase embedded in a continuous cationic polyamine PE matrix. As a reference, pure matrix membranes were prepared by forming a thin polyamine (PEI or PVAm, Fig. 2a and b) layer on a polyethersulfone (PES) support membranes. The cross-linker was epichlorohydrin (ECH, Fig. 2c) or glycerol diglycidyl ether (GDE, Fig. 2 d). The support was a commercial UF membrane by GE-Osmonics. Thus, obtained membranes were already demonstrated to have low-scaling properties for phosphate-super-saturated solutions mimicking the Shafdan effluent (Levchenko, 2016). Charge-mosaic NF (CM-NF) membranes were prepared by a similar procedure but with the addition of negatively charged 200 - 500 nm nanoparticles dispersed in the coating solution of an amino-functional polymer. The first option reported here employed MOF-type nickel hexacyanoferrate $\text{Na}_2\text{NiFe}(\text{CN})_6$ particles prepared by precipitation

reactions (Wu, 2016). Such materials were recently reviewed in the context of batteries and electrocatalysis as attractive highly cation-conductive materials (Canepa *et al.*, 2017).

NF membranes were prepared using the dip coating method. The optimal coating solution composition for preparing the amine polymer was 20-25 g/L PEI (600-1000 kDa, Aldrich), or PVAm (XEOREX™ RS 1300, gift from BASF), 2.5-3.5 g/L GDE and 30-50 g/L glycerol (to prevent UF membrane pore collapse upon drying) in ethanol, water or their mixtures. The solution was prepared by dissolving PEI or PVAm, cross-linker, and glycerol in ethanol and stirred for 2 h before coating. Ethanol was a preferred solvent for making membranes without particles, as it dissolves PEI, GDE, and glycerol, better wets PES support membrane and dries faster, yielding a more uniform and reproducible coating. Particle dispersion of 30 g/L MOF particles were prepared using a published arrested growth procedure by mixing appropriate precursor salts in presence of a Ni-binding agent (citric acid salt) (Sun, 2018).

Prior to coating, the PES support coupons were immersed in pure solvent for 24 h to remove soluble components and then fixed in plastic frames and immersed in the coating solution for 1 min. Thereafter, the frame with membrane was hung vertically in a convection oven and dry-cured at 30 °C for another 24 h. For preparing charge-mosaic membranes, the solvent was always water and support was first covered with a particles dispersion to let them settle on the surface and dried, and thereafter was coated with the coating solution of polymer and hung vertically to drain and dry followed by drying in an oven, similar to pure polymer coating. Water was a preferred solvent for MOF dispersion, as its high dielectric constant helps stabilize the dispersion.

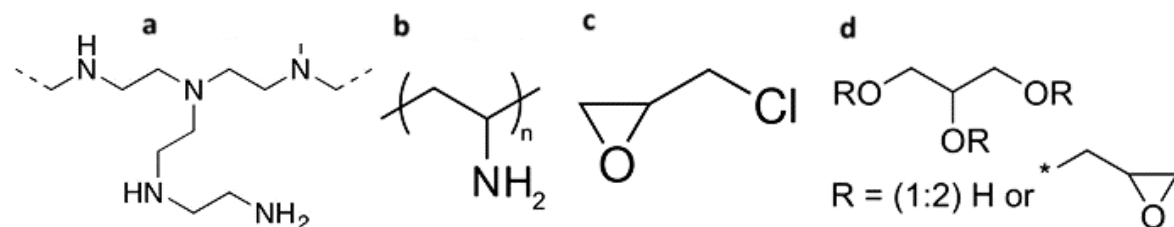


Figure 2: (a) Branched PEI monomer, (b) PVAm monomer, (c) ECH crosslinker, (d) GDE crosslinker.

The approach for fabrication of negatively charged NF (nNF) membranes is based on previous work own work (Bernstein, 2012). For that, commercial polyethersulfone (PES) ultrafiltration membranes are modified by a UV-initiated “grafting-from” method (Fig. 3).

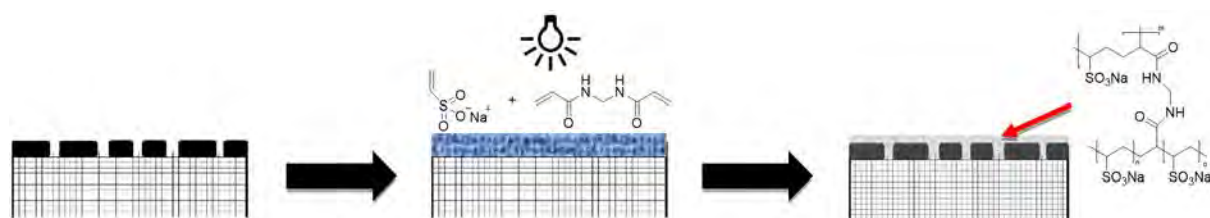


Figure 3: Schematic overview on the preparation of nNF membranes by UV-initiated “grafting-from” based on direct activation of the membrane polymer PES and radical cross-linking graft copolymerization.

In order to obtain a high negative charge density in the selective layer of the nNF membrane, vinylsulfonic acid (VSA) was used as functional monomer and methylenebisacrylamide (MBAA) was used as cross-linker monomer. With the aim to optimize rejection and permeability, different parameters such as base membrane type (molecular weight cut-off, MWCO), monomer concentration and crosslinker monomer fraction, as well as irradiation time and irradiation intensity were varied.

Membrane testing and scaling experiments were performed on a laboratory crossflow setup. Single-salt feed solutions of MgCl₂, NaCl, and Na₂SO₄ contained 1 g/L for all salts. Flux was determined by weighing the permeate and rejection by measuring the conductivity of the feed and permeate.

RESULTS AND DISCUSSION

Preparation of NF membranes containing MOF

Comparison of the performance of similarly prepared pure polyamine membranes showed that both PEI and PVAm membranes (without MOF, Fig. 3a) had single-salt rejections in the range 80-90% for $MgCl_2$, 40-50% for NaCl, and 5-30% for Na_2SO_4 . This pattern is typical of positively charged membranes. However, PVAm was somewhat more selective than PEI, suggesting that the effective charge of PVAm was larger (Table 1).

It was also found that PEI degraded and dissolved MOF particles, apparently, due to competitive complexing and leaching Ni^{2+} ions from the $Na_2NiFe(CN)_6$ structure. On the other hand, PVAm did not show such an effect and acted to stabilize MOF dispersions. The resulting mixed-matrix membrane then clearly showed cubic MOF particles, 200-300 nm large, dispersed in a PVAm matrix (Fig. 4b).

Unfortunately, the performance of mixed-matrix membranes did not show any principle difference from the pure-PVAm membranes (see last line in Table 1), suggesting that MOF particles were not contributing significantly to cation permeation. Indeed, results by the Smith group published recently indicated that Na^+ permeability of $Na_2NiFe(CN)_6$ was several orders of magnitude lower than anion permeability of PVAm and PEI (Shrivastava, 2018). The ion permeability mismatch was apparently too large to produce a mosaic effect. Therefore, we have abandoned the use of this type of MOF particles and, at present, are focusing on other cation-conductive materials, including the polymer particles to be developed by the German partner.

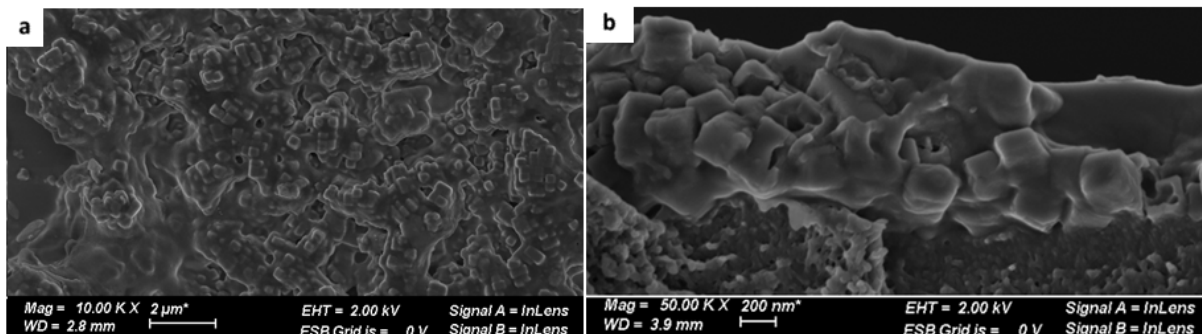


Figure 4: (a) PVAm& NP membrane top view (b) PVAm& NP membrane cross section.

Table 1: PEI membrane cross-linked by GDE (PEI_{GDE}); PVAm membrane cross-linked by ECH ($PVAm_{ECH}$); charge-mosaic membrane with PVAm cross-linked by ECH (CM-NF $PVAm_{ECH}$).

Membrane	Flux, LMH/bar	Single Salt Rejection, %		
		$MgCl_2$	NaCl	Na_2SO_4
PEI_{GDE}	5-6	85	50	30
$PVAm_{ECH}$	4-5	90	45	10
CM-NF $PVAm_{ECH}$	6-7	85	40	5

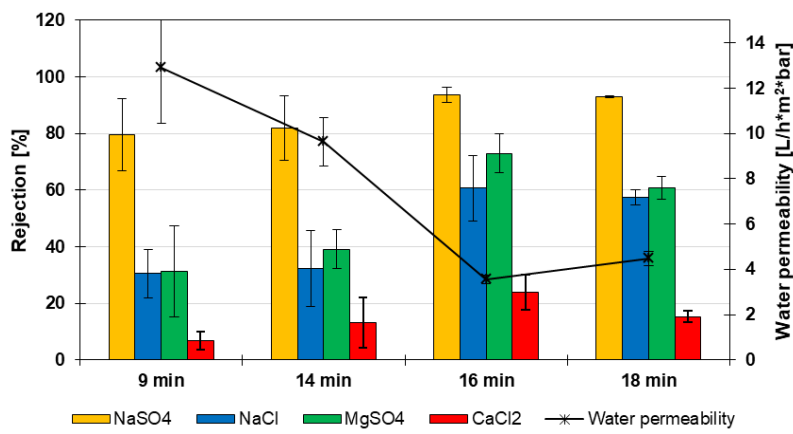


Figure 5: Separation performance of nNF membranes (measured at a transmembrane pressure of 8 bar and using single salt solutions with 1 g/L in water), obtained with a monomer solution containing 250 g/L VSA and 1.75 mol% MBAA in water, and a PES membrane with MWCO = 30 kg/mol at varied UF irradiation time (UV intensity 20 mW/cm²).

Negatively charged NF membrane via graft functionalization

The formation and composition of the grafted cation-exchange hydrogel layer as well as resulting separation performance were studied for systematically varied parameters. Figure 5 shows the salt rejection and pure water permeability as function of UV irradiation time.

A strong influence of UV irradiation time and thus degree of grafting (not shown here) on salt rejection and permeability is observed; with increasing irradiation time, the salt rejection increases, while the permeability decreases. The prepared nNF membranes show the rejection order: Na₂SO₄ > NaCl ≥ MgSO₄ > CaCl₂. This can be explained by a major influence of the Donnan effect. The first membrane prototype for tertiary desalination from this project, the nNF membrane obtained by a strong cation-exchanger hydrogel grafting at an UV irradiation time of 18 min (cf. Fig. 5), is currently further evaluated with mixed salt feeds without and with additional water matrix components.

CONCLUSIONS

MOF-polyamine thin-film composite membranes were prepared and tested. Unfortunately, their separation performance did not show any significant difference from polyamine-only membranes. This indicates that MOF conductivity was too low to produce a charge-mosaic-type selectivity. Therefore, the focus has been shifted to other types of negatively charged cation-conductive particles, including the polymer particles to be developed by the German partner. In parallel, the feasibility of adapting the properties and separation performance of grafted cation-exchange hydrogel layers on ultrafiltration membranes toward negatively charged NF membranes had been shown so that the effects of a partial improvement of membrane selectivity on tertiary desalination performance can already be studied.

ACKNOWLEDGEMENT

Financial support from the Nancy and Stephen Grand Technion Energy Program (GTEP) as well as the *German-Israel Water Technology Cooperation* by Israeli Ministry of Science, Technology and Space (MOST) and the German Federal Ministry of Education and Research (BMBF; 02WIL1488) are gratefully acknowledged.

REFERENCES

- Bernstein R., Antón E., Ulbricht M. (2012). UV-photo graft functionalization of polyethersulfone membrane with strong polyelectrolyte hydrogel and its application for nanofiltration, *ACS Appl. Mater. Interfaces* 4, 3438.
- Canepa P., Sai Gautam G., Hannah D. C., Malik R., Liu M., Gallagher K. G., Persson K. A., and Ceder G. (2017). Odyssey of Multivalent Cathode Materials: Open Questions and Future Challenges. *Chem. Rev.*, 117, 4287–4341.
- Elkayam R., Michail M., Mienis O., Kraitzter T., Tal N., and Lev O. (2015). Soil Aquifer Treatment as Disinfection Unit *J. Environ. Eng.*, 141(12): 05015001.
- Levchenko S. and Freger V. (2016). Breaking the Symmetry: Mitigating Scaling in Tertiary Treatment of Waste Effluents Using a Positively Charged Nanofiltration Membrane. *Environ. Sci. Technol. Lett.*, 3, 339–343.
- Raveha E. and Ben-Gal A. (2015). Irrigation with water containing salts: Evidence from a macro-datanational case study in Israel. *Agric. Water Manag.*, 170, 176–179.
- Shrivastava A. and Smith K. C. (2018). Electron Conduction in Nanoparticle Agglomerates Limits Apparent Na⁺ Diffusion in Prussian Blue Analogue Porous Electrodes. *J. Electrochem. Soc.*, 165(9), A1777-A1787.
- Sun H., Zhang W. and Hu M. (2002). Prussian Blue Analogue Mesoframes for Enhanced Aqueous Sodium-ion Storage. *Crystals* 8, 23.
- Wu X., Wu C., Wei C., Hu L., Cao Y., Ai X., Wang J., Qian J. and Yang H. (2016). Highly Crystallized Na₂CoFe(CN)₆ with Suppressed Lattice Defects as Superior Cathode Material for Sodium-Ion Batteries. *ACS Appl. Mater. Interfaces* 8, 5393–539

Root and Rhizosphere Hydraulic Properties

Gaochao CAI¹, Mohanned Ali ABDALLA¹, Andrea CARMINATI¹, Or LITIG² and Nimrod SCHWARTZ^{2*}

¹ University of Bayreuth, Soil Physics, 95444 Bayreuth

² Hebrew University of Jerusalem, Soil and Water Sciences, 716100 Rehovot

*Corresponding author's e-mail: nimrod.schwartz@mail.huji.ac.il

ABSTRACT

Root water uptake (RWU) accounts for ~80% of the total terrestrial evapotranspiration, affecting crop growth and yield, hydrological processes, carbon cycle, and more. Despite the importance of this process, relatively little is known about the interactions between the soil and the plant and the impact of this interaction on RWU, especially under water drought and saline conditions. The objectives of the proposed research are to identify in what conditions RWU becomes limiting, how root and rhizosphere properties affect crop tolerance to drying and salinity stresses, which root and rhizosphere traits allow reducing abiotic stresses, and which irrigation management can result in optimal stress tolerances in tomatoes.

To reach these objectives, we are conducting simultaneous measurements of water potential in the plant and the soil at both the laboratory and field scale. A physically based model of water flow in soil, rhizosphere and plants is used to interpret the experimental results and to run scenarios.

KEYWORDS

Drought; Drip Irrigation; Matric potential; Root water uptake; Salinity; Soil moisture

INTRODUCTION

Water use for irrigation accounts for ~ 51% of the total water usage in Israel (IWA, 2015). Irrigation efficiency has been largely improved thanks to the introduction of drip irrigation practices that reduce water losses due to evaporation from the soil surface and drainage of water below the root zone. Despite having been successful in increasing irrigation efficiency (Deng et al., 2006), drip irrigation might result in the accumulation of salts at the root surface, which can induce strong osmotic stresses in crops (Sun et al., 2012).

The objective of this project is to establish a method to measure the effect of soil drying and salt accumulation on soil-plant-water relations (root and rhizosphere hydraulic conductivity and leaf water potential) and estimate to what extent and in what conditions (soil texture and transpiration rates) the loss in soil hydraulic conductivity and salt accumulation limit the ability of plants to sustain transpiration demands.

To understand the effect of soil stress (soil moisture and salinity) on soil-plant-water relations it is not sufficient to measure plant transpiration, but it requires the measurements of the water potential in the plant, for example in the leaves. As the soil dries and salts accumulate at the root-soil interface, the leaf water potential drops. It is claimed that stomata regulation (i.e., closure) allows plants to avoid that the leaf water potential decreases to very negative values at which the xylem cavitates (Sperry and Love, 2015). The hypothesis is that stomata close at the onset of hydraulic stress when the leaf water potential starts to decrease more rapidly than the increase in transpiration. This concept has been introduced for trees, for which xylem cavitation is expected to be the primary cause of cavitation. However, also crops such as tomato have been reported to cavitate (Skelton et al. 2017).

Additionally, it has never been proven that the primary cause of hydraulic limitation is the xylem and not the soil. The claim of Sperry and Love (2015) is based on the argument that because of the uncertainty in hydraulic conductivities of dry soils and the area of water adsorbing roots, it is pragmatic to assume that "root investment is just sufficient to approach the xylem limit." However,

for improving water use efficiency and identifying root traits that favor water acquisition from drying soils, questioning this hypothesis is necessary. In particular, it should be tested for which plant species, soil types, and atmospheric conditions (light intensity, air humidity, and temperature), the soil is the limiting factor for water flow and to what extent stomata regulate to control transpiration and attenuate the drop in leaf water potential.

Once the soil hydraulic limits to transpiration and the stomata regulation are understood and we have a mechanistic model of transpiration regulation based on soil-plant hydraulics, one can formulate a hypothesis on the effect of irrigation on transpiration and growth.

Here, we claim that in the same way as stomata close at the onset of soil hydraulic limitation, irrigation should also be performed at this onset. Since the soil-hydraulic limitation is plant, soil, and atmosphere specific, the optimal irrigation schedule should also be a plant, soil, and atmosphere specific.

In this project, we aim to identify such optimal irrigation schedule for varying tomato varieties showing a contrasting degree of drought and salinity tolerance. As soil stress depends on how the water is distributed in the soil profile, we performed experiments at two scales:

1) In relatively small pots we tested the relation between leaf water potential, soil water potential and stomata conductance at high temporal resolution. The small pots allow the use of a specially designed root pressure chamber, in which the soil-root system is enclosed in a pressure chamber and the water in the leaf xylem is maintained at atmospheric pressure (Passioura, 1980; Carminati et al., 2017).

2) In lysimeter scale experiments, it is tested how water is distributed in the soil during root water uptake (RWU). Due to linearity in soil hydraulic properties, water depletion increases nonlinearly with the dimension of the soil samples. Therefore, to mimic field conditions and study the effect of heterogeneous soil drying on the leaf water potential, a lysimeter scale study is planned. In this experiment, soil moisture and root distribution are measured with electrical resistivity tomography (ERT). Leaf water potential is measured using psychrometers. In this extended abstract, we present the preliminary results of the project.

MATERIAL AND METHODS

Pressure chamber method

The root pressure chamber system measures the transpiration rate (T) and the leaf xylem water potential. It is composed of two parts: the root pressure chamber with a cuvette above and the main controller with a touchable display panel (Fig. 1). Tomatoes were grown in sealed polyvinyl chloride (PVC) columns with the roots and soil in the pressure chamber and the shoots in the cuvette where the transpiring rate was changed by altering the light intensity. The transpiration rate of the plant was calculated by multiplying the difference in humidity between the outgoing and ingoing air with the flow rate of the ingoing air. The relative humidity and temperature of the ingoing and outgoing air were measured every 10 seconds by the sensors (Galltec-Mela, Bondorf, Germany) that were installed below and above the cuvette. The air passing through was stirred by a fan that was installed top inside the cuvette. Four groups of light emitting diode (LED) lights were distributed outside of the cuvette. The light intensity was measured by the radiometric sensor (Gamma scientific, San Diego, USA) that was installed below the fan. The leaf water potential was determined by applying pneumatic pressure to the roots to bring the water in the cut leaf to atmospheric pressure. That pressure applied is called balancing pressure, P , and it is equal to the tension in the leaf xylem before pressurization (Passioura, 1980). A meniscus system with a capillary tube and an infrared detector was connected to the cut leaf to maintain the hydraulic continuity and monitor the pressure in the cut leaf. The movements of the meniscus indicated the pressurized status of the plant to the applied pressure. The xylem water potential was determined when the meniscus was maintained (fluctuation $\leq \pm 2$ mm) for an adjusted pressure for at least 10 minutes.

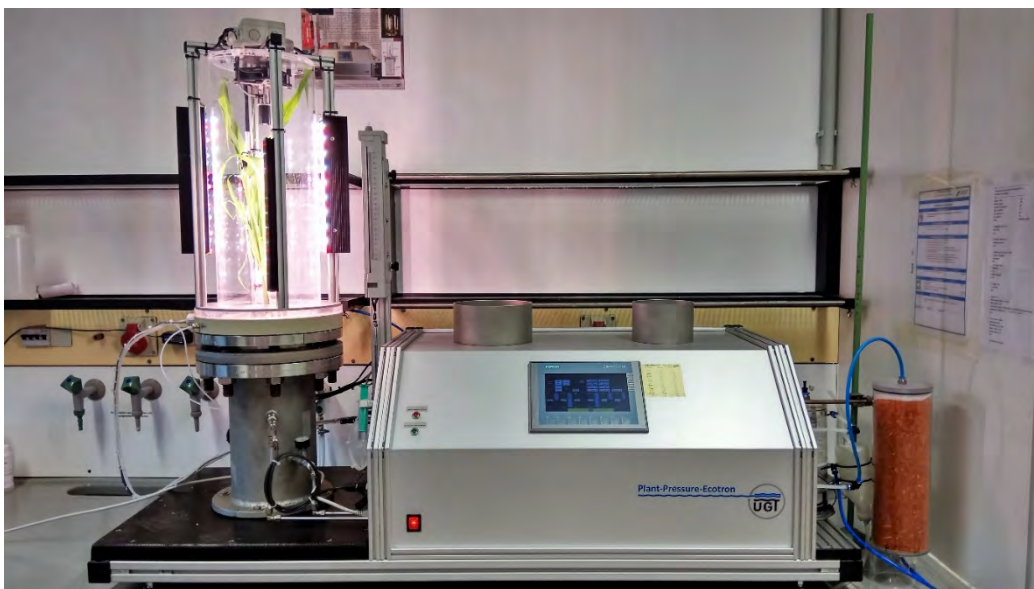


Figure 1: The root pressure chamber system is composed of a root pressure probe where the root-soil is pressurized with a mixture of N₂ and ambient air. The shoot is enclosed in a cuvette where varying light intensity and air humidity can be applied. Transpiration is measured by measuring the humidity of the incoming and outgoing air and air flow rate. Leaf water potential is measured by maintaining the water pressure in the xylem of an excised leaf at atmospheric pressure, which is achieved connecting a cut branch to a thin capillary and monitoring the height of water in thin capillary constant. The method allows simultaneous measurements of the relationship between water potential and transpiration for varying water content.

Lysimeter experiments

We design a lysimeter system that enables simultaneous measurements of xylem water potential, transpiration, and mapping of the soil water content (see Figure 2). Each lysimeter unit contains a 70L pot, a high-resolution scale (150D, Mettler Toledo), a psychrometer (PSY1, ICT International) and 128 stainless steel electrodes for electrical imaging. We filled three pots with red sandy loam soil and planted one grafted tomato plant in each pot. We use M82 for the scion and “strong,” “medium,” and “weak” tomato rootstock (Rootility) for each pot. Every three days, 120% of the transpired water was added to each pot. Two months after planting, the stem of each plant was connected to the psychrometer and irrigation was ceased. We continuously monitored the stem water potential, the transpiration of each pot, the temperature, the radiation, and the relative humidity. For each pot, we conducted a daily electrical resistivity tomography survey (using the DAS-1 electrical impedance tomography system, MPT). The results from the electrical surveys were inverted using the R3 software (A. Binley, Lancaster University).



Figure 2: The lysimeter system during an electrical survey.

PRELIMINARY RESULTS

Pressure chamber method

Preliminary experiments were carried out with a drought-sensitive tomato cultivar (from Rootility). The connection between the leaf xylem and the meniscus was achieved with a thin capillary (Figure 3a).

The challenge was to seal the chamber at the plant collar. This problem was solved by testing different gluing materials and timing of application (ca. 2 weeks after planting). Transpiration rate was measured by subtracting the relative humidity of the incoming and outgoing air (RHin and RHout) and multiplying by the air flow rate (Figure 3b). The results showed an excellent match with gravimetric/complementary measurements. The measurements of the leaf water potential

based on the position of the meniscus showed an accuracy higher than 0.1 bar (10 kPa, Figure 3b), which is acceptable considering the stress that we expect to impose on tomatoes during soil drying and salinity (up to 1.5 MPa).

The measurements showed the expected relationship between leaf water potential (P) and transpiration rate (T) for decreasing volumetric soil water contents θ . At high water contents, the relationship was linear (Figure 3b). For decreasing water contents the relationship became slightly nonlinear, with an increase in leaf suction (P) at high transpiration rates T . In severely dried soils ($\theta=0.05$) the leaf suction was high already at low transpiration and it rapidly and non linearly increased when transpiration was increased. Interestingly, high transpiration rates could not be sustained at this water content.

The point on this trajectory when the curves become nonlinear and bend compared to the trajectory in wet soils ($\theta=25\%$, yellow line Figure 3c) is when hydraulic stress occurs. This is the point when the soil should be irrigated. Note that this critical water content depends on the transpiration rate.

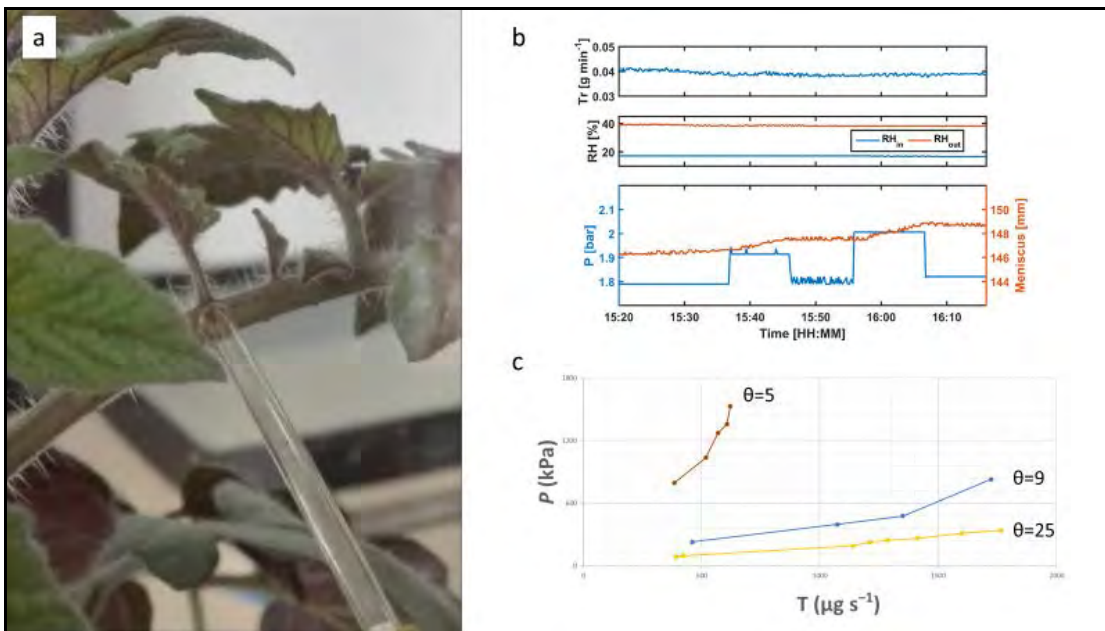


Figure 3: Results of the pressure chamber experiments performed by the German group in Bayreuth. a: connection between an excised tomato leaf and a thin capillary which is connected to a meniscus whose position is measured by a laser. b: Test measurements of the accuracy of the transpiration measurements (T), relative humidity of the incoming and outgoing air (RH_{in} and RH_{out}), and sensitivity of the meniscus to the applied pressure (P). c: Measurements of the relation between applied pressure P (corresponding to the leaf water potential) and transpiration rate T for tomatoes in soils with different water contents θ (given as %).

Lysimeter experiments

In Figure 4, the time series of the xylem water potential for the three different plants is shown. First, the diurnal pattern is clearly demonstrated. A clear difference between the response of the plants to water stress is observed. Plant A does not show a significant decrease in the xylem water potential, while the xylem water potential of plant C and plant B starts to decrease from day 9, and day 4, respectively. Note that the only difference between the plants is the rootstock.

Results from the ERT surveys are shown in Figure 5. Examples for the inverted images are shown in panels (d) and (e), and a 1D plots of the resistivity along the center of the pots vertical axis for plants A, B and C are shown in panels (a), (b) and (c),

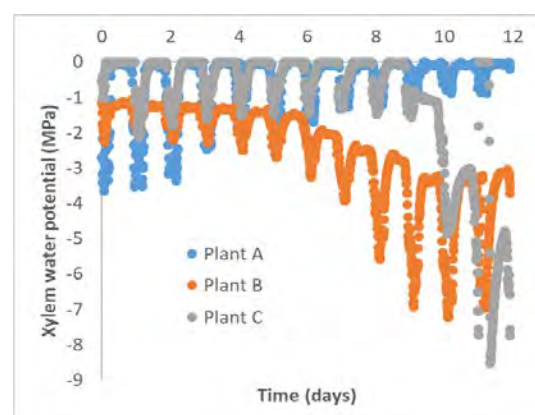


Figure 4: Xylem water potential as a function of time for the three different tomato plants.

respectively. For all plants, the electrical resistivity increases with time as a result of a decrease in water content (due to transpiration) and an increase in the salt concentration (accumulation at the root zone). Two resistivity patterns are observed. For plants B and C, the resistivity is highest at depths ranging from 15 to 20 cm. For plant A, the highest resistivity is in the shallow zone of the soil. The zones of increases resistivity can be associated with zones of high RWU, as this is the main process controlling the resistivity in the pots. Interestingly, RWU patterns can be linked to the xylem water potential. For plant A, the xylem water potential is highest (less negative) while for plants B and C with deeper RWU, a more negative xylem water potential develop with time.

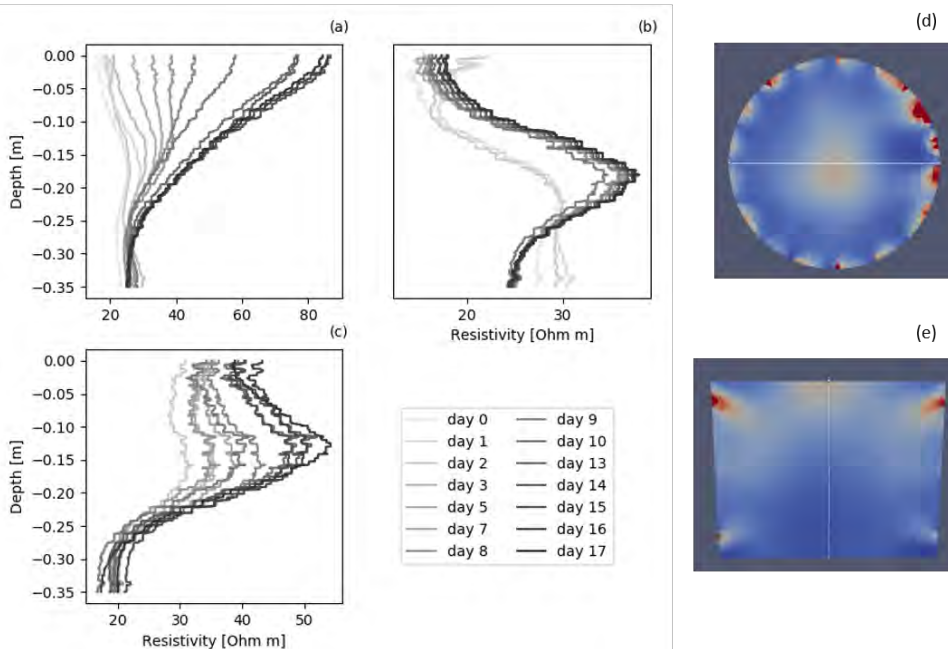


Figure 5: Vertical cross section of the electrical resistivity at the centre of pots A, B and C (in panels a, b and c, respectively) for different times. Day zero represent the time of the last irrigation. Examples for top view and cross section view of the pot ERT image (panels d and e, respectively).

FUTURE DIRECTIONS

After having tested the methods, the next steps are:

- 1) to measure the relationship between leaf water potential and transpiration rate in tomatoes with contrasting drought and salinity tolerance (including drafted varieties);
- 2) to measure this relationship during varying drip irrigation frequency and intensity;
- 3) to test whether irrigating at the onset of soil hydraulic stress (nonlinearity in the leaf water potential-transpiration relationship) is an optimal strategy.

CONCLUSIONS

We have shown a method to measure the relationship between leaf water potential and transpiration rate in drying soils. This method gives the onset of soil hydraulic stress, and this is the experimental base to test the hypothesis that irrigation should be scheduled at the onset of hydraulic stress. The concept will be applied in field-scale experiments in which soil moisture and root distribution are measured with ERT.

ACKNOWLEDGMENT

The position of Gaochao Cai and Or Littig are funded by the German-Israeli Cooperation in Water Technology Research (BMBF-MOST, Project: WT1704 / 02WIL1489 /ID13 3-14907 Rhizosphere).

REFERENCES

- Carminati A., Passioura J.B., Zarebanadkouki M., Ahmed M.A., Ryan P.R., Watt M. and Delhaize E. (2017). Root hairs enable high transpiration rates in drying soils. *New Phytologist*, 216:771-781.
- Deng X.-P., Shan L. and Zhang H. (2006). Improving agricultural water use efficiency in arid and semiarid areas of China. *Agric. Water Manag.* 80(1): 23–40.
- IWA. (2015). Total water consumption by sectors. Available at <http://www.water.gov.il/Hebrew/ProfessionalInfoAndData/Allocation-Consumption-and-production/20156/goals-2015.pdf>.
- Passioura, J. (1980). The Transport of Water from Soil to Shoot in Wheat Seedlings. *J. Exp. Bot.* 31, 333–345.
- Skelton R.P., Broadribb T.J. and Choat B. (2017). *New Phytologist*, 214: 561–569.
- Sperry, J. S. & Love, D. M. (2015). What plant hydraulics can tell us about responses to climate-change droughts. *New Phytol.* 207, 14–27.
- Sun, J., Y. Kang, S. Wan, W. Hu, S. Jiang, and T. Zhang. (2012). Soil salinity management with drip irrigation and its effects on soil hydraulic properties in north China coastal saline soils. *Agric. Water Manag.* 115: 10–19.



Project Group 2017

Improved Degradation and Enhanced Infiltration Rates in SAT by Hydraulic Manipulation

Felix BARQUERO¹, Shany BEN MOSHE², Alex FURMAN², Joseph GUTTMAN³, Falk HAENDEL¹, Fritz KALWA¹, Christian KONRAD⁴, Rudolf LIEDL¹, Jana SALLWEY^{1*} and Noam WEISBROD⁵

¹ Institute for Groundwater Management, TU Dresden, 01069 Dresden, Germany

² Faculty of Civil and Environmental Engineering, Technion, 32000 Haifa, Israel

³ MEKOROT - Israel National Water Co. Ltd., 61201 Tel Aviv, Israel

⁴ G.U.B. Ingenieur AG, 08004 Zwickau, Germany

⁵ Blaustein-Institute for Desert Research, Ben-Gurion University, 8499000 Sde Boker, Israel

*Corresponding author's e-mail: jana.sallwey@tu-dresden.de

ABSTRACT

The research project aims to increase geohydraulic and biological-chemical knowledge on soil aquifer treatment (SAT) processes to optimise the operational management of existing SAT plants and to enable the effective planning of new plants. Most of the desired water treatment during SAT is aerobic. With limited land availability in urban or peri-urban regions, SAT needs to be optimized in a way to maximize the infiltration capacity while maintaining the remediation potential of the unsaturated zone.

Increasing the oxygen availability at various depths can tremendously improve the water quality and biodegradation efficiency in SAT. Column experiments conducted with intermittent infiltration schemes confirmed that higher oxygen values in the soil lead to higher degradation rates of dissolved organic carbon (DOC) and ammonium. Next to an increase of oxygen through prolonged drying phases, biodegradation proved to be enhanced and stabilized through airsparging.

Small-diameter wells were tested as a hydraulic measure to shift part of the treatment into deeper strata, thereby enhancing recharge performance, while minimizing land demand. Laboratory experiments showed that while the recharge potential of these wells is high and physical clogging can be managed well, biological clogging management is still a matter of concern.

The project is conducted in close cooperation with MEKOROT, the operator of the SHAFDAN treatment plant and its associated infiltration ponds near Yavne. While the assessment focuses on this site, results will be applicable to other SAT sites as well. To better understand the general potential of the SAT concept in Central Europe we conducted a preliminary assessment for SAT schemes in a case study in Germany. With the results of the research project, we hope to promote use of SAT as well as increase its acceptance by decision makers and administrations.

KEYWORDS

Soil aquifer treatment, water reuse; biodegradation; optimization; small-diameter wells, infiltration

INTRODUCTION

In recent years, the need for irrigation water is constantly rising. To meet the demand, the reuse of treated waste water has proven to be an economic measure, given satisfying water quality. SAT is a mean to increase the quality by using the unsaturated zone as a bioreactor for pretreated waste water, percolating intermittently for mainly aerobic degradation of DOC, nitrogen species and other contaminants.

The metropolitan area of Tel Aviv is constantly growing, leading to an increase in total waste water amount as well as a price increase for infiltration area. Due to this, the effectiveness of the existing SAT infiltration areas in the Shafdan needs to be further improved. To find optimal ways for SAT-operation, hydrogeophysical methods can be useful to better control the infiltration process and the resulting oxygen availability in real time and the biogeochemistry in the vadose zone (Haaken

et al., 2016). Entrapped air plays a key role here, since it acts as a hydraulic impediment for the infiltrating water but is also essential for biodegradation in the deeper vadose zone, where oxygen is scarce (Mizrahi et al., 2016).

The SATPlanner project started in 2017 and aims at enhancing the degradation of the secondary treatment residues by controlling the resultant redox processes in the vadose zone. To do so, either the wetting-drying cycle of the infiltration basin can be changed, or the basin can be replaced by one or more infiltration wells, which can be cheap and easy to drill, if the well diameter is small (Händel et al. 2014). The wells, however, can be subject to clogging, which needs to be assessed first.

METHODS

Laboratory investigations

A large-scale column of 6 m length, filled with undisturbed material from the infiltration ponds near Yavne, is currently used to test different hydraulic loading cycles (HLC) in combination with different waste water types monitoring oxygen levels and biodegradation. The optimal HLC for each waste water type (20 combinations are being tested) shall provide a basis for optimizing the SAT efficiency in the field facilities.

A 1 m column was recently constructed to test the ability of additional air injection through a compressor (airsparge) for enhancing drying, and biodegradation of organic matter and nitrogen species. Various operation modes are to be tested while the dissolved oxygen (DO) and ORP

(oxidation-reduction potential) are monitored, and water quality samples are collected. Operation modes will range from air injection to expedite drying (i.e. injection during drying mode) to continuous water infiltration and air injection.

For well clogging assessment, six identical well-aquifer models (Figure 1) were built to mimic the surrounding of infiltration wells with different setups. Two models were set up with a gravel pack of the same diameter as the well screen of two other models (63 mm), where the filter slots were in direct contact with the sediment. The remaining two models were filled with gravel only to compare the clogging in sand with clogging in gravel. Clogging was assessed under a constant flow rate, by observing the increase in hydraulic head difference and calculating the resulting

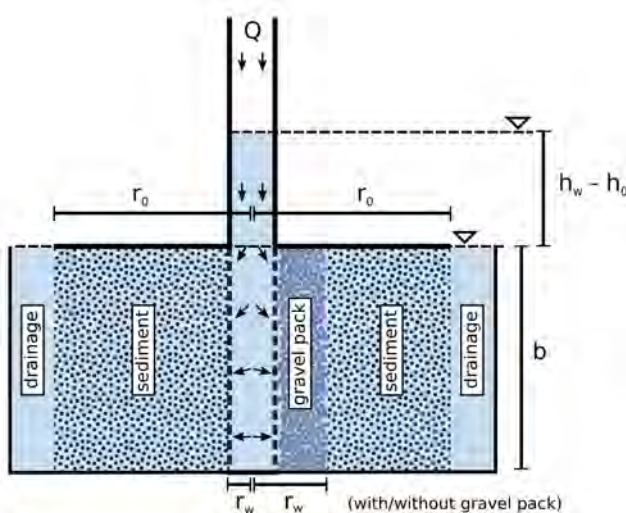


Figure 1: Aquifer-well model, with well diameter (r_w), model diameter (r_o), inflow (Q), hydraulic head difference (h_w-h_0) and model thickness (b)

hydraulic conductivity with Dupuit-Thiem. Physical and biological clogging was assessed by making two experimental runs for nutrient-rich and turbid waters, respectively. Nutrients were added in form of glucose, nitrogen and phosphate; suspended solids were added in form of clay particles. Table 1 shows the tested well setups.

Field investigations

Two new hydrological station were constructed at Yavne 1 (small) site, at the infiltration basin ends. Each station includes sensor clusters every 25 cm from the soil surface to 2 m below ground, with sensors for water content, temperature, electrical conductivity, ORP, gas phase oxygen, and for some depths pH. A sampling port is installed at each depth. We set infrastructure for air injection at three depths at each station. This pond is undergoing a unique operation (roughly 8/4 days wetting/drying), that would significantly expand our database. Results from this site are currently being gathered but will not be presented here.

Numerical modeling

Numerical modeling is essential for a good process understanding and for upscaling from laboratory to field scale. SAT hydraulic and geochemical modeling is currently calibrated to the

long-column experiments. Results are not shown in this manuscript for space. Geochemical modeling is based on PHREEQC (Parkhurst and Appelo, 2013) as imbedded in HYDRUS/HP1 (Jacques and Simunek, 2005). Models consider Richards' equation for water flow, advection-dispersion for solute transport (ammonium, nitrate, nitrite, dissolved oxygen) with multiple Monod and first order reaction for various solute reactions and soil sorption. Biomass growth and decay are modeled (but without microbial movement). Oxygen transport is considered in the gas phase through advection. The model also includes a section for aboveground reactions, executed using PhreeqC (independent of HP1) and Matlab platform. A 2D/3D version is yet to be executed.

Analyses of potential sites for SAT systems

Analyses for the selection of potential sites for the construction of SAT-systems were carried out for parts of Israel and for the area of "Südheide" in Lower Saxony (Germany). Existing methods for site selection analysis have been adapted and advanced. They consider the presence of unconsolidated underground material, the existence of waste water treatment plants (WWTP) and their distance to potential users of the water and available areas. This data was overlain in GIS to display potential sites. During the second step, detailed information, like the geohydraulic parameters of the subsoil or aquifer, the depth of the groundwater table, the groundwater flow direction, existing groundwater uses, and the quality of the wastewater, were interpreted for the potential sites.

SELECTED RESULTS AND DISCUSSION

Influence of operational dynamics on soil aeration

Figure 2 presents one exemplary result from the large column studies, depicting the DO concentrations at four depths through a two-stage flooding-drying campaign (HLC 60/180 min wetting/drying, followed by 60/240 min; see appendix for further details). Increasing the drying period (DP) after ~2000 min, we expected to observe increased aeration and some recovery of DO concentrations deeper than 75 cm (where the shorter DP led to DO depletion). At 75 cm depth, DO concentrations increased by ~60% and reached an average of ~6.4 mg/L during longer DP (compared to an average of ~3.7 mg/l during the shorter DP, after the initial drop around the third cycle).

In the deeper parts of the profile, a delayed, moderate yet significant response to the increase in DP was observed (DO recovery was observed after around 2700 min for 375 cm and 3700 min for 575 cm). The minimum DO concentrations recorded through the two-stage experiment averaged 0.79, 1.32 and 1.62 mg/L for depths of 175, 375 and 575 cm, respectively. These ranges of DO concentrations below 1.5 m underground are common in many SAT sites around the world (Amy et al., 2007) and explain the insignificant aerobic bacterial activity found under these conditions. Following each of the longer DP, DO concentrations in the 175 cm sensor fluctuated periodically in response to the wetting and drying periods and reached 4.1 mg/L on average following the drying events. In the two deepest sensors, DO concentrations stabilized around ~3.9 mg/L in the 375 cm sensor and ~3.25mg/L in the 575 cm sensor. As sustaining the shorter drying periods of stage 1 would result in total DO depletion at ~175 cm depth, these are very important observations. They indicate that longer DP not only enhance oxidizing conditions at a given depth, but also increase the share of the profile that did not develop anaerobic conditions.

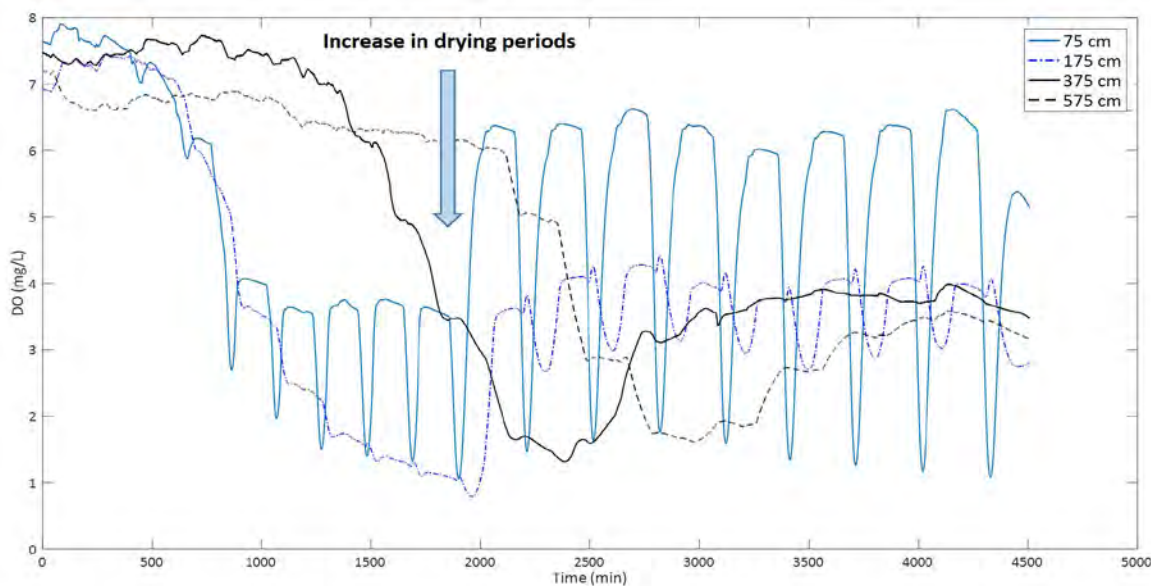


Figure 2: DO concentrations shifting the HLC from 60/180 min to 60/240 min

In a field study conducted in the Israeli SHAFDAN site in 2015-2016 ORP values through the wetting and drying cycles were recorded in a series of aquifer recharge campaigns over a year (Orgad et al., 2017). A comparison is brought in appendix, but in brief, patterns are similar but with different time scales that are attributed mostly to dimensionality.

Potential of airsparging for additional soil aeration

The aim is to investigate artificial aeration at different soil depths and its influence on qualitative parameters (e.g. DOC, ammonium) and further the extent to which the drying times can be shortened by additional aeration, allowing for larger infiltration quantities. First results are promising and show that for infiltration cycles with short drying times (1h infiltration, 2h drying) the oxygen saturation can be kept constant over time and the DOC removal can be stabilized at a high level (Figure 3). The same scenario run without airsparging leads to complete oxygen depletion and significantly reduced DOC removal rates.

In a second step, the scenario was changed to a HLC of 2 h: 4.5 h. The 4.5 h DP was stepwise reduced always including a constant aeration phase of 1 h. Results show that even for a reduction from 4.5 h to 3 h for the DP high levels of maximum DO could be achieved (90% in the upper soil, 60% in the lower soil). These results indicate that installation of airsparging helps to recover oxygen levels quicker in during the DP, giving the possibility to prolong the infiltration phases and to increase the infiltration capacity.

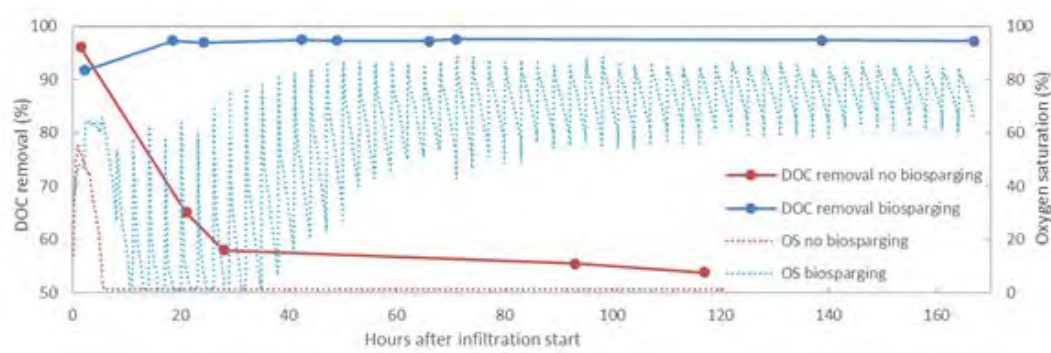


Figure 3: Effect of additional aeration on oxygen saturation and DOC removal

Well clogging assessment

Figure 4 shows the results of the well clogging assessment. To make the results more palpable, only averaged values of the identical setups – 2x 63 mm without gravel pack, 2x 63 mm with gravel pack,

and 2x 63 mm in gravel aquifer – are presented. While physical clogging led to a 95 % reduction of the original hydraulic conductivity after 2 h, biological clogging reached this value only after 36 h. However, as these values depend very much on specific factors (clay and nutrient concentration, temperature, etc.), they cannot be generalized. More interesting is the evolution of clogging, where physical clogging shows strong differences between the setups with/without gravel pack and in the gravel aquifer. Biological clogging seems to evolve rather similarly for all setups, leading to the conclusion that the advantages of a gravel pack become less pronounced, when only bioclogging is expected (as it is the case with most treated effluents).

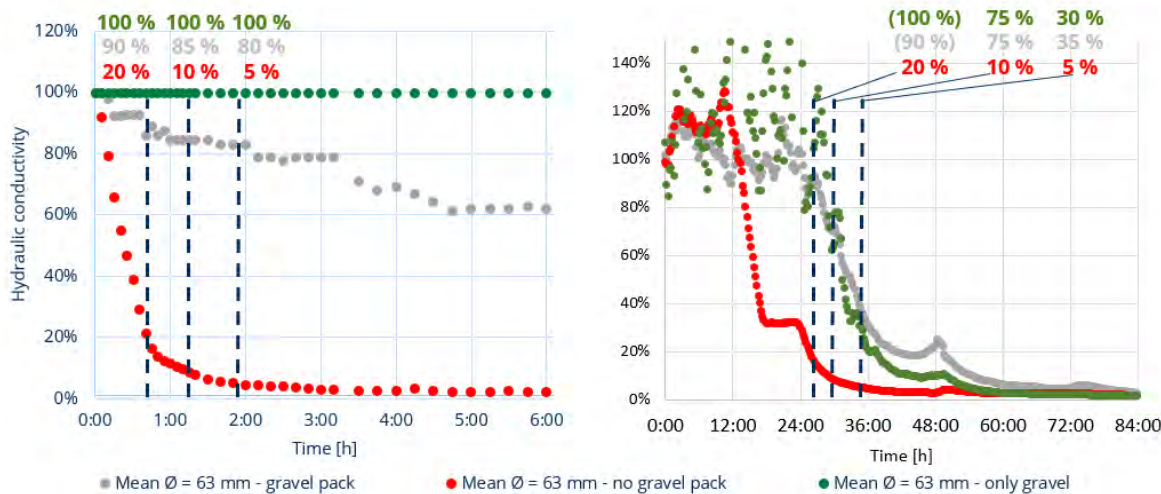


Figure 4: Decrease in hydraulic conductivity around a well due to physical clogging (left) and biological clogging (right)

SAT site selection and site assessment

The site selection analysis for Israel shows that unconsolidated rock formations are (a) the Coastal Aquifer, (b) local Neogene and quaternary formations in the Negev and Arava, (c) alluvial formations in the area of Bet-She'an and the Jordan Valley in the Eastern Mountains and the Kinneret Basin, and (d) the western Jezre'el Valley fill aquifer of Neogene-Quaternary age in the Western Galilee Basin (Sneh et al., 1998; Weinberger et al., 2012). More than seventy WWTP sites have already been researched, the greatest density of which is in the coastal region. Here, the implementation of additional SAT-systems was not considered due to extensive use of the Coastal Aquifer for drinking water production. Possible sites for SAT-systems in the areas (a) and (d) are currently under review.

For the Südheide region of Germany, information about the land use, depth of the groundwater table, rivers, and the location of protection zones (for drinking water, natural, and military purposes) were compared with seventeen locations of WWTPs. Four WWTP sites were excluded due to the land use (forest or settlements) or shallow groundwater tables. Detailed information concerning the parameterization of the subsoil, the designation of specific areas, and the groundwater dynamics were compiled for the remaining thirteen sites. The planning of a potential SAT-system for at least one site will finalize this part of the project.

CONCLUSIONS

The application of additional SAT-systems in Israel is primarily restricted by the presence of unconsolidated aquifers and by the concurrent uses of the aquifers. Thus, enhancement of existing SAT schemes is inevitable. This study presents three promising measures for enhancement of infiltration quantity: improved operational dynamics, additional airsparging and integration of small diameter wells. The insights obtained from corresponding experiments and modelling, along with methods for site selection, as well as from experiences published in the literature, will form the basis for the planned guidelines on SAT site planning and enhancement.

ACKNOWLEDGEMENT

This study was supported by the German Federal Ministry of Education and Research (BMBF) and the Ministry of Science, Technology and Space (MOST), Israel with grant No. 02WIL1451A and Israeli Project Number 2689.

REFERENCES

- Gary, A. and Drewes, J. (2007). Soil aquifer treatment (SAT) as a natural and sustainable wastewater reclamation/reuse technology: fate of wastewater effluent organic matter (EfOM) and trace organic compounds. *Environmental monitoring and assessment* 129 (1-3), pp 19-26.
- Haaken, K., A. Furman, N. Weisbrod, and A. Kemna (2016). Time-lapse electrical imaging of water infiltration in the context of soil aquifer treatment. *Vadose Zone Journal*, 15 (11).
- Händel, F., Liu, G., Dietrich, P., Liedl, R., Butler Jr., J. (2014). Numerical assessment of ASR recharge using small-diameter wells and surface basins, *J. Hydrol.*, 517, pp 54-63.
- Jacques, D., & Šimůnek, J. (2005). User manual of the multicomponent variably-saturated flow and transport model HP1: Description, Verification, and Examples, Version 1.0. BLG-998, SCK•CEN, Belgium.
- Mizrahi, G., Furman, A. and Weisbrod, N. (2016). Infiltration under confined air conditions: Impact of inclined soil surface. *Vadose Zone Journal*, 15 (9).
- Orgad, O. (2017). Seasonal operation mode for a SAT system. In: MSc. Thesis Ben-Gurion University of the Negev, Israel.
- Parkhurst, D.L., and Appelo, C.A.J., 2013, Description of input and examples for PHREEQC version 3--A computer program for speciation, batch-reaction, one-dimensional transport, and inverse geochemical calculations: U.S. Geological Survey Techniques and Methods, book 6, chap. A43, 497 p., available only at <http://pubs.usgs.gov/tm/06/a43>.
- Sneh, A., Bartov, Y., Weissbrod, T. and Rosensaft, M., (1998). Geological Map of Israel, 1:200,000. Isr. Geol. Surv. (4 sheets).
- Weinberger, G., Livshitz, Y., Givati, A., Zilberbrand, M., Tal, A., Weiss, M., and Zurieli, A. (2012). The natural water resources between the Mediterranean Sea and the Jordan River. Hidrological Service of Israel.

Development of a Textile Reinforced Pipe System with Integrated Monitoring Function

Yiska GOLDFELD^{1*}, Gali PERRY¹, Gözdem DITTEL² and Thomas GRIES²

¹Faculty of Civil and Environmental Engineering, Technion - Israel Institute of Technology, Haifa 32000, Israel

²Institut fuer Textiltechnik of RWTH Aachen University, Otto-Blumenthal-Strasse 1, 52074 Aachen, Germany

*Corresponding author's e-mail: yiska@technion.ac.il

ABSTRACT

The study aims to develop a smart self-sensory textile reinforced concrete (TRC) pipe system that has capabilities to provide an early detection of water leakage and water infiltration through cracked and damaged zones. The proposed smart-sensory system is integrated into the reinforcement system and thus can overcome some of the drawbacks of traditional sensory systems that are inherently separated from the structural system. Therefore, the current study aims to prove the feasibility of the smart pipe system by developing, designing, constructing and analyzing a hybrid pipe made of textile reinforced concrete. The paper outlines the necessary steps to accomplish this goal by summarizing the experimental and theoretical investigations conducted at the Technion and at RWTH Aachen University during the first two years of the project, and by presenting the next steps to be taken by the two groups.

KEYWORDS

Smart pipe system; Water leakage detection; Self-sensory system; Textile reinforced concrete.

INTRODUCTION

A multi-functional intelligent water delivery system is a key component of a modern and sustainable built environment. Sustainability requirements such as the demand for a significant reduction in the consumption of natural resources and inadequacy of the water distribution through such systems motivate the development of effective, safe, lightweight and economical pipe systems with advanced monitoring techniques. The proposed study offers to handle this challenge by developing hybrid water pipe element which is a unique infrastructural configuration by saving up to 50 % of the materials and components weight and offering an integrated monitoring function that can early detect water infiltration. Compared to conventional building materials, the proposed TRC pipe is lighter, stronger, more durable and less affected by corrosion. Furthermore, the integrative nature of the proposed sensory system can overcome some drawbacks of the traditional sensory systems that are inherently separated from the structural system (Capadevila et al. 2011, Liu et al. 2013). These conclude to savings in production, transportation, installation and maintenance and address the major challenges of water loss in transport systems and ecological alternatives for building materials. The proposed self-sensory system continues to function also in scenarios of progressive failure mechanism where traditional sensing devices usually failed to produce meaningful information. This is crucial in cases of water pipe systems that have limited accessibility such as underground water pipe systems. In such cases, it is important to have a reliable estimation of the magnitude of the water infiltration and as result to estimate the amount of water loss from the time it is detected till the time it is corrected. To realize the concept, the investigation considers various aspects related to design and production of the smart TRC pipe. This paper addresses the aspects achieved so far and presents the missions that should be completed in order to prove the feasibility of the Smart Pipe concept.

SELF-SENSORY TEXTILE

For the development of the Smart-TRC pipe system, the chosen reinforcement materials consist of two types of rovings: rovings made of AR-glass fibers and rovings made of carbon fibers, material properties are given in Quadflieg et al. (2017) and Dittel et al. (2019).

In this configuration, the main reinforcement is the AR-glass rovings, which is electrically isolating, and sensory carbon rovings are replacing two adjacent AR-glass rovings in the perpendicular direction. The carbon rovings are part of the reinforcement system and, by taking advantage of their electrical conductivity, they also serve as the sensory agents. Therefore, the position and configuration of the carbon rovings along the TRC element should answer both purposes. Due to their advanced mechanical properties they should be positioned in accordance to the direction of the tensile stress, which is perpendicular to the potential cracked surface. Its exact optimal orientation is, therefore, dependent on the geometry of the structural elements, the boundary conditions and the loading scheme. Accordingly, in case of pipe system the carbon rovings should be positioned along the circumferential direction.

The implementation of the sensory carbon rovings within the textile mesh is performed as an integrated part of the production process. Therefore, the cost associated with converting the textile into a self-sensory one is not expected to be a significant factor.

SENSORY CONCEPT

Infiltration of water occurs at cracked and damaged zones along the pipe. In such scenarios the carbon rovings are exposed to water which influences the electrical properties of the electrical circuit built up by the carbon rovings. Several sensing concepts were investigated as part of the current project, Goldfeld and Perry (2018a, 2018b), and it was found that a consistent and clear electrical reading is obtained if two adjacent carbon rovings are electrically linked due to infiltration of water. A schematic layout of the chosen electrical setup is illustrated in Fig. 1. One end of each carbon roving is connected to one of the terminals of the AC power source. Due to wetting, the electrical characterization is altered, and a pronounced and sensitive electrical reading is obtained. One of the advantages of the chosen sensing concept is that only one end of each roving is connected to the DAQ which simplifies the installation of the electrical connection. The proposed electrical connection will be water resistance t (IP 67) that can be easily connected to the DAQ system. It will be integrated before casting the pipe and considered in the design of the special mold.

Restricting the electrical terminals to one end of the rovings limits the sensing capacities to an integrative mode, and accordingly limits the system to identifying wetting events without the ability to identify the exact location of the event along the roving. Segmentation of the monitoring system can overcome this obstacle and is particularly relevant to pipeline applications in which precast elements are placed head to tail, yielding a system that is segmented by nature. In such applications, the sensing concept aims to detect the wetting and the severity of the infiltration but is not designated to pinpoint the exact location of the event within the segment. Since carbon rovings are an integrated part of the structural system, they continue to function also in scenarios of progressive failure mechanism, which is crucial in case of water pipe systems. Furthermore, such a hybrid system that continues to function, structurally and sensory, can be corrected and fixed and it is not necessitated to replace the damaged segment.

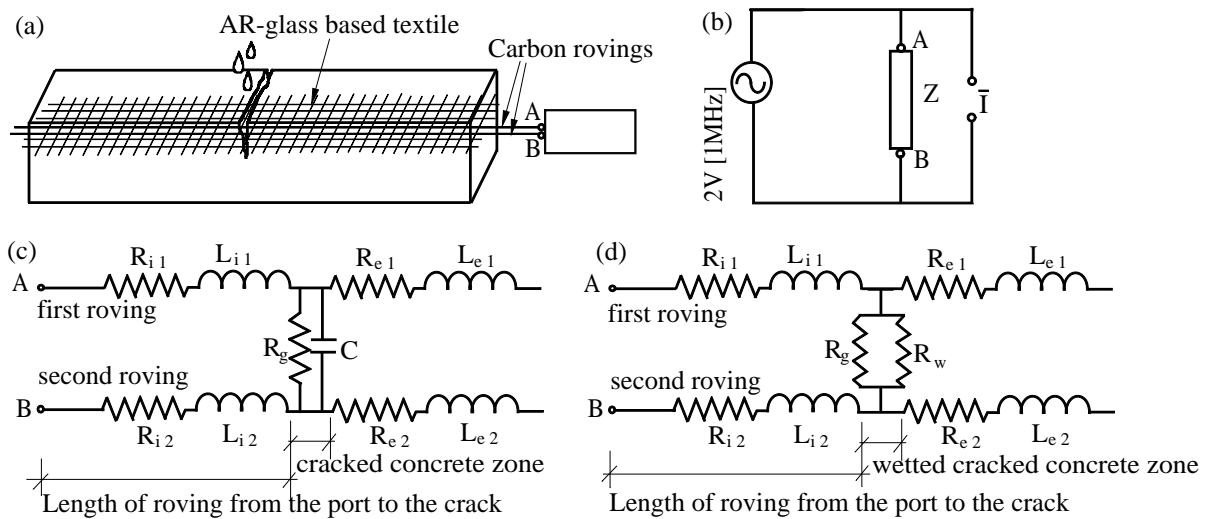


Figure 1: (a) Schematic layout of wetting event; (b) electrical setup of AC circuit; (c) electrical circuit at dry position; (d) electrical circuit at the wetting event, Perry et al. (2019b)

OPTIMAL TEXTILE CONFIGURATION

In order to develop a smart TRC pipe element, the chosen self-sensory textile reinforcement should meet two requirements at once, as the reinforcement system as well as the sensory one. Therefore, the chosen textile configuration should yield an advanced structural performance with the capability to sense and distinguish between the magnitude of the water leakage. The goal is to find the optimal textile configuration with respect to the two requirements.

Structural performance

The structural response of TRC systems is significantly influenced by the micro-structural mechanism and particularly by the bonding mechanism of the rovings and the cementitious matrix, e.g. Peled et al. 2017. Since each roving consists of thousands of tightly packed filaments, the cementitious matrix does not penetrate into the entire roving cross-section. Only filaments located along the interphase with the concrete matrix (called the sleeve filaments) are bonded to the concrete matrix, while filaments within the core of the roving are almost isolated from the concrete body. Accordingly, the sleeve filaments transfer the tensile load by adhesion shear stress and tend to break due to cracking, while the core filaments transfer the load by friction, which is much lower than adhesion and characterized by delayed activation. At progressive damage scenarios, the core filaments tend to pull-out rather than to break. Therefore, in order to increase the ultimate load and improve the structural performance, it is desired to improve the bond between the core and the sleeve filaments and to increase the volume fraction of the sleeve filaments, for example, by using different binding procedure (Hegger et al. 2006), applying pre-treatment procedure such as coating (Gao et al. 2007), or improving the penetrability of the cementitious matrix (Brockmann 2007). In order to further improve the structural performance, the current study investigates the mutual effects of binding and coating (Perry et al. 2019a). Summary of the averaged structural response of representative TRC beams under flexural loading is presented in Fig. 2a. It is demonstrated that the effect of the type of binding is most pronounced in uncoated textile, in such a case, textiles with relatively flat cross-section are preferable. While, in case of coating, relatively more circular cross-sections yield an improved structural response. Therefore, from a structural point of view, coated Counterlaid-Tricot textile is a preferable configuration.

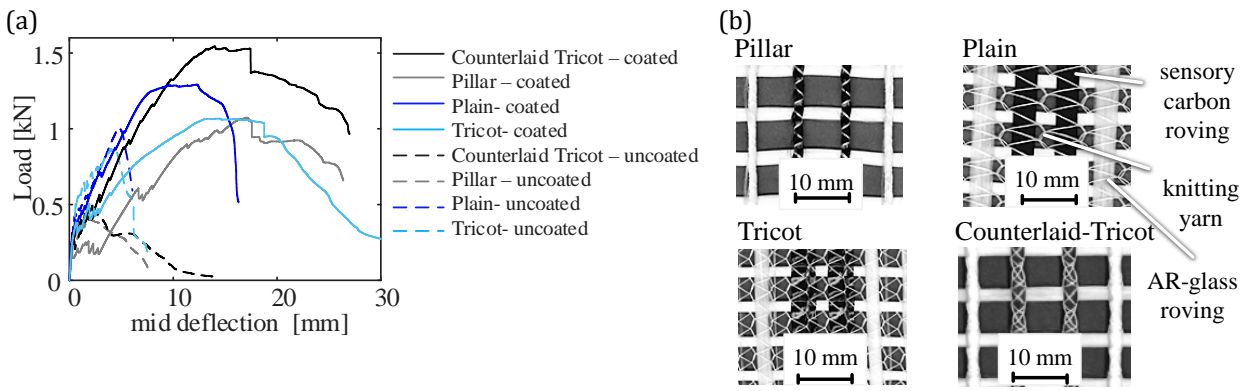


Figure 2: (a) Averaged Load-deflection curves, Perry et al. (2019a); (b) Pictures of the different textile configurations, Dittel et al. (2019).

Sensory capabilities

The chosen textile configuration should also adjust the requirement of the self-sensory system. The goal is to investigate the capabilities of the various textile configurations to detect and mainly distinguish between the magnitude of water infiltration through cracked zones, which is associated to the severity of the cracking. The hypothesis is that the micro-structural mechanism is also reflected by the sensitivity of the measured electrical signal. The study focused on two types of textile binding as representative cross-sectional roving shapes, Counterlaid-Tricot and Plain. Each type was investigated in uncoated and coated configurations. Eight TRC beam samples were casted and mechanically loaded up to cracking. The cracked zones were monitored, and each zone was separately examined by performing a wetting event, Perry et al. (2019b). Representative results are given in Fig. 3. It is demonstrated that the type of binding and coating, which significantly affect the structural response, reflect and affect the measured electrical signal. It is found that there is a trade-off mechanism between the structural response and the sensory capabilities. While coating or special type of binding may improve the structural performance, they can lead to a limited sensory capability to distinguish between the magnitude of the water infiltration.

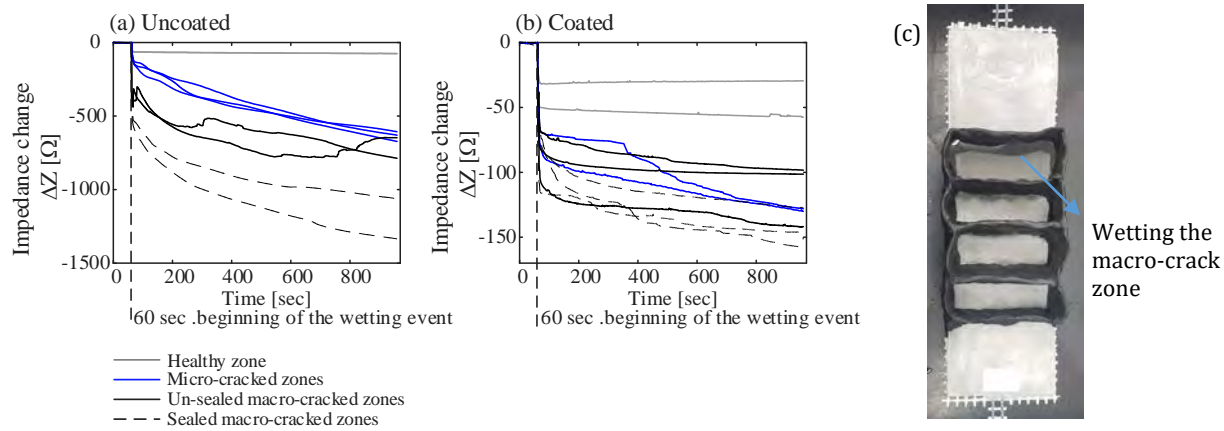


Figure 3: Impedance change due to wetting the Counterlaid-Tricot based TRC beams: (a) Uncoated textile; (b) Coated textile; (c) Picture of the wetting event, Perry et al. (2019b).

The observed trade-off mechanism between the structural performance and the sensitivity of the monitoring capabilities, with respect to the textile configuration yields the conclusion that the optimal textile configuration should be determined upon the desired application. With respect to the circular geometrical properties of the pipe the study offers to combine the two requirements by a special filament winding procedure that is proposed in the next section.

DESIGN OF SMART TRC PIPE SYSTEM

In order to realize the Smart Pipe concept, the investigation considers the production feasibility of the pipe and its adjustment to acceptable standards and building codes. It is performed by merging

the structural requirements and the sensory capabilities of the textile with respect to the production feasibility. It involves the following aspects:

Load cases and distribution: The first step of designing the smart TRC pipe considers its adjustment to acceptable standards. Investigation of the load cases associated to the pipe system shows that according to acceptable Israeli, German and European standards (IS 27, DIN V 1201, EN1916, respectively) the major load case that the pipe should be designed for is concentrated compression load at the top of the pipe. Schematic layout of the pipe deformation with respect to the stress and crack distribution is given in Fig. 4a. An advanced structural model of TRC pipe with circular cross-section takes into consideration the nonlinearity of the concrete and the unique micro-structural mechanism of the textile within the cementitious matrix.

Textile geometry and configuration: The study offers a filament winding textile configuration for the TRC pipe. Such a configuration answers both the structural and the sensory requirements. It also eliminates inadequate connections that occurred in case of a biaxial warp knitted textile, which lead to potential weak points (Dittel et al. 2019). Coated AR-glass rovings are placed along the longitudinal direction. AR-glass rovings and a pair of uncoated carbon rovings are wound along the circumferential direction. Schematic demonstration is given in Fig. 4b. This configuration enables to capture the cracking, which according to the design load case are formed parallel to the longitudinal direction and therefore can be detected by the sensory carbon rovings. This configuration will be further investigated both from a practical point of view with regard to the casting capabilities, as well as from a structural performance point of view with respect to the structural analysis.

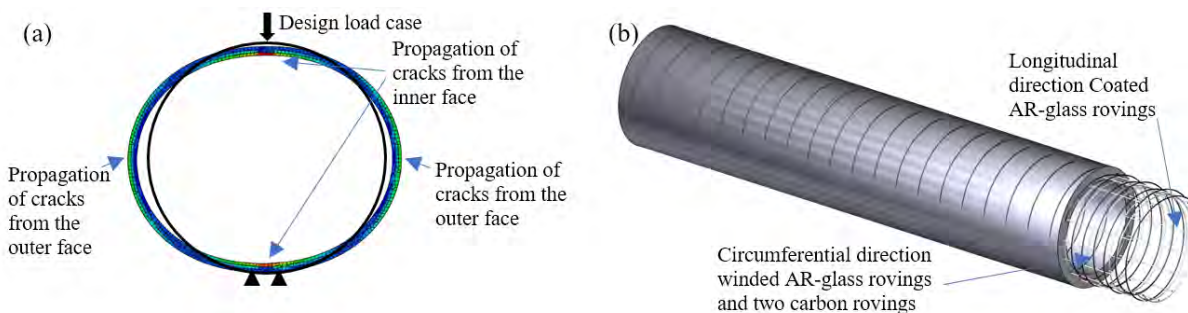


Figure 4: (a) Schematic deformation and stress distribution of pipe model; (b) Schematic layout of TRC pipe.

Concreting method: Two concrete mixtures are found to be suitable for smart thin-walled TRC production: a commercial grout mixture, Sika Grout 214, and a special mixture developed by Brockman (2007). The tensile (7.5-10 MPa) and compression (70-75 MPa) strength, of both mixtures, are suitable for the structural requirements and the maximum size of the aggregate suits to the properties of the textile mesh. In order to allow fast production process, to eliminate phenomena of water blinding and to obtain suitable concrete flow through the mesh and along the pipe, the mixture was adjusted with 2.35 liters of water per 25 kg of dry material. It will be further adjusted during the production of a prototype smart pipe.

A special multi-parts mold is designed in order to construct the TRC pipe, which considers the positioning of the reinforcement rovings within the pipe according to the proposed filament winding configuration, the production process and the electrical connection.

SUMMARY AND CONCLUSIONS

The current paper outlined the various aspects related to the development of the Smart Pipe concept, among them: the sensory concept; the optimal textile configuration with respect to the structural and sensory requirements; the development of the filament winding concept for the smart TRC pipe; the adjustment of the design to acceptable design standards; and the concreting and production feasibilities. The promising results presented in this paper, and the goals that are considered for the coming year prove the feasibility of the smart pipe concept that enable to further bring the concept into realization.

ACKNOWLEDGEMENT

The research is funded by the BMBF – MOST Joint German-Israeli Water Technology Research Program, Grant No. WT1602/02WIL1452. Ms. Perry would like to acknowledge the support of the Young Scientists Exchange Program (YSEP) of the BMBF – MOST Cooperation in Water Technology Research. The authors are also grateful for the help of Eng. Barak Ofir, Mr. Elhanan Yitzhak, and the staff of the National Building Research Institute, and of the students, technical and administrative staff of ITA-RWTH Aachen University.

REFERENCES

- Brockmann, T., (2007) "Mechanical and fracture mechanical properties of fine-grained concrete for TRC structures" In Advances in Construction Materials, Gross, C. U. (ed.), pp. 119-129. Springer, Berlin.
- Capadevila, S., Roqueta, G., Guardiola, M., Jofre, L., Romeu, J., and Bolomey, J. Ch. (2011) "Water infiltration Detection in Civil Engineering Structures Using RFID" Proceedings of the 6th European Conference on Antennas and Propagation (EUCAP), pp. 2505-2509, 2011
- Dittel, G., Heins, K., Gries, T. (2019) "Development and design of smart textile reinforcement for concrete pipes", Proceedings of the ACI Convention, Ohio, USA, October 20-24, 2019, to be presented.
- Gao, S.L., Mäder, E. and Plonka, R., (2007) "Nanostructured coatings of glass fibers: improvement of alkali resistance and mechanical properties", *Acta Materialia*, 55(3):1043-1052.
- Goldfeld Y. and Perry, G. (2018a) "Electrical characterization of smart sensory system using carbon based textile reinforced concrete for leakage detection", *Materials and Structures*, Vol. 51, No. 17, pp. 1-17.
- Goldfeld Y. and Perry, G. (2018b) "A-R Glass/Carbon-Based Textile Reinforced Concrete Elements for Detection Water Infiltration within Cracked Zones", *Structural Health Monitoring*, DOI: 10.1177/1475921718808223.
- Hegger, J., Will, N., Bruckermann, O. and Voss, S. (2006) "Load-bearing behaviour and simulation of textile reinforced concrete", *Materials and Structures*; 39(8):765-776.
- Liu, T., Huang, Y., Zou, D., Teng, J. and Li, B. (2013) "Exploratory study on water seepage monitoring of concrete structures using piezoceramic based smart aggregates", *Smart Materials and Structures*, 22:8.
- Peled, A., Bentur, A. and Mobasher, B. (2017) "Textile Reinforced Concrete", CRC Press Taylor and Francis Group.
- Perry, G., Dittel, G., Gries, T. and Goldfeld, Y. (2019a) "Mutual Effect of Textile Binding and Coating on The Structural Performance of TRC Beams", submitted for publication.
- Perry, G., Dittel, G., Gries, T. and Goldfeld, Y. (2019b) "The Effect of Textile Configuration on the Monitoring Capabilities of Smart Carbon-based TRC elements to detect water infiltration", submitted for publication.
- Quadflieg, T., Goldfeld, Y., Dittel, D., Gries, T. (2017) "New Age Advanced Smart Water Pipe Systems Using Textile Reinforced Concrete", 15th Global Conference on Sustainable Manufacturing, Technion-IIT, Haifa, Israel, September 25-27, 201

Nanomembranes for Cost-Effective Hybrid Desalination-Filtration of Wastewater

Doron AURBACH^{1*}, Eran AVRAHAM¹, Markus KLAPPER^{2*}, Nicole WUTKE², Armin GÖLZHÄUSER^{3*}, Andre BEYER³, Albert SCHNIEDERS^{4*}

¹ Bar-Ilan University, Department of Chemistry, IL-52900 Ramat-Gan

² Max Planck Institute for Polymer Research, Ackermannweg 10, D-55128 Mainz

³ University of Bielefeld, Universitätsstraße 25, D-33615 Bielefeld

⁴ CNM Technologies GmbH, Morgenbreede 1, D-33615 Bielefeld

*Corresponding authors e-mail: aurbach@mail.biu.ac.il, klapper@mpip-mainz.mpg.de, ag@uni-bielefeld.de, albert.schnieders@cnm-technologies.com,

ABSTRACT

Our joint work aims to provide an improved and efficient treatment of brackish water and wastewater using carbon nanomembrane (CNM) multilayer electrodes, to meet increasing regulations governing the allowable levels of total dissolved solids (TDS) and suspended solid particles (SSP) in potable water, and assessing the potential reduction in initial capital investment as well as the estimation of operating costs of wastewater treatment.

Suggested herein is an innovative route for brackish and wastewater purification technology by using ultrathin (1 – 3 nm), mechanically robust, large area CNMs with tailored pore sizes and surface charges for efficient and cost-effective removal of salt and solid suspended particles from brine feed resources. In this project, we tailor CNM multilayers with and without surface functionalization as electrodes (German partners) for the Capacitive Deionization (CDI) process to maximize the efficiency of the water purification technology (Israeli partner). In addition, an innovative low energy-hybrid approach for CDI-filtration, a one-step process for wastewater treatment, is proposed, taking advantage of the fast transport and surface area properties of the tailored CNM multilayers.

KEYWORDS

Water technology, carbon nanomembranes, ballistic transport, desalination, osmosis

INTRODUCTION

Fresh water is limited in Israel and therefore desalinated brackish water sources are used for the water supply (Glueckstern 2000). The total production of desalinated water from brackish sources is currently 30 million cubic meter (MCM/year), and planned production is expected to reach 80-90 MCM/year by the year 2020 (Glueckstern, 2000). Thus far, thermal distillation (Rifert, 1990), membrane separation, reverse osmosis (RO; Lee, 2011), microfiltration systems (MFS; Saboyainsta, 2000), electrodialysis (ED; Xu, 2008) are the most common desalination processes. Although these processes can achieve high salt removal, they have several major disadvantages including high energy consumption, high maintenance costs, and equipment fouling problems.

Due to the increasing population of Israel and due to intensive agriculture (especially: watering of fields), re-use of wastewater (either for re-circulating or as potable water) is necessary (Friedler, 2001), and this cannot be done solely by desalination process and a filtration pre-treatment step is required. Consequently, a new technology for water purification of brackish and wastewater is needed to satisfy the increasing water demand of the country. For this purpose, the development of a technology with novel separation functions is a key objective, as the above-mentioned methods are costly and have equipment-fouling problems. Recently, Capacitive Deionization (CDI) was developed and this process opens new avenues for water purification (Suss, 2015). CDI is an electrochemically controlled desalination technology that removes ions from salt water by electro-

sorption via a two-step, non-faradaic process occurring in the electrical double layer region (Grahame, 1947). During the CDI process, ions in the feed water flowing through a spacer between the cathode and the anode are removed by electrostatic attraction. Subsequently, when the electrodes are short-circuited (regenerated), the adsorbed ions are released from the electrodes. Beside this self-cleaning ability of its surfaces, CDI is reported to have many environmental and energy consumption advantages over thermal distillation desalination and membrane separation desalination methods because CDI does not require chemical treatment to regenerate membranes nor high pressure for water recovery (Porada 2013). Activated Carbon (AC) has been the most widely employed material for CDI electrodes (Noked 2011). The high surface area of AC is mostly governed by the presence of micropores (<2nm).

MATERIALS AND METHODS

A promising approach to fabricate functional carbon membranes with well-defined pores, is to exploit the self-assembly of molecules. Self-assembled monolayers (SAMs) can be created from amphiphilic aromatic molecules. These SAMs can be crosslinked via electron-beam or EUV-photon irradiation and thus transformed into CNMs (Figure 1) (Eck, 2005; Nottbohm, 2008). Multilayers of such CNMs can be prepared as well. By pyrolysis, it is possible to turn CNMs into nanocrystalline graphene maintaining properties like carbon density and porosity. Due to the atomic thinness of graphene and CNMs, we observe a fast water transport of components permeating through nanomembranes (Yang, 2018) instead of a solution-diffusion transport as in conventional membranes. This means that there will be no collision of molecules with the pore wall during the permeation through a pore, just size exclusion at the pore entrance (Turchanin, 2016) and single-file motion (Yang, 2018).

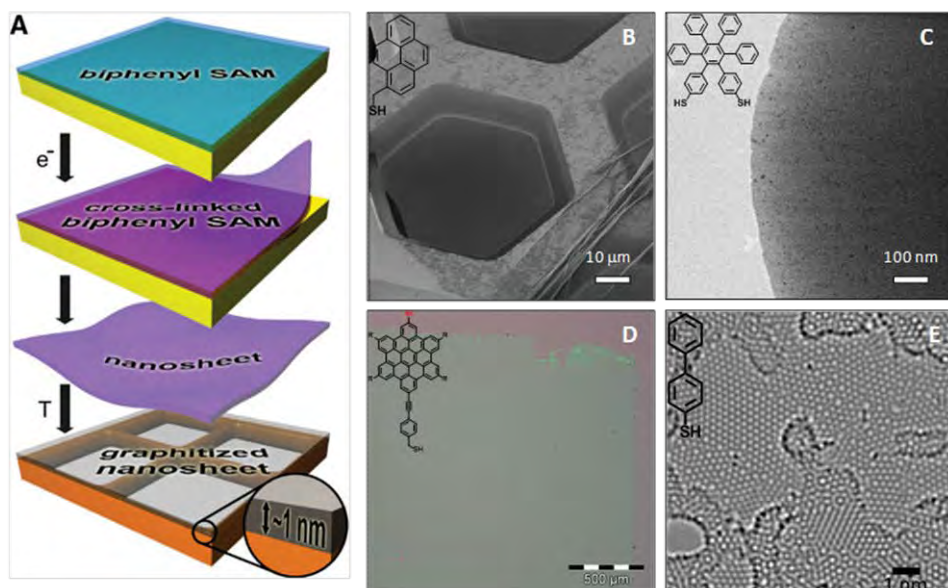


Figure 1: (A) Schematic illustration of carbon nanomembrane (CNM) fabrication (Turchanin, 2011). (B)-(C) Helium ion microscopy (HIM) images of free-standing CNMs. (D) Optical image of a CNM transferred to a SiO₂-surface. (E) HR-TEM image of pyrolyzed CNM (Angelova, 2013).

Cost effective brackish water desalination with conventional CDI

The engineering of 2D ultrathin (0.5 – 3 nm), mechanically robust, large area multilayer carbon nanomembranes (CNMs) or graphene to function as electrode materials in the conventional CDI process can be very attractive for water desalination. These materials not only preserve desirable high surface area along with excellent electric conductivity and chemical tolerance, but also the in-plane nanopores shorten the permeation paths of ions between the layers, as the mechanism changes from a solution-diffusion transport to a ballistic transport and thus, significantly enhance CDI performance (Figure 2). Furthermore, the incorporation of nitrogen in the CNMs can enhance electrosorption by electrodes. The assembly of CNM materials with defined pore size and pore distribution is a key factor in this proposed joint research.

Approach 1: Removal of salt by CDI

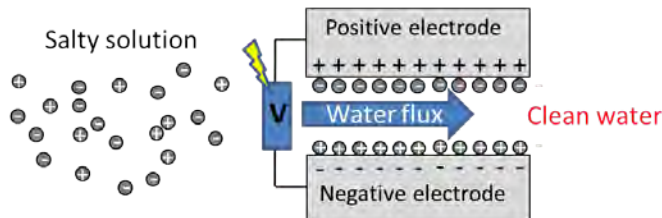


Figure 2: Schematic illustration for conventional CDI.

The joined project is divided in work packages that strongly depend on each other. MPIP synthesized linear polyaromatic thiols with different end functionalization. We wanted to compare the properties of the corresponding CNM to each other, as the Bielefeld and CNM Technologies team observed that terphenyl structures seem to result in more stable and dense CNMs than biphenyls. Furthermore, MPIP synthesized biphenyl thiols with alkene and alkyne functions to investigate the influence of additional electrons in the structures on the crosslinking of SAMs (self-assembled monolayers). The amine functionalized biphenyl thiol was synthesized as well, to investigate the influence of heteroatoms on the filtration properties of the CNMs denoted as (NBPT - nitro-biphenyl-4-thiol). However, in terms of filtration capabilities, NBPT- CNM shows the best results (provided in figure 3) and all the following results (including integrated membrane) through this report, stands for NBPT-CNM

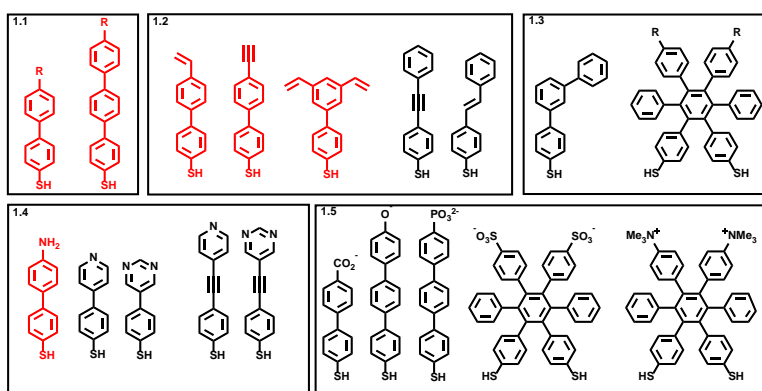


Figure 3: Structures of the synthesized (red) and planned (black) precursor molecules

The main benefit that is associated with nanofiltration is that high retention of micro-solutes can be attained under much lower pressures compared to reverse osmosis. However, implementation of nanofiltration in industry is limited because its low to moderate retention of monovalent ions. Within the frame of this joint proposal, we present a new thinking of a new design of bifunctional membrane. German and Israeli Partners developed a jointly am multilayer setup of the membrane. The bifunctional membrane consists of 3 layers, where at first CNM is transferred on top of a commercial UF membrane (German partners) providing filtration capabilities, following by deposition ("direct transfer") of highly porous carbonaceous material on the bottom side of the UF membrane (Israeli partners) providing monovalent ion capturing, thus retention of micro solutes

and dissolved solutes can be attained, yet applying low pressures, part of the energy in the process can be recovered.

A variety of carbonaceous materials were evaluated considering the following: The electrode should sustain high current densities in order to cope with the high permeability of the CNM; Good adhesion between the electrode material and the UF membrane should be provided and the electrode material should possess relatively high capacitance in order to alleviate the number of discharge cycles along the process.

The Bar-Ilan group constructed a first cell for the investigation of the membranes from CNM technologies. The Integrated membrane is assembled in the 3-electrode filtration cell (A full description of the setup and cell components is provided in Figure 4). A synthetic solution containing SP (PEG 400) and DS (NaCl , 500ppm) is admitted to the filtration cell.

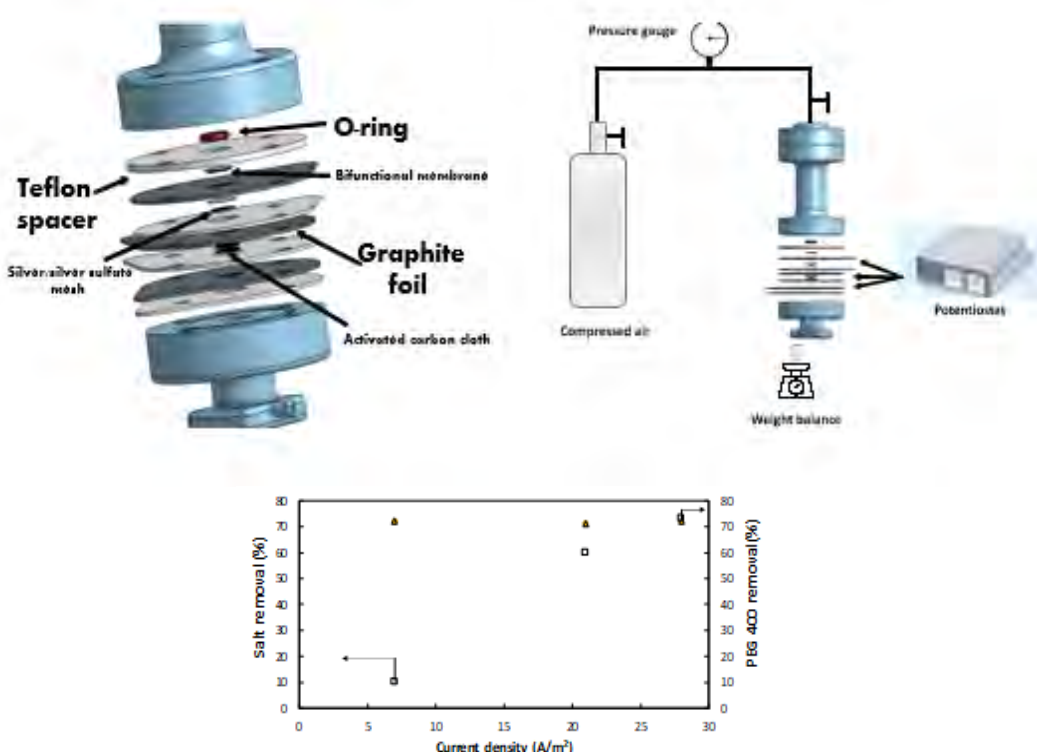


Figure 4: Illustration of 3 electrode cell dead end filtration set up and components and Salt removal rates and SP(PEG 400) retention rates at various current densities and constant applied pressure of 1.2 bar

Two parameters are considered; Pressure application (correlated with the permeate flux) and the current applied to the integrated membrane. physical and electrochemical characteristics of the activated carbon cloth electrode including the imaging of the integrated membrane are presented. For example, a retention of 80% of NaCl (feed solution 500ppm) and >70% of PEG 400 are demonstrated when the current density and the pressure were 30 A/m² and 1.7 bar (corresponds to about 120 LMH) correspondingly. Comparable experiments with feed solution containing 1000 ppm NaCl with higher current density (~50 A/m², resulted with 60% salt retention (in this case the current exceeds the limit of water discharge). This clearly indicates that with these membranes, salt retention is possible and the proof of concept achieved.

In the second part of this joint project, a new concept of combined oxidation and filtration was demonstrated. We explore a new integrated membrane design for combined secondary wastewater effluent treatment of dual action of membrane separation and advanced oxidation process (AOP) exploiting dissolved oxygen in the water. The bifunctional membrane consisting of CNM layer on top of a commercial ultrafiltration membrane (microlon™), and the bottom layer is a sprayed coated (partially exfoliated) reduced graphene oxide (PE-rGO) thin film.

Partially exfoliated graphene particles were produced via fast exposure of as-prepared GO particles to pre-heated furnace (at 450° C) and consecutively were sprayed coated on the reverse side of the UF membrane support.

The integrated membrane showed pore size cut off value of about 5nm and permeability of about $35 \text{ Lm}^{-1}\text{Hr}^{-1}\text{bar}^{-1}$. Electrochemical measurements demonstrate the catalytic activity of the integrated membrane toward hydrogen peroxide generation with low overpotentials. A synergistic action of electrochemical oxidation by application of cathodic potentials to the integrated membrane concurrently with pressure application was demonstrated using a synthetic solution consisting of Methylene Blue (MB), as the organic micro-pollutant probe and PEG 1000. Degradation of MB (70%) and good rejection (>70%) of suspended particles (<5nm) at pressures lower than 1.5 bar were obtained.

The concept shown opens up new strategies toward more efficient secondary wastewater effluent management and may contribute mitigating the ubiquitous increasing occurrence of micro- and biorecalcitrant contaminants in water environments (see Figure 5).

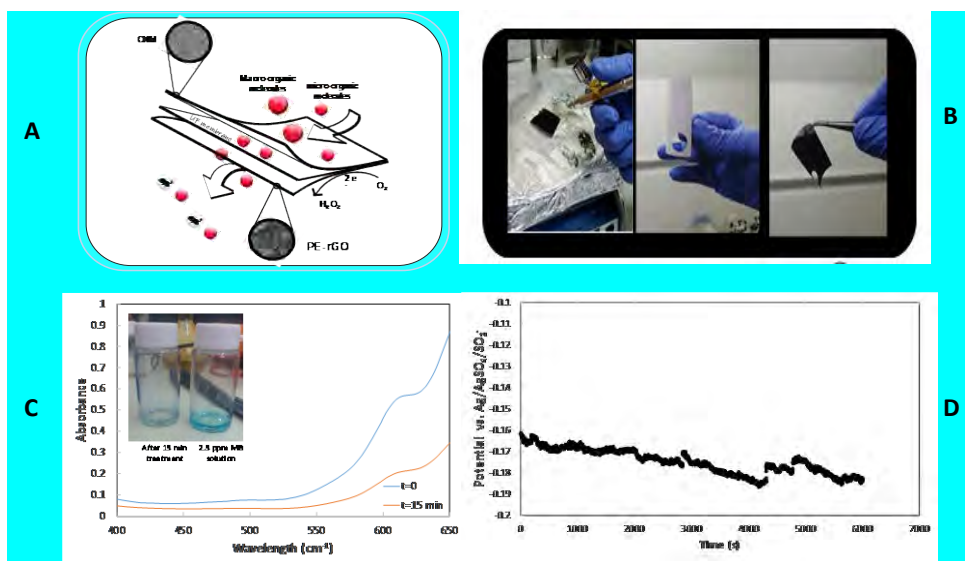


Figure 5: A) Illustration of 3 layered membrane assembly, B) picture of two sides of the integrated membrane, C) degradation at the MB concentration, D) potential- time profile

CONCLUSIONS

We focus on the development of a more energy-efficient water purification and wastewater treatment process, which guarantees the future water supply in Israel based on a versatile and cheap technology. It will allow more extensive watering of agricultural land and increase the yield. We expect that this technology can be used in a decentralized way, as it needs less energy and smaller devices (small membranes, low pressure). Thus, transport of water over long distances to and from treatment facilities will be avoided.

The project aims to provide an innovative large-scale process for water desalination and wastewater treatment. The process should prevail over other conventional processes in terms of operation costs and process complexity, and thus opening new opportunities toward technology exportation to potential companies, for instance, the Israeli manufacturing cooling towers. Such developments are quite complex and require the expertise from organic chemistry, physics, electrochemistry and process development which is perfectly combined in the consortium of the project. A broad variety of precursor molecules, have already been synthesized, used in the layer formation and the most successful systems have been investigated by CNM for upscaling. Bar-Ilan build first cells being suitable for studying the membranes in the filtration process.

Initial results from these measurements have shown the proof of principle, filtration and separation processes could be achieved. In the residual months of the project optimization of the processes will be in the focus. In particular, the control of the quality of the membranes in the nano and sub-nano scale level is challenging. This optimization includes the stability of the membranes but also the control of the pore size and the ion retention behavior. Another focus will be also the development of a stable desalination process considering the electrostatic effects in the cells.

ACKNOWLEDGEMENTS

We thank BMBF and MOST for financial support within the German-Israeli Cooperation in Water Technology Research. We also thank Y. Yang, P. Dementyev, and N. Meyerbröker for fruitful discussions.

REFERENCES

- Angelova, P.; Vieker, H.; Weber, N.-E.; Kurasch, S.; Lorbach, D.; Wunderlich, K.; Reimer, O.; Terfort, A.; Feng, X.; Klapper, M.; Müllen, K.; Kaiser, U.; Gölzhäuser, A. Turchanin; A. (2013). A Universal Scheme to Convert Aromatic Molecular Monolayers into Functional Carbon Nanomembranes. *ACS Nano*, 7, 6489–6497.
- Eck, W.; Küller, A.; Grunze, M.; Völkel, B.; Gölzhäuser, A. (2005). Free-standing nanosheets from cross-linked biphenyl self-assembled monolayers. *Adv. Mat.* 17, 2583–2587.
- Friedler, Eran. (2001). "Water reuse—an integral part of water resources management: Israel as a case study." *Water policy* 3.1. 29-39.
- Glueckstern, P., and M. Priel. (2000). "Desalination of brackish and marginal water sources in Israel—past, present and future." *3rd Israel Desalination Society Conference, Tel-Aviv, Israel*.
- Grahame, David C. (1947). "The electrical double layer and the theory of electrocapillarity." *Chemical reviews* 41.3. 441-501.
- Lee, Kah Peng, Tom C. Arnot, and Davide Mattia. (2011). "A review of reverse osmosis membrane materials for desalination—development to date and future potential." *Journal of Membrane Science* 370.1. 1-22.
- Noked, Malachi, Abraham Soffer, and Doron Aurbach.(2011). "The electrochemistry of activated carbonaceous materials: past, present, and future." *Journal of Solid State Electrochemistry* 15.7-8. 1563-1578.
- Nottbohm, C. T.; Beyer, A.; Sologubenko, A. S.; Ennen, I.; Hütten, A.; Rösner, H.; Eck, W.; Mayer, J.; Gölzhäuser, A. (2008). Novel carbon nanosheets as support for ultrahigh-resolution structural analysis of nanoparticles. *Ultramicroscopy* 108, 885–892.
- Porada, S. (2013)."Review on the science and technology of water desalination by capacitive deionization." *Progress in Materials Science* 58.8. 1388-1442.
- Rifert, V. G., P. A. Barabash, and N. N. Golayad. (1990). *Methods and Processes of Thermal Distillation of Water Solutions for Closed Water Supply Systems*. No. 901249. SAE Technical Paper.
- Saboyainsta, Luciana V., and Jean-Louis Maubois. (2000). "Current developments of microfiltration technology in the dairy industry." *Le Lait* 80.6. 541-553.
- Suss, M. E. (2015). "Water desalination via capacitive deionization: what is it and what can we expect from it?." *Energy & Environmental Science* 8.8. 2296-2319.
- Turchanin, A. Gölzhäuser, A. (2016). Carbon Nanomebranes. *Adv. Mater.*, 28, 6075-6103.
- Turchanin, A.; Weber, D.; Büenfeld, M.; Kisielowski, C.; Fistul, M. V.; Efetov, K. B.; Weimann, T.; Stosch, R.; Mayer, J.; Gölzhäuser, A. (2011). Conversion of Self-Assembled Monolayers into Nanocrystalline Graphene: Structure and Electric Transport. *ACS Nano*, 5, 3896–3904.
- Xu, Tongwen, and Chuanhui Huang. (2008). "Electrodialysis-based separation technologies: A critical review." *AIChE journal* 54.12. 3147-3159.
- Yang,Y.; Dementyev, P.; Biere, N.; Emmrich, D.; Stohmann, P.; Korzetz, R.; Zhang, X.; Beyer, A., Koch, S.; Anselmetti, D.; Gölzhäuser, A. *Rapid Water Permeation Through Carbon Nanomembranes with Sub-Nanometer Channels*, ACS Nano **12**, 4695, 2018.

Closing the Urban Water Loop – Integrated Urban Water and Wastewater Management for Increased Sustainability

Manfred SCHÜTZE¹, Jens ALEX¹, Ofer SNIR², Hagit NETA², Yael GILBOA², Olga VDOV², Michelle PORTMAN² and Eran FRIEDLER²

¹ ifak e.V., Department of Water and Energy, 39106 Magdeburg, Germany

² Technion, Haifa 32000, Israel

*Corresponding author's e-mail: manfred.schuetze@ifak.eu

ABSTRACT

This paper summarises the current state of the CLUWAL project aiming at providing simulation support for holistic water management and, in particular, in assessing the impact of rainwater harvesting and greywater reuse on the entire urban water cycle. Simulation modules within an overall simulation and evaluation framework were developed. Detailed studies on rainwater harvesting potential, based on a stochastic model for rainwater generation and water demand, as well as an in-depth analysis of risks associated to greywater reuse illustrate the application of the CLUWAL methodology. Furthermore, social aspects are considered by experts' interviews and a questionnaire-based survey among water users.

KEYWORDS

Greywater; integrated urban water system model; Life Cycle Assessment; Quantitative Microbial Risk Assessment; rainwater harvesting

INTRODUCTION

Population growth, rising living standards, and urbanisation are placing pressure on available water resources, necessitating new approaches to urban water management to achieve economic, environmental, and social sustainability (Daigger, 2009; Sapkota *et al.*, 2015). Numerous water saving technologies and methods have been developed and applied. However, their application is usually rather fragmented, *i.e.* focusing on individual subsystems of the urban water cycle (*e.g.* wastewater treatment and reuse, rainwater harvesting - RWH, greywater treatment and reuse - GWR), but an integrated approach, analysing their interactions in a broader framework looking both at the water and the wastewater sections of the urban water cycle is yet missing.

The CLUWAL project aims at using water sources within the city in a sustainable manner, by providing methods and tools for the analysis of potential alternative water sources (*e.g.* RWH, stormwater harvesting) and water reuse (*e.g.* treated wastewater and greywater) of different scales in order to increase sustainable urban water management. CLUWAL illustrates the application of the procedures and quantifies the reuse and water saving potentials for case studies of different climates in Israel and Germany, whilst considering, *inter alia*, social and health aspects, thus, the sustainability of these alternatives.

MODELING

In order to simulate and analyse the effects of measures such as RWH and stormwater harvesting and of water reuse (*e.g.* GWR), a modelling framework was developed, allowing to model all related components of the urban water system. Whilst detailed models for individual components do exist (*e.g.* SIMBA#, EPANET, MODFLOW), an overall assessment requires integration of all elements of the urban water system in a convenient way. In order to set up an Integrated Urban Water Model (following the model classification by Bach *et al.*, 2014), modules such as those shown in Fig. 1 were set up. Deliberately, simplified modelling approaches were chosen, in order to allow long-term

simulations and application of methods of systems analysis (*e.g.* Monte-Carlo simulation). Nevertheless, each sub-module can be substituted by more detailed modelling approaches (*e.g.* detailed Activated Sludge Models, hydrodynamic sewer modelling), which can be done within the same modelling framework. As a base for module implementation, the general purpose simulation system Simba# (Ogurek *et al.*, 2015) was chosen. It is characterized by a state-of-the-art graphical user interface, is equipped with state-of-the-art numerical solvers and provides, through its flexible architecture and scripting features, the base for the model developments within this project. Furthermore, it is widely used in environmental engineering research and practice.

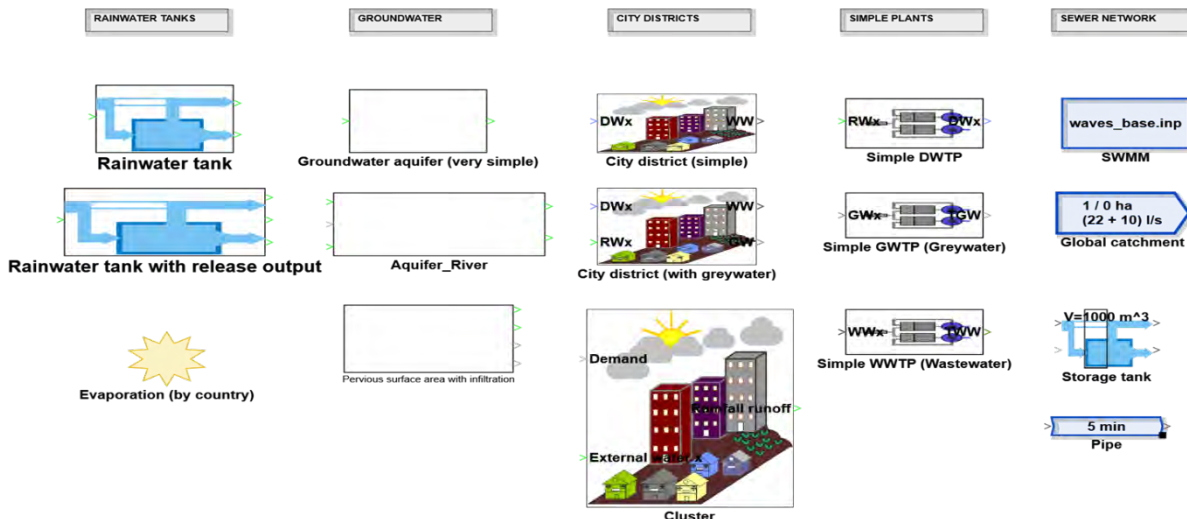


Figure 1: The CLUWAL modelling library (present draft version)

Figure 2 illustrates that, using these blocks, the entire water system can be modelled. These modules were used to simulate RWH strategies and evaluating them according to different criteria, as outlined below. As the interactions of the surface water system with groundwater are of crucial importance on one hand, but detailed groundwater modelling would lead to “getting lost in detail”, a simplified groundwater model was developed, implemented and validated against data from an aquifer in Portugal (Rojas and Schütze, 2018). In order to integrate simulation modelling with evaluation of the water system related to a Life Cycle Assessment (LCA), the modelling blocks are linked to evaluation routines, permitting simulation and LCA-related calculations to be done in a single step. A similar framework such as the one described by Schütze *et al.* (2019) is envisaged.

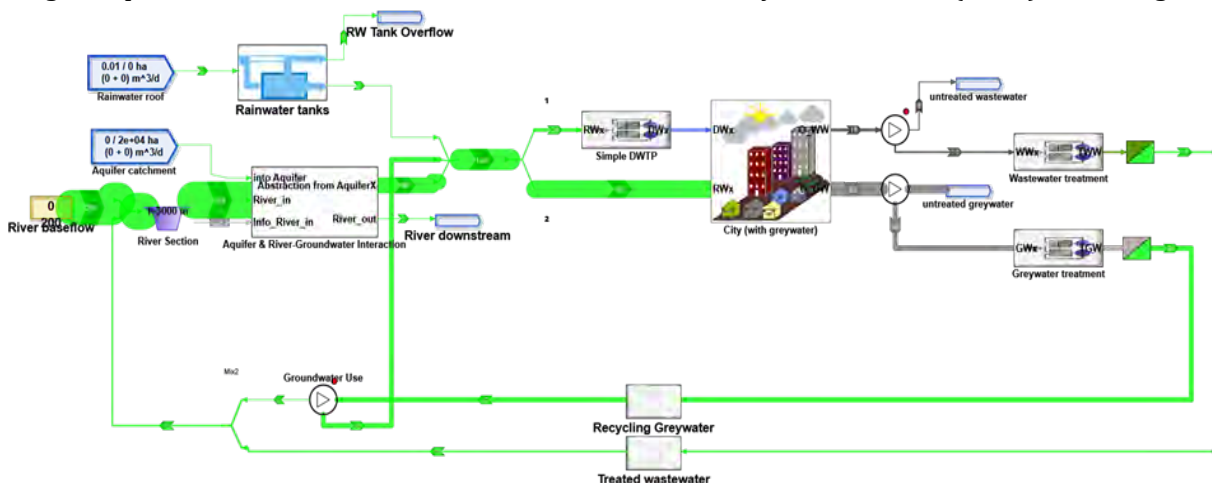


Figure 2: General model of the entire water system using the modules shown in Fig. 1.

RAINWATER HARVESTING (RWH)

RWH practice were studied thoroughly in recent years, as it has the potential to mitigate some of the negative hydrologic effects of urbanisation. RWH as modelled in this research is the collection of

precipitation from rooftops, storing the water and supplying it for on-site toilet flushing. Based on a mass-balance approach, inflows (rainfall), outflows (demand) and overflows to the urban drainage system are calculated for each time step, thus yielding the volume of water available for the next time step. Real rainfall data is used in the developed model as an input either as full season time series or as a single rain event. Demand data is drawn stochastically in two levels: 1) random selection of households to the modelled building; 2) for each household in the building, a random diurnal consumption is drawn from its pool of days. After rainfall is determined for the season and demands are determined for the next day, the mass balance is solved for each time-step. In order to assess the effects of RWH on urban stormwater flows, high temporal resolution was selected (10 min. time-step).

As an example to the system's performance, the simulation was run for 100 randomly selected rain-seasons for a 20 m³ rainwater tank serving a building of 40 apartments with 150 dwellers and roof area of 840 m². Two performance estimators were examined and displayed (fig. 3): Peak overflow reduction in

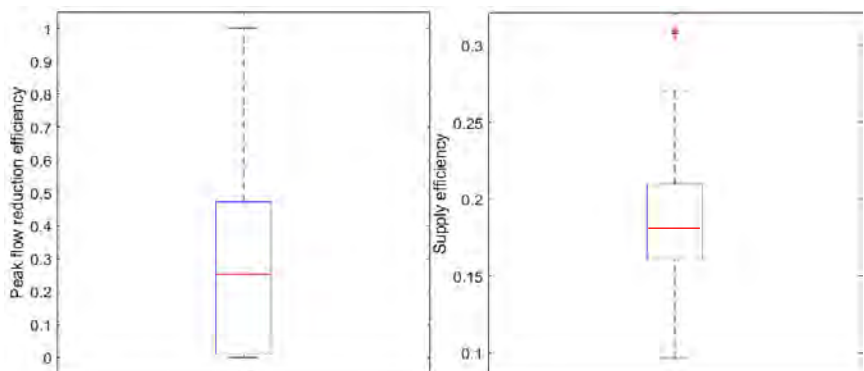


Figure 3: RWH model performance estimators

comparison to the same building without RWH, and supply efficiency (proportion of the total demands supplied by rainwater). For these conditions peak overflows were reduced by 30% (median value), and the RWH system supplied of 18% (median value) of the overall winter toilet flushing demand.

Incorporation of further features to RWH systems could improve its performance in both runoff peak flows reduction and water supply. Modelled features include air-conditioning (A/C) water harvesting, which produce significant amounts of condensed water in the Israeli climate. The model predicts A/C water could supply 8% of the toilet flushing water demand during summer (for the building described above). Another model feature is real-time volume controls, that can control release of water from the tank, when weather forecasts indicate that overflow will occur due to predicted significant rain events (Xu *et al.*, 2018). While reducing supply efficiency from 18% to 14%, this feature could improve peak overflow reduction from 30% to 70% (median values) from the modeled building.

HEALTH CONCERN

Hybrid water systems, comprising of centralized and distributed water infrastructure, contain water streams of different qualities for potable and non-potable uses. A main characteristic of hybrid systems is the use of non-potable water (*e.g.* for garden irrigation and toilet flushing). Toilet flushing, sprinkle irrigation, and some treatment systems, create bio-aerosols that may compromise human health if critical amounts are inhaled, ingested, or come into contact with human skin (Benami *et al.*, 2016; Blanky *et al.*, 2017; Busgang *et al.*, 2018). Therefore, implantation of hybrid systems bears possible long-term health risks under normal operation and higher short-term ones due to malfunction of the system's elements. Quantitative microbial risk assessment (QMRA) is a methodology for predicting health risks associated with waterborne pathogens (Haas *et al.*, 1999). In the present study, several exposure scenarios to reclaimed GW and rainwater were explored. The QMRA model developed is fully stochastic, where all parameters in all scenarios, for each event, were drawn from distributions taken from the literature.

Results, as expected, show that untreated reclaimed water in most scenarios exceeded the maximum acceptable risk level set by the WHO. Nevertheless, by exercising minimal precaution measures (*e.g.* hand washing), illness probabilities are significantly reduced. Moreover, using alternative water sources (*i.e.* GW or rainwater) after treatment dramatically reduces illness probability.

An example of annual illness probabilities vs. pathogen concentrations and ingested volume is presented in Fig. 4. The plot presents tolerable annual probability of illness (P_{max}), results for raw and treated GW (prior to disinfection), and contour lines depict plains of theoretical annual probability, where each line represents a different number of events (n) per year.

Integration between Life Cycle Assessment (LCA) and the QMRA is currently being performed. This will provide a new angle to the overall sustainability assessment tool by adding human health issues (related to waterborne diseases) not yet available in LCA.

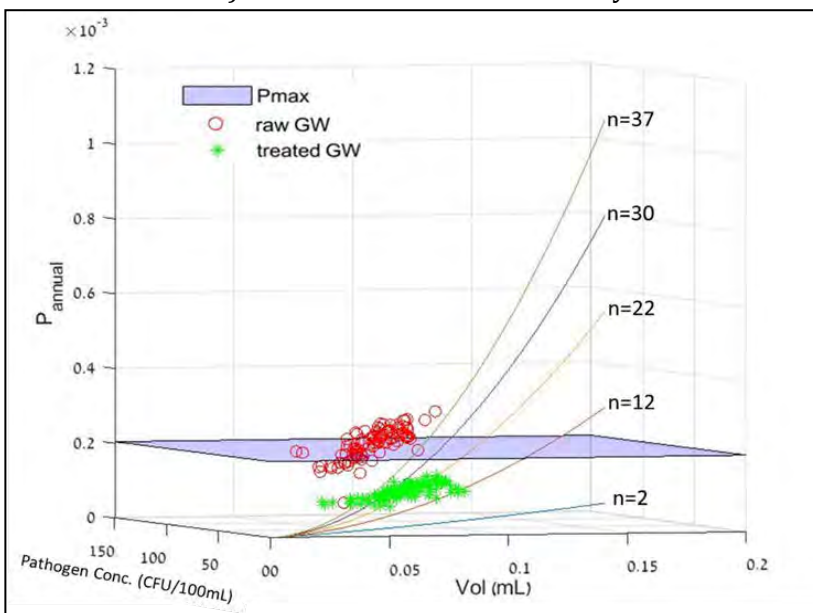


Figure 4: Annual illness probabilities (P_{annual}) from garden work and lounging due to reusing GW containing *Salmonella* s.p. as a function of pathogen concentration (PC) and volume.
Red circles - raw GW, green stars - treated GW, P_{max} - maximum tolerable annual probability. Contour lines - theoretical annual probability plains calculated by multiplying the entire PC range with entire volume range (as opposed to drawing random values)

SOCIAL SUSTAINABILITY EVALUATION

Social sustainability, or more precisely termed as socio-economic evaluation, identified two broad categories of relevant literature. The first deals with perception studies, particularly those related to the adoption of new practices and technologies in the realm of water use. The second deals with mixed methods in social science research, particularly focusing on distinguishing between perceptions, attitudes and behaviours and how these can be examined and explored with regard to the adoption of environmental technologies and practices. The work required to perform the socio-economic evaluation consists of two steps: a) in-depth semi-structured interviews with key informants (experts); and b) a questionnaire administered to at least 300 households, targeted at GWR systems and RWH end-users. The first, consisting of in-depth open-ended interview responses, provides the basis for development of the second questionnaire. The interviewed experts are familiar with urban water use and management in Israel and are from the private, public and academic sectors.

Interviews were analysed using thematic analysis; key ideas, concepts and themes were gathered from reviewing the interview transcripts in a systematic way and divided into major open (not pre-set) code categories (Gibbs, 2008). Three major "codes" or themes that emerge from the responses so far are: importance of reuse opportunities within the water provision system; centralised vs. decentralised practices and reuse opportunities; reliance on public sector action / responsibility. Thus, the potential end-user questionnaire will include five sections. The first will ask for general demographic information about the respondent. Sections 2-4 will cover the above-mentioned themes. The 1st (Sec. 2) will be addressed with questions indicating the respondents' level of concern for water conservation (WC) and WC practices on a sliding scale (highly agree to highly disagree). Example questions are: I am deeply concerned about near-future water shortages in my city; I am more concerned about drinking water shortages than about shortages in irrigation water. The 2nd theme (Sec. 3) seeks to clarify preferences regarding systems' set-up from a

logistical/technical standpoint, particularly whether systems will be individually, locally, municipally, or regionally operated / owned. In this section, questions are asked about potential uses of greywater and collected rainwater (for what household uses, *e.g.*, flushing toilets, washing cars). Many of these questions will be based on previous work done by Friedler (2008) and Opher and Friedler (2016). Under the 3rd theme (Sec. 4), which was discovered as crucial in the open-ended expert interviews, questions will be asked about the level of trust that potential end-users place in the ability of the government (local, regional or national) to ensure proper functioning of decentralised technologies. The last section will cover willingness-to-pay (WTP) and a relatively new concept – willingness-to-avert (WTA) – which will establish the value of the two practices dealt with in this study based on a monetary figure. It is possible that this section will also use a pairwise comparison method (as typical in multi-criteria decision analysis or what is known as AHP (Malczewski, 2006; Patton, 2015; Portman *et al.*, 2016)) using three criteria: compliance and enforcement, cost and convenience (logistics) and health risks. This will then be fed into the LCA to be conducted in other parts of CLUWAL.

WTP is an accepted method of studying the importance users place on environmental practices and innovations. It has been used in numerous studies regarding myriad resources employing complex (*e.g.*, Roder *et al.*, 2019) to simplistic survey (*e.g.*, Farrugia, 2017) and analysis techniques. In this study, as WTP is only a small component of the survey, a more simplistic approach will be applied, however, while we ask about WTP for GWR and RWH, a unique aspect will be questions about WTA. While the WTP approach for valuation has been applied to averting water related to floods (*e.g.*, Roder *et al.*, 2019), it has not been explored with regard to averting GWR and RWH. Questions in this last part will include: What would be the most you would be willing to pay for a properly functioning GWR system in your home / community (range offered)? If you could save 50% on your current water bill, what would you be willing to pay for a properly functioning GWR system in your home or community? Comparable questions will be asked on RWH systems and some questions about WTA of these practices (GWR & RWH) will also be included. Overall, in addition to feeding other parts of the research, questionnaires will be used to determine stakeholder preferences for adoption of different GWR and RWH use practices and will contribute in this way to the overall literature regarding stakeholder adoption of water reuse practices (*e.g.*, Inbar, 2015, Bakare *et al.*, 2016, Mankad *et al.*, 2019).

INTEGRATION AND CASE STUDIES (Kfar Saba, Israel)

To estimate effects on urban drainage systems, a district of Kfar Saba city was hydrologically modelled in EPA's SWMM software. Spatial analysis was used to estimate roof areas, and impervious and pervious areas. Incorporation of RWH systems is expected to affect amounts and patterns of roof runoff, thus resulting in changes of drainage flows. To evaluate these effects, a historical rain event in Kfar Saba of February 2017 was modelled. The hydrological model produced similar results to measured drainage flows. Incorporating RWH resulted in peak flow reduction of 20% (max. flow at the drainage system outlet was reduced from 592 to 476 m³/h). However, as the storm progressed, rainwater tanks are filled up as demands were unable to cope with rainfall volume, and thus flow reduction decreased over time.

CONCLUSION/OUTLOOK/NEXT STEPS

The modelling approach proved to be useful for detailed analysis of RWH potential, and the application is being extended to include other alternative decentralised water sources. The QMRA supplies a quantitative measure of the associated microbial health risk and is being integrated into an LCA framework. Social aspects are revealed through in-depth interviews with experts that will serve as a basis for a survey of the general public attitudes and perceptions towards non-conventional water sources. These also will be later integrated into the LCA framework. It is envisaged that the CLUWAL project will contribute to more sustainable management of the urban water cycle.

ACKNOWLEDGEMENTS

This research is funded by the German Federal Ministry of Education and Research (BMBF) and Israel Ministry of Science and Technology (MOST) (Ref. 02WIL1454; WT1604).

REFERENCES

- Bach P. M., Rauch W., Mikkelsen P. S., McCarthy D. T., Deletic A., 2014. A critical review of integrated urban water modelling – Urban drainage and beyond. *Env. Model. & Soft.*, **54**, 88 – 107
- Bakare B. F., Mtsweni S., Rathilal S. 2016. A pilot study into public attitudes and perceptions towards greywater reuse in a low cost housing development in Durban, South Africa. *J. of Wat. Reuse and Desal.*, **6**, 345-354.
- Benami M., Busgang A., Gillor O., Gross, A. 2016. Quantification and risks associated with bacterial aerosols near domestic greywater-treatment systems. *Sci. Tot. Env.*, **562**, 344–352.
- Blanky M., Sharaby Y., Rodríguez-martínez S., Halpern M., Friedler, E. 2017. Greywater reuse - Assessment of the health risk induced by Legionella pneumophila. *Wat. Res.*, **125**, 410–417.
- Busgang A., Friedler E., Gilboa Y., Gross, A. 2018. Quantitative microbial risk analysis for various bacterial exposure scenarios involving greywater reuse for irrigation. *Water (Switzerland)*, **10**(4), 1-15.
- Campusano A., Butler D., Ward S., Burns M. J., Friedler E., DeBusk K., ... Han M. 2017. Urban rainwater harvesting systems: Research, implementation and future perspectives. *Wat. Res.*, **115**, 195–209.
- Daigger G. T., 2009. Evolving urban water and residuals management paradigms: water reclamation and reuse, decentralization, and resource recovery. *Wat. Env. Res.*, **81**, 809-823
- Farrugia M. T. 2017. Public perceptions on coastal erosion in the Maltese Islands: a case study of St George's Bay (St Julians) and Pretty Bay (Birżeppuġa). *Natural Hazards*, **86**, 587-604.
- Friedler E. 2008. The water saving potential and the socio-economic feasibility of greywater reuse within the urban sector – Israel as a case study. *Int. J. of Env. Studies*, **65**, 57-69.
- Gibbs, G. R. 2008. *Analysing qualitative data*. Sage, Thousand Oaks.
- Haas C. N., Rose J. B., Gerba, C. P. 1999. *Quantitative Microbial Risk Assessment*. John Wiley & sons, NY
- Inbar A. 2015. *Perceptions and Attitudes toward Greywater Recycling – A Review*. In: Gross A., Maimon A., Alfiya Y., Friedler E. *Greywater Reuse*. CRC Press. pp 215-218
- Malczewski J. 2006. GIS-based multicriteria decision analysis: a survey of the literature. *Int. J. of Geographical Information Sci.*, **20**, 703-726.
- Mankad A., Walton A., Gardner J. 2019. Psychological predictors of public acceptance for urban stormwater reuse. *J. of Hydrology*, **572**, 414-421.
- Ogurek M., Alex, J., Rieger L., Schraa O., Schütze M. (2015): A novel integrated approach for designing, testing and implementing WRRF process control solutions; WEFTEC; Chicago, September 2015
- Opher T., Friedler E. 2016. Comparative LCA of decentralized wastewater treatment alternatives for non-potable urban reuse. *J. of Env. Manage.*, **182**, 464-476.
- Patton M. Q. 2015. *Qualitative Research & Evaluation Methods: Integrating Theory and Practice*. Sages.
- Portman M. E., Shabtay-Yanai A., Zanzuri A. 2016. Incorporation of socio-economic features' ranking in multicriteria analysis based on ecosystem services for marine protected area planning. *PLoS ONE*, **11**.
- Roder, G., P. Hudson, P. Tarolli. 2019. Flood risk perceptions and the willingness to pay for flood insurance in the Veneto region of Italy. *Int. J. of Disaster Risk Reduction*, **37**, 101172.
- Rojas K., Schütze M. 2018. *Modelling groundwater recharge and abstraction*; Internal report; ifak, Magdeburg
- Sapkota M., Arora M., Malano H., et al.. 2015. An overview of hybrid water supply systems in the context of urban water management: Challenges and opportunities. *Water*, **7**(1), 153-174.
- Schütze, M., Wriege-Bechtold, A., Zinati, T., Söbke, H., Wißmann, I., Schulz, M., Veser, S., Londong, J., Barjenbruch, M., Alex, J. (2019): Simulation and visualization of material flows in sanitation systems for streamlined sustainability assessment; *Wat. Sci. Tech.*, <https://doi.org/10.2166/wst.2019.199>
- Xu W. D., Fletcher T. D., Duncan H. P., Bergmann D. J., Breman J., Burns M. J. 2018. Improving the multi-objective performance of rainwater harvesting systems using real-time control technology. *Water*, **10**(2), 1-19.

Industrial Wastewater Treatment and Reuse Process

Amit GROSSMANN¹, Yonas Zeslase BELETE¹, Stefan LEU², Sammy BOUSSIBA², Clemens POSTEN³, Franziska SCHWERTNER³, Laurenz THOMSEN⁴, Song WANG⁴, Amit GROSS¹, Roy BERNSTEIN¹

¹ Zuckerberg Institute for Water Research and ²Microalgal Biotechnology Laboratory, French Associates Institute for Agriculture and Biotechnology of Drylands, The Jacob Blaustein Institutes for Desert Research, Ben-Gurion University of the Negev, Sede-Boqer Campus 84990, Israel

³ Institute of Process Engineering in Life Sciences, Karlsruhe Institute of Technology (KIT), Fritz Haber Weg 2, 76131 Karlsruhe, Germany

⁴ Department of Physics and Earth Sciences, Jacobs University Bremen, Campus Ring 1, 28759 Bremen, Germany

*Corresponding authors' e-mail: royber@bgu.ac.il; clemens.posten@kit.edu; l.thomsen@jacobs-university.de

ABSTRACT

In this study, we present the results of an anaerobic membrane bioreactor (AnMBR) coupled with microalgal cultivation for advanced treatment of food industry wastewater, together with results of a membrane-based harvester towards a low-energy harvesting process. The wastewater contained high concentrations of organic matter (COD, 2g/L), total nitrogen (TN, 160 ppm), and total phosphate (TP, 9 ppm). The AnMBR efficiently reduced total suspended solids by over 99.9%, and the COD in the influent by about 97% while the TN and TP concentrations did not change. The AnMBR effluent was used as a growth medium for cultivation of several microalgae species in a lab and outdoor experiments. The microalgae biomass growth, TN and TP uptakes, and water loss due to evaporation in the outdoor system changed seasonally according to the irradiation values. The microalgae effluent (following harvesting) reached the required standards for reuse within 2 and 6 days in the spring and fall, respectively and in 12 days during winter. Indoor studies in Germany revealed that a local strain isolated from a wastewater treatment plant has a great potential for the treatment of the AnMBR effluent. Preliminary harvesting experiments using a new membrane-based harvester revealed that fouling is a critical challenge and that the energy for fouling control can be optimized by varying process parameters. These results indicate that the integrated process tested is efficient in treating high-strength industrial food wastewater with a positive water balance. The energy and environmental balances of the system are currently under investigation.

KEYWORDS

food industry wastewater, microalgae cultivation, anaerobic membrane bioreactor, nutrient and water recovery, microalgae harvesting

INTRODUCTION

The main challenges for sustainable wastewater treatment are improving the effluent quality, reducing the energy consumption, and recovery of the energy and nutrients stored in the wastewater (Diaz-Elsayed et al., 2019). Consequently, a modern WWT scheme requires the integration of multiple technologies. The use of anaerobic membrane bioreactors (AnMBR) presents a promising alternative for organic matter decomposition due to two main advantages: it produces very high effluent quality with absolute removal of bacteria and viruses; and the energy stored in wastewater can be recovered as biogas. Particularly, AnMBR is most suitable for high strength industrial wastewater specifically from food processing, where total organic carbon concentration (TOC) is high and mostly biodegradable. Still, for AnMBR to become the main-stream solution several challenges should be overcome including (and most of them are studied in this project): (i) membrane fouling management; (ii) reduction of high dissolved biogas in the effluent; (iii) the relatively low quality of the produced biogas which contains 30% CO₂, and (iv) low nutrient removal in AnMBRs which requires post-treatment steps. On the other hand, low nutrients removal and CO₂ production provide ideal substrates for microalga cultivation, an efficient, environmentally

friendly and sustainable method for nutrient recovery and CO₂ fixation (Yadav et al., 2019). Valuable microalgae biomass production can upgrade the effluent quality for reuse or release by reducing the nutrients and TOC levels assisted by CO₂ supplementation derived from biogas combustion or following biogas upgrading (separating the CO₂ from the biogas). The combination of AnMBR with microalgae cultivation has been previously described (Viruela et al., 2016), however, for the treatment of effluent containing relatively low N concentration, resulting in low microalgae productivity (Pachés et al., 2018), and low CO₂ fixation. Also, these studies were done under a controlled environment (indoor) and/or at short-term outdoors studies. Furthermore, the nutrients cycle, the energy balance and in specifically the energy required for microalgae harvesting were usually overlooked. The overall goal of our research is to investigate and develop a long-term sustainable food processing wastewater treatment technology based on an AnMBR-microalgae management scheme including: (1) adaptation and integration of AnMBR and microalgae for economical and sustainable industrial wastewater treatment; (2) production of high quality effluent; and (3) full recovery of nutrients and energy potential from the wastewater. This scheme is also expected to mitigate the environmental hazards typically associated with organic-rich industrial wastewater such as GHG emission. Here, we present a long-term experiment on potato-chips factory wastewater using AnMBR followed by microalgae post-treatment for nutrient removal in a lab-scale and under a continuous yearlong outdoors operation. We also present an evaluation of the energy required for membrane-based microalgae harvesting.

METHODS

AnMBR: A high-throughput lab-scale submerged AnMBR (15 L) equipped with six membranes (PES 150 kDa, Microdyn-Nadir, Germany) was built and operated for 2 years (Grossman et al., 2019). The reactor was fed with real industrial wastewater taking from a potato snack factory (Strauss – Frito-Lay, Sha'ar Hanegev, Israel). The wastewater properties are listed in Table 1. The filtration was conducted under sub-critical flux with 9 min filtration and 1 min backwash. The critical flux of the procedure are described by Diez et al., (2014).

Microalgae cultivation in Israel: Several microalgae strains were tested: BZ-2, a highly thermotolerant, fast-growing *Coelastrella* species, similar to *Coelastrella saipanensis*, was used as the benchmark species assessed during all four seasons and compared to the following other species: *Scenedesmus desertii*, a fast-growing locally isolated *Scenedesmus* strain; *Chlorella sp*, a heat tolerant, very fast growing Chlorella species isolated in Sede Boker, Israel (Belete et al. 2019); *Scenedesmus Bremen*, a *Scenedesmus* species isolated in Germany for wastewater applications.

During the initial research period those algae species were adapted to and tested in AnMBR effluent supplemented with Fe-EDTA and microelements in Erlenmeyer flasks as described previously (Belete et al 2019). Repeated independent semi-continuous effluent treatment periods were then performed outdoors as follows: 4 in July-August 2018; 3 in November-December 2018; 5 during January/February 2019, and 4 in May 2019. Algae were cultivated in 2.5 L column PBRs in MBLs innovative proprietary high-efficiency cultivation approach, mixed by bubbling with about 1 L/min air/2% CO₂ mixture.

Microalgae cultivation in Germany: The microalgae cultivation experiments in Germany were conducted thus far in a lab-scale. The AnMBR effluent was lyophilized in Israel and sent as a powder to Germany where it was re-dissolved and used as the growth medium for the cultivation studies. Two microalgae were studied - Phyto2015H and *Coelastrella sp.*. The microalgae were inoculated into AnMBR effluent (300 mL) with an initial biomass concentration of 100 mg/L in biological triplicates in a temperature-controlled room (21±1 °C) with a light intensity of 100 µmol/m⁻²/s and with a light regime of 18 h light/ 6 h darkness for 4 days. Aeration was provided by an air compressor. The decrease in volume caused by evaporation was compensated by ultra-pure water every day.

Characterization: Microalgae growth and water properties were assessed as recently described (Belete et al 2019).

RESULTS AND DISCUSSION

Long-term AnMBR of food processing wastewater

Table 1 presents the average quality of the influent, effluent, during the first 6 months of operation. The results in Table 1 show that the DOC and TSS removal was steady and greater than 97%, indicating its high biodegradability. The latter resulted in relatively low sludge production with SRT/HRT ratio of at least 30 (30 ml/day for every 1 L volume of the reactor) as typically found in AnMBRs. As expected, the N and P concentrations in the influent and the effluent were similar. The biogas production was about 9 L/day, with a specific biogas yield of 0.19 L CH₄/gr COD removed. The biogas was composed of ~75% CH₄, and ~25% CO₂, that is suitable for direct combustion. Trace of H₂S (~1000 ppm) was also found, likely because of S present in the feed. The relatively high specific methane yield indicates an efficient methanogenic activity. The results in Table 1 also demonstrate that the effluent quality and biogas production were relatively stable yearlong. This reason was that the AnMBR operated under constant conditions throughout the experiment.

The trans-membrane pressure (TMP) of the membranes was also relatively stable during the experiments (-15-(-40) mBar)) and the membrane did not require chemical cleaning. This suggests that the membrane fouling was low. The reasons for the low fouling were probably the low flux (4 LMH), much lower than the critical flux (\approx 12 LMH), the long HRT (3 days), and because biogas sparging and backwashing were implemented (Grossman et al., 2019). Such low HRTs and fluxes are typically applied for AnMBR treating industrial wastewater in order to achieve a high enough COD removal (Dereli et al., 2012). Nevertheless, in order to lower the energy demand of the system, it is necessary to reduce the intense biogas sparging and frequent backwashing; this is currently being investigated by using modified membranes. In addition, the valorization of the sludge by hydrothermal carbonization is also being explored to recover the full potential of the wastewater.

Table 1: Water quality and process performance in the SAnMBR.

Parameter	Units	Influent (feed)	Effluent (permeate)	Removal (%)
TSS	mg/L	2093.5 \pm 199.1	<10	>99.9%
TOC	mg/L	1520.0 \pm 715.1	32.3 \pm 6.5	97.9%
DOC	mg/L	916.2 \pm 95.1	32.3 \pm 6.5	96.5%
TCOD	mg/L O ₂	4560.0 \pm 2145.3*	96.9 \pm 19.5*	97.9%*
SCOD	mg/L O ₂	2748.6 \pm 285.3*	96.9 \pm 19.5*	96.5%*
TN	mg/L	164.7 \pm 80.6	153.7 \pm 15.8	6.7%
TP	mg/L	9.2 \pm 4.5	9.2 \pm 4.5	-
pH	-	7.0 \pm 0.2	7.3 \pm 0.2	-
EC	µS/cm	2.4 \pm 0.3	4.0 \pm 0.4	-

* Calculated COD according to TOC concentrations (1:3 – TOC:COD)

Long-year microalgae cultivation in Israel

Several algae species were cultivated outdoor in a semi-continuous mode during four seasons, with 3 – 5 repeated growth cycles each (dilution in fresh AnMBR effluent and cultivation to reach the stationary phase). Biomass, nutrient and TOC concentrations were plotted with time and analyzed by linear regression and statistical tools. Furthermore, biomass productivities were normalized versus daily radiation (Figure 1).

The summary of the uptake/growth rates based on linear fitting, as well as the number of days needed to reach the required TN and TP levels for irrigation in Israel (TN<20ppm, TP<1ppm) are presented in Table 2. The microalgae biomass of all three strains increased with time at a similar growth rate strongly dependent on irradiation (Fig.1a and Table 2). The TN and TP uptake rates were also linear during 5-6 days and reached the required Israeli standards for irrigation (Inbar, 2007). Interestingly, the DOC was hardly consumed throughout experiments and remained between 30 to 40 ppm, and was at times slightly higher than the standard for irrigation (\approx 30 ppm DOC). The standards for discharge into rivers are stricter with a limit of 10 mg/l for TN and 1 mg/L TP (Inbar, 2007). It is noted that algal growth and consequently nutrient removal were lower during the winter, when both radiation and temperatures are lower. Nutrients uptake could not be significantly improved by using a *Scenedesmus* (Sec. G) strain originally isolated in Germany. Statistical analysis (not presented) showed that the irradiation was the dominant factor and not the temperature; thus low-temperature tolerance strain could not improve nutrients uptake during

winter time. Nonetheless, new strains will be further study. Currently, *Coelastrella sp* performed good as or better than other species tested during all seasons (Fig. 1), which justify its selection as the primary species to be assessed in the long term up-scaled pilot plant. Furthermore, the variability in treatment efficiency is planned to accommodate by using a novel pilot facility under construction at BGU.

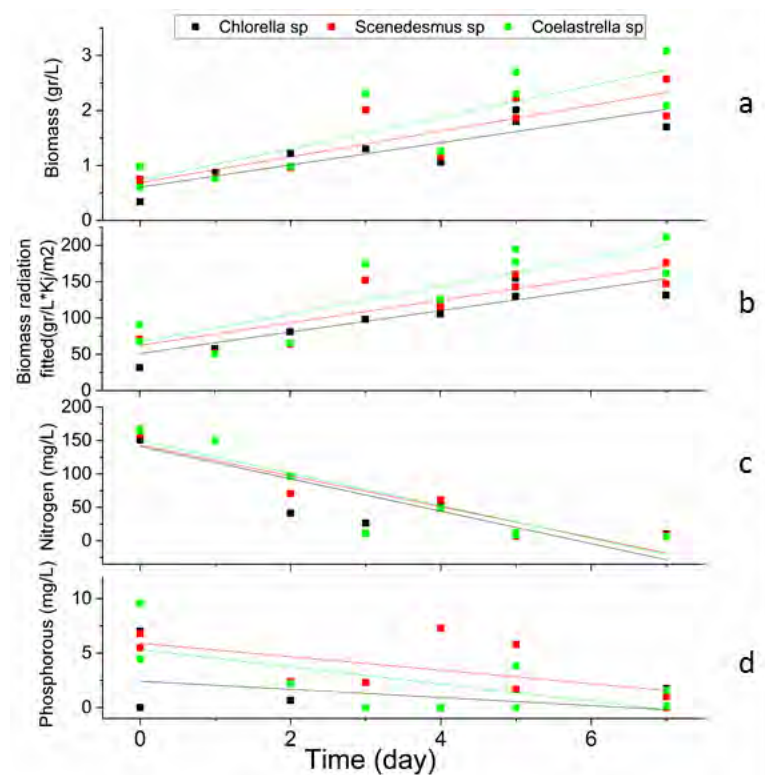


Figure 1: Average microalgae growth (a) microalgae growth normalized to daily irradiation (b) total nitrogen update (c) and total phosphate uptake (d) of three different strains in the outdoor microalgae cultivation studies in Sde Boker during November ($n=3$).

Table 2: Average TN and TP uptakes, microalgae growth and microalgae growth normalized to daily irradiation of different strains during three seasons in the outdoor studies in Sde Boker. And, the number of days in the outdoor cultivation studies that are needed to reach the nutrients levels in the microalga effluent suitable for discharge in Israel.

Month		N		P		Biomass	Biomass/Rad
		N uptake rate (mg/L·day)	Concentration after day 2 (mg/L)	P uptake rate (mg/L·day)	Concentrat ion day 2 (mg/L)	growth rate (gr/L·day)	growth rate (gr/L·day·kJ·m ⁻²)
July/ summer	<i>Sce.</i>	-37.90	8.4	-	<0.1 ppm	0.43	14.46
	<i>Coe./ Super</i>	-39.07	6.3	-	<0.1 ppm	0.39	11.93
		after day 6		after day 6			
Nov./ fall	<i>Chl.</i>	-24.22	≈4	-0.37	0.18	0.20	14.73
	<i>Sce.</i>	-23.03	≈4	-0.62	2.18	0.23	15.49
	<i>Coe.</i>	-24.28	≈4	-0.79	0.59	0.29	19.11
		after day 12		after day 12			
Jan./ winter	<i>Chl.</i>	-11.71	11.91	-1.07	<0.1	0.14	12.34
	<i>Sce.G</i>	-13.50	1.18	-0.88	<0.1	0.18	15.65
	<i>Coe.</i>	-10.90	18.42	-0.82	<0.1	0.18	15.40

Growth in Germany

Lab-scale microalgae cultivation studies with the effluent from Israel were conducted in Germany with the two strains - Phyto2015H and *Coelastrella sp.* Both algae displayed almost linear growth curves during 4-day cultivation and reached 94 (*Coelastrella sp.*) and 112 mg/L/d (Phyto2015H), after 4-day cultivation. The biomass productivity of Phyto2015H was significantly higher (evaluated using ANOVA) than that of *Coelastrella sp.* ($p<0.05$). Both species exhibited approx. 99% ammonium within 24 h, resulting in nutrient removal rates of approx. 23.5 mg/L/d. Both species kept growing over time, even though there was no ammonium available in the medium. Therefore, algae either stored the ammonium or started to use the organic nitrogen source (e.g. amino acids) from the effluent. To gain more insights into the various nitrogen sources, the N content in biomass and amino acids concentration in the effluent needs to be measured in the next step. Orthophosphate-P removal rates of 1 mg/L/d and 0.9 mg/L/d were achieved by Phyto2015H and *Coelastrella sp.*, respectively. Orthophosphate-P was removed completely by Phyto2015H after day 4.

Energy and water balance

Water balance: water evaporation may be prohibitively high in desert areas as Sde Boker which will lessen the process feasibility. However, thanks to an improved PBR concept with 2-3 fold areal productivity, water loss by evaporation during a treatment period was 10-15 L/day in summer out of 35 L treated, and 1 – 2 L/day in winter out of 10L effluent treated.

Microalgae harvesting: The final step of the described process above is a solid/liquid-separation of effluent and algae by a two-step approach: a filtration unit will reach about 20 g/L and a second unit operation depending on later usage of biomass. Therefore, a membrane-hollow-fiber based pilot-scale filtration plant was developed, allowing measuring several parameters (temperature, pH, turbidity, inflow, and pressure) online and simultaneously. A process control system was set up, in order to control the filtration process towards high effluent quality and efficiency concerning algae growth. Preliminary results using model foulants (Baker's yeast) showed that fouling is a significant problem, especially when the filtration is done without gas-sparging. Thus, the development of a fouling-reduction strategy such as aeration, back-flushing or relaxation is required. The critical filtrate flux - an important parameter in membrane filtration in biological reactors - was measured by the so-called "flux-step"-method (Le Clech et al., 2003) using a culture of the green algae *Chlorella vulgaris* (dry biomass: 2 g/L). The critical flux was 0.19 l/(min·m²) (Fig2a&b). When the gassing rate increased to 30 L/min the critical flux increased to 0.23 L/(min·m²) (Fig2b). This indicates that the critical flux correlates with the applied gassing rate and that the tradeoff between the increase in the critical flux and the rate, in relation to the energy

cost, needs to be evaluated. Other operational parameters including low fouling membranes will also be investigated in the new system.

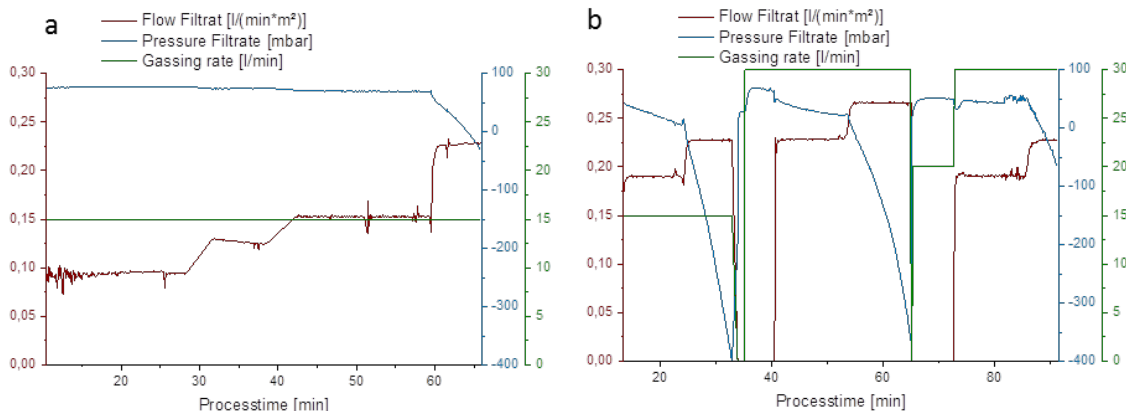


Figure 2: (A) Determining the critical flux for a gassing rate of 15 L/min and (B) evaluating the critical flux for different gassing rates (15 L/min and 30 L/min).

CONCLUSIONS

An AnMBR was successfully applied for high removal of TSS and TOC from food industry wastewater while extracting the energy from the organic matter as biogas and maintaining low-fouling. Outdoor microalgae cultivation as a post-treatment step effectively removed the nutrients to the required level for effluent reuse, besides during the winter time, probably due to low irradiation levels. Strain selection provided an optimal strain for year-long treatment, but a strain with high growth rates in winter time is still needed. A new membrane-based harvesting system was built for advanced harvesting studies. Preliminary results indicated that fouling is a significant challenge which can be lessened by optimizing process conditions. Future study will focus on finding microalgae strain for wintertime, study energy and nutrients cycle of the proposed system, and study membrane-based harvesting system.

REFERENCES

- Belete Y.Z., Leu S., Boussiba S., Zorin B., Posten C., Thomsen L., Wang S., Gross A., Bernstein R. *Bioresour Technol.*, 2019, accepted.
- Dereli, R.K., Ersahin, M.E., Ozgun, H., Ozturk, I., Jeison, D., van der Zee, F., and van Lier, J.B. *Bioresour Technol.*, 2012, 122, 160-170.
- Diaz-Elsayed, N., Rezaei, N., Guo, T., Mohebbi, S., and Zhang, Q. *Resour. Conserv. Recycl.*, 2019, 145, 94-112.
- Diez, V., Ezquerra, D., Cabezas, L.J., García, A., Ramos, C. *J. Membr. Sci.*, 2014, 453, 1-11
- Grossman, A.D., Yang, Y., Yogeve, U., Camarena, D.C., Oron, G., and Bernstein, R. *Environ. Sci.: Water Res. Technol.*, 2019, 5, 1145-1156.
- Inbar, Y. *Wastewater reuse-Risk assessment, decision-making and environmental security* (Springer), 2007, 291-296.
- Le Clech, P., Jefferson, B., Chang, I.S., and Judd, S.J. *J. Membr. Sci.*, 2003, 227, 81-93.
- Pachés, M., Martínez-Guijarro, R., González-Camejo, J., Seco, A., and Barat, R. *Enviro technol*, 2018, 1-10.
- Viruela, A., Murgui, M., Gómez-Gil, T., Durán, F., Robles, Á., Ruano, M.V., Ferrer, J., and Seco, A. *Bioresour Technol.*, 2016, 218, 447-454.
- Yadav, G., Dash, S.K., and Sen, R. *Sci. Total Environ.*, 2019, 688, 129-13.



Project Group 2016

Aquifer Recharge as Sustainable Storage Solution for Desalinated Water

Anat BERNSTEIN^{1*}, Hagar SIEBNER¹, Raz STUDNY¹, Daniel KURTZMAN², Barak IZRAEL², Yoram KATZ³, Kaori SAKAGUCHI-SÖDER⁴, Berhane ABRHA⁴, and Christoph SCHÜTH⁴

¹ Zuckerberg Institute for Water Research, Ben-Gurion University of the Negev

² Institute of Soil, Water and Environmental Sciences, ARO Volcani Center

³ Mekorot

⁴ Institute of Applied Geosciences, Technical University Darmstadt

*Corresponding author's e-mail: anatbern@bgu.ac.il

ABSTRACT

Aquifer recharge is suggested as an intermediate storage solution for surpluses of Israel's desalinated water. Due to the hydro-chemical differences between desalinated water and naturally recharging rain water and runoff, aquifer recharge by desalinated water is expected to present (1) raise in HCO_3^- and Mg^{2+} following dissolution of carbonates and ion exchange processes, and (2) formation of halogenated disinfection by-product. With the grand challenge of assuring sustainable storage solution for future usage, our study aims in getting a deeper understanding of the processes accompanying aquifer recharge with desalinated water.

To this end, in the reported period the following activities were performed: On the quantitative level, vadose zone and groundwater modelling was performed (partially reported before). Column experiments were further conducted to account for major ions processes. On the organic geochemistry level, continuous monitoring in flood event was conducted. Well controlled infiltration experiments were performed, and accompanying laboratory experiments were conducted (due to space limitation, only main findings are reported). Additionally, isotope methods were developed as a tool for studying the fate of THM in the subsurface. These were implemented to study isotope fractionation along reductive dehalogenation. Further work will be done to isotopically analyse THM in field samples.

KEYWORDS

Aquifer recharge; desalinated water; geochemistry; modelling; stable isotopes; disinfection by-products

INTRODUCTION

During the last decade, desalinated water is produced in Israel in increasing volumes, making sea water the main source for domestic water supply in the country (~75%). Following variations in demand and production, aquifer recharge may be a practical tool for managing surpluses of desalinated water by providing intermediate storage. In Israel, this was suggested as a solution for water production surpluses in rainy years or seasons and as a temporal solution during maintenance of the national water carrier.

The hydro-chemical properties of desalinated water lead to specific processes during aquifer recharge, including (1) raise in HCO_3^- and Mg^{2+} following dissolution of carbonates and ion exchange processes, and (2) formation of halogenated disinfection by product (DBP).

With the grand challenge of assuring sustainable storage solution for future usage, our study aims in getting a deeper understanding of the processes accompanying aquifer recharge with chlorinated desalinated-seawater. This will enable optimization of the recharge technology, both on the physical aspects of infiltration (capacity, rates), as well as water quality aspects (minerals, DBPs). These research goals are tested in the lab, as well as in the field - at the Menashe Infiltration basin and with model simulations.

METHODS (Relevant for the reported period only)

Groundwater model - A regional conservative-transport groundwater model (65 km^2) was set using the MT3DMS solver as described in the 2nd annual report (Ganot et al., 2018b). Transport of a conservative tracer which is typical to reverse-osmosis desalinated seawater (e.g. ${}^2\text{H}$) was simulated considering advection and dispersion processes. Simulations were further verified by the isotope composition of groundwater sampled in wells within the model domain.

Field site and monitoring system – A monitoring system was formerly installed in the Menashe site. The system includes suction cups installed at 0.5, 1.0, 2.0 and 3.0 m depth along the unsaturated zone, and two monitoring wells penetrating the shallow aquifer (20-30 m depth). The infiltration pond is surrounded by production wells that are sampled twice a year (see former reports).

Water isotope composition - The isotopic composition of water ($\delta^{2\text{H}}$, $\delta^{18\text{O}}$ ‰) was analyzed in all field samples using Cavity Ring Down Spectrometer (Picarro L2130-i Analyzer).

Isotope analysis of disinfection by-products – Methods for Cl-CSIA and Br-CSIA for selected THMs were developed based on Sakaguchi-Söder et al. (2007). Standard GC/qMS with purge and trap (P&T) was used to conduct Cl- and Br-CSIA using the methods. Chlorine and carbon isotope enrichment factors were determined for CF during the reductive degradation process.

Small scale infiltration experiment - A small scale controlled infiltration experiment was carried out in January 2017. Desalinated water was led to infiltrate within a defined 1.3-m diameter concrete ring. Infiltrated water was sampled by suction cups installed along the vadoze zone. Free chlorine (Eutech Instruments C-201) and general geochemical parameters (pH, EC, temp, dissolved oxygen; WTW MultiLine 3420) of the water samples were measured in the field. Additionally, water samples were taken to the lab for THM concentrations (EPA Method 551.1), water stable isotopes, and major ions.

RESULTS AND DISCUSSION

Monitoring and sampling at the Menashe Site (2014-2019)

As part of this project and in continuation to MARSOL project (EU-FP7, 619120) we were able to monitor and sample water levels, electrical conductivity (EC), major ions and water stable isotopes for almost 5 years now (see different monitoring data at Ganot et al., 2017, 2018a, 2018b, as well as in the Appendices). We will continue the bi-annual sampling effort also beyond this project in order to have a long-term picture of changes in the aquifer.

Flow and Deuterium-Transport model

A unique flow and ${}^2\text{H}$ transport groundwater model was set and calibrated jointly by Mekorot (Yoram Katz) and Volcani Center (Yonatan Ganot and Daniel Kurtzman). The calibrated model was used for simulation of 50 years of managed recharge with desalinated (Figure 1). More details can be found in the publication Ganot et al., 2018b.

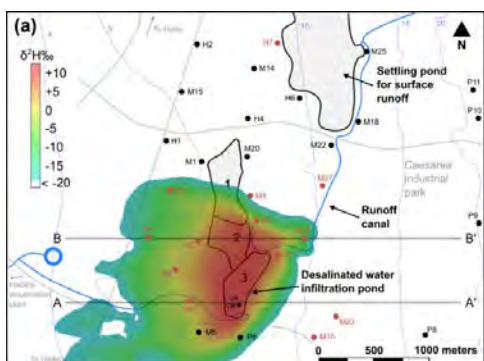


Figure 1. (a) Scenario simulation of the spread ${}^2\text{H}$ in the top layer of the aquifer model at 2065. All years 2016-2065 were simulated as the year 2015;

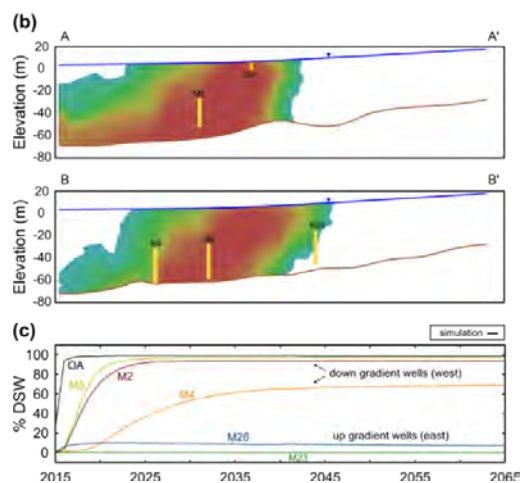


Figure 1 (b) Cross sections AA' and BB' at 2065;4

Figure 1 (c) Percentage of desalinated seawater in pumped water in relevant wells according to the 50 years simulation. Note that the desalinated water plume will not spread very far and will reach a steady state in all wells (adopted from Ganot et al., 2018b).

Column experiments with sediments from Menashe site

Column experiments were performed for testing major ions behavior under controlled laboratory conditions. Columns were ran with either desalinated water that is enriched with Ca^{2+} and HCO_3^- (Ashkelon plant water), or water containing no Ca^{2+} and HCO_3^- (distilled water). Column sediments originate from Menashe infiltration pond. Experiments were conducted for up to 2500 pore volumes (PV). The first 80 PVs are here presented (Figure 2).

The high concentrations in the first 1-3 PVs are due to water that was not flowing and had long residence time in the column. The Ca^{2+} concentration in the effluent reaches quickly the inlet concentration of the enriched water. Whereas in the distilled water in which the inlet concentration is close to zero the effluent contains $\sim 10, 15 \text{ mg/L}$ Ca^{2+} discharged from the sand and beach rock columns, respectively, showing the dissolution potential of the non-enriched water vs. no dissolution in the enriched water (Figure 2 top). Note that for Mg^{2+} the concentration are more than an order of magnitude smaller, and there is a larger relative difference between the concentration of the two types of water in both sediments. In the non-enriched water concentrations of Mg^{2+} stabilize after 20-30 PVs, whereas with the enriched water, where the cation exchange potential is high, there is a decrease in the Mg^{2+} concentrations throughout the 80 PVs. Some dissolution or disillusion followed by cation exchange releases small concentrations of Mg^{2+} ($<0.5 \text{ mg/L}$) when non enriched water passes through the sediment, much higher in the beach-rock than in the sand (Figure 2 bottom).

A continuous monitoring of head in the inlet and discharge from the column, and keeping the outlets at constant head enables continuous calculation of the saturated hydraulic conductivity (K) by the Darcy Law. Only a slight decrease in K was observed with time, probably due to small continuous compaction of the sediment in the column. No dramatic changes in K due to opening of new pathways or clogging of them caused by dissolution/precipitation were observed.

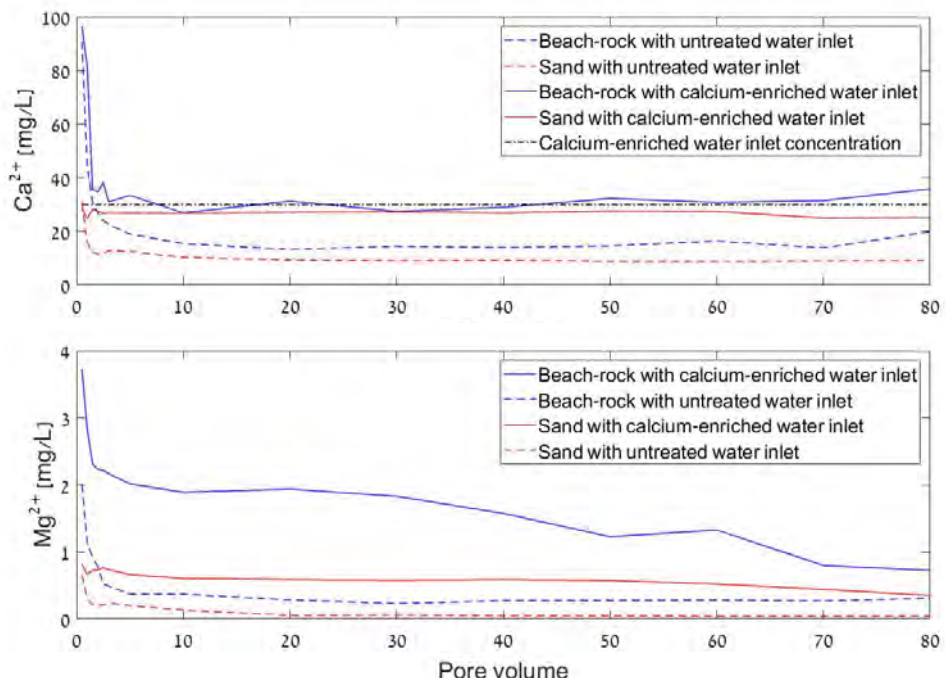


Figure 2. Ca^{2+} (upper panel) and Mg^{2+} (lower panel) in the column effluents. Concentrations are mean values of 4 replicates of each treatment. Mg^{2+} inlet concentrations are below the detection limit.

Trihalomethane formation during aquifer recharge with chlorinated desalinated water (due to space limitation, only selected results are presented)

Desalinated water was recharged to the vadose zone in a small scale infiltration experiment. During this infiltration event, chlorine concentrations measured at the outflow of the pipe varied between 0.3-0.4 mg/l. Water isotopes measurements indicated that this water is indeed desalinated water. Bromide concentrations were <30 µg/l and DOC of 0.9 ± 0.5 mg/l were measured in the ponding water, prior infiltrated. Average residence time within the ring was ~ 32 min.

Total THM in the desalinated water at the pipe outlet were 0.8-1.0 µg/l. Concentrations only slightly increased above this background concentration in the pond, with maximal concentrations of 1.6-1.8 µg/l. Concentrations also did not dramatically change along the vadose zone (1.0 – 3.6 µg/l at different depths and durations, Figure 3). This has indicated that the THM are quickly formed in the pond water (average residence time of 32 min) and are not significantly formed or removed along the vadose zone.

In the second experiment, bromide was added at an average concentrations of ≈ 2 mg/l. Total THM in the desalinated water at the pipe outlet were 0.9 µg/l. Concentrations were this time significantly higher, with total THM formed in the pond of 5.8-6.4 µg/l and similar concentration along the soil profile (4.4 – 9.3 µg/l) and speciation changed towards brominated forms. Nevertheless, THM concentrations are still more than an order of magnitude lower than drinking-water standard.

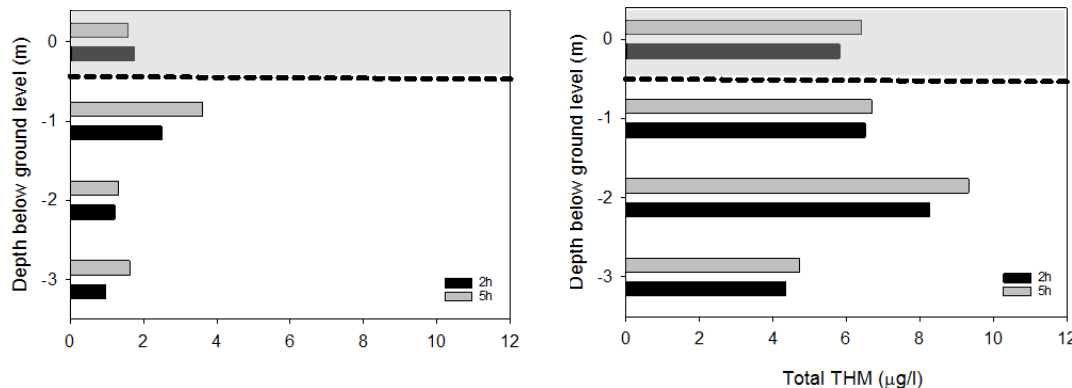


Figure 3. Total THM after 2 and 5 hours along the vadose zone for desalinated water (left) and desalinated water with the addition of $\approx 2 \text{ mg/l}$ bromide (right)

A full scale infiltration event took place in the site, with total infiltration volume of 2.2 MCM in ≈ 3 weeks. Total THM concentrations were monitored in the pond and vadose zone 4, 13, and 20 days after infiltration began. In accordance to the small scale infiltration experiment, THM concentrations in the vadose zone were similar to those in the pond. Nevertheless, a significant decrease was monitored in total THM along the event (Figure 4). The temporal variability may theoretically be the result of Br- variability, but results indicate a rather uniform Br- concentration along the entire flood event - $33 \pm 6 \text{ µg/l}$ in pond water and $42 \pm 5 \text{ µg/l}$ in the vadose zone. Also DOC concentrations were uniform along the flood, with concentration of $17.1 \pm 0.7 \text{ mg/l}$ in the pond and $17.4 \pm 1.5 \text{ mg/l}$ along the vadose zone. Water isotopes indicate no change in water source during the flood event. Thus, this shift may also be attributed to other factors such as volatilization, temporal variations in chlorine concentrations which cannot be monitored, or changes in DOC type.

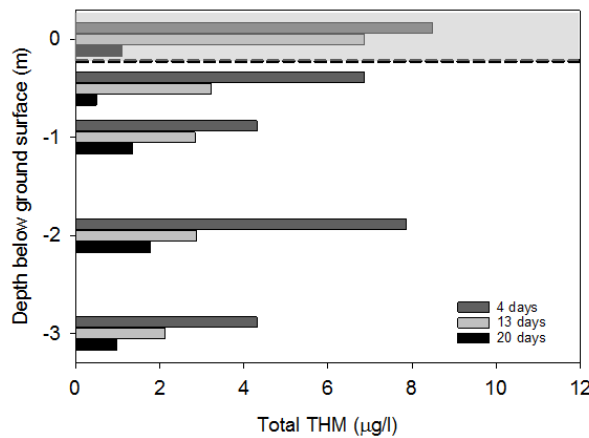


Figure 4. Total THM concentrations in the pond and along the vadose zone during a full scale infiltration event.

It may be questioned whether THM formation fully occurs within the pond, or also in the unsaturated zone. A significant difference is observed in chlorine consumption between the organic matter types (Figure 5), with a more rapid consumption when using compost as opposed to humic acids. The water average residence time in the peak of the full scale flood was 4 days (estimated by infiltration rate of $\approx 0.5 \text{ m/d}$, and water column of 2 m). Experiments for chlorine consumption (2.0 mg/l) show that the residual chlorine (typically $\leq 0.5 \text{ mg/l}$) should be fully consumed at the water DOC within this timescale. Thus, THM formation is expected to occur at the surface water, and not further formed along the vadose zone.

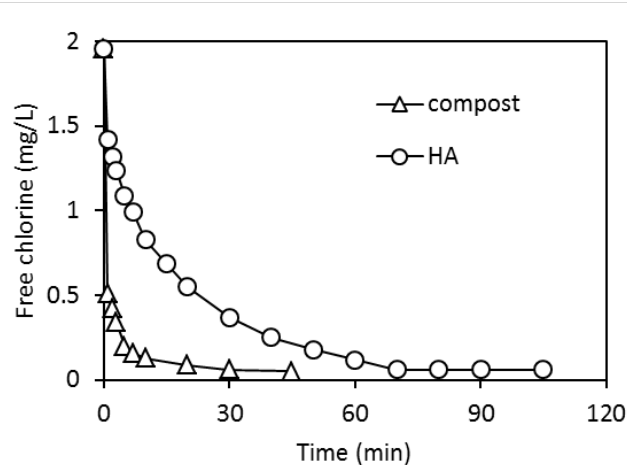


Figure 5. Chlorine consumption as a function of time (min) when introduced with 10 mg/l DOC from compost or humic acids (HA)

Monitoring of THM in adjacent wells surrounding the infiltration ponds were carried out, and presented maximal concentrations of \approx 2 $\mu\text{g}/\text{L}$ at wells downstream to the pond. Water isotopes have indicated that water in these wells present an increasing proportion of desalinated water (see Appendix A2). These concentrations were surprising, as it was expected that concentrations will be significantly diluted downstream to the pond. Stable isotope analysis of chloroform (see below) may possibly provide explanation for this observation.

Isotope method development and application for trihalomethanes (THM)

Shifts in THM stable isotopes may shed light on degradation processes these compounds follow in the sub-surface. Additionally, since chloroform (CF) concentrations underneath the infiltration pond were \approx 2 $\mu\text{g}/\text{L}$, and in wells downstream rather similar (despite the expectation of much lower concentrations due to dilution) it may be possible that CF has different sources in this site. This as well may possibly be identified using isotope tools.

Following the extremely low THM concentrations in the site (dominated by CF), compound-specific isotope methods (CSIA) were optimized. For CSIA of CF, a precision of \pm 0.31 ‰ was achieved for chlorine isotope composition ($\delta^{37}\text{Cl}$) when analysing 10 mL of aqueous sample containing 3 $\mu\text{g}/\text{L}$ CF (on-column mass = 30 ng). However, samples with CF concentration down to 1.5 $\mu\text{g}/\text{L}$ were determined at the MAR site, and precision became significantly deteriorated (\pm 1.53 ‰). To achieve our target precision for $\delta^{37}\text{Cl}$ of \pm 0.5 ‰ or better, the enrichment of CF in the water phase or modification of the system for a larger volume (e.g. 10 mL \rightarrow 20 mL) is of must.

A couple of commercial SPE cartridges were identified for a successful enrichment of CF for Cl-CSIA. A certain level of isotope fractionation that seems to occur during the enrichment process still needs to be minimized. Groundwater was sampled during spring 2019, and will be analysed after achieving this goal.

For the determination of chlorine and carbon enrichment factors of CF following degradation processes, a series of experiments were implemented. CF was reductively dehalogenated in the presence of palladium on alumina as a catalyst and hydrogen gas as an electron donor. Degradation experiments were conducted using an innovative sampling method, which was designed not to generate headspace during the experiment.

Chlorine (Figure 6) and carbon isotope enrichment factors (ϵ) were determined using Rayleigh's equations. The chlorine and carbon isotope enrichment factor were derived as -3.28 ± 0.23 ‰ and -17.79 ± 0.98 ‰, respectively. Our outcome is comparable to the investigation by Torrento et al (2017) with higher precisions.

In the course of degradation process, CF has transformed to dichloromethane, chloromethane and methane. Using newly developed Cl-CSIA methods for dichloromethane and chloromethane, it is planned to determine additional sets of chlorine and carbon isotope enrichment factors for these degradation products.

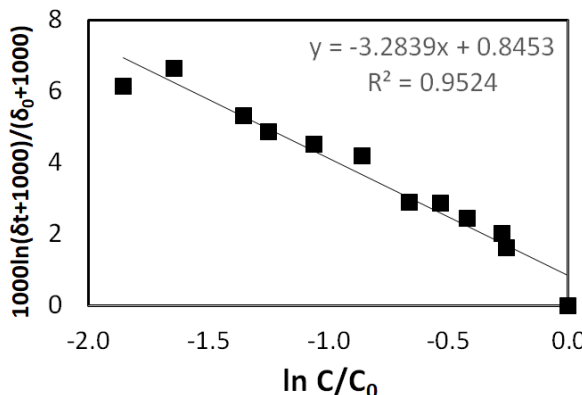


Figure 6. Stable chlorine isotope fractionation of the residual fraction of chloroform during abiotic reductive dechlorination using Pd/Al₂O₃(10%wt)

CONCLUSIONS

- A unique aquifer flow and ²H transport groundwater model was calibrated to isotope data and used for MAR scenario s
- Column experiments with non-enriched water show the possible in-situ enrichment with Ca²⁺ and to lesser extent with Mg²⁺ due to flow through the calcareous beach rock.
- THM are formed at low concentrations during aquifer recharge with desalinated water, at the ≈ 2 µg/L range
- If water with higher bromide concentrations are introduced, THM concentrations increase during MAR to the ≈ 7-8 µg/L range. These concentrations are an order of magnitude lower than drinking water regulations.
- THM formation occurs at the surface water, prior infiltration to the vadose zone.
- CSIA methods enable precise analysis of δ¹³C and δ³⁷Cl in chloroform at concentration of 3 µg/L. Further effort is dedicated to improve this limit of quantification by a factor of two.
- Reductive dehalogenation of chloroform is accompanied by significant carbon and chlorine isotope effects.
- Isotope analysis of chloroform in groundwater samples is further planned.

ACKNOWLEDGMENTS

This work is funded by the German Federal Ministry of Education and Research (BMBF) and by the Israel Ministry of Science, Technology and Space (MOST), project WT1401. TUD gratitude goes to Dr. Thomas Schiedek and Ms. Claudia Cosma for their technical support in the laboratory. BGU acknowledge Ms. Vinolia Shyntychea. ARO acknowledges Mr. Ido Nitzan (lab and field technician).

REFERENCES

- Ganot, Y., R. Holtzman, N. Weisbrod, I. Nitzan, Y. Katz and D. Kurtzman (2017). Monitoring and modeling infiltration-recharge dynamics of managed aquifer recharge with desalinated seawater. *Hydrology and Earth System Sciences* 21: 4479-4493.
- Ganot, Y., Holtzman, R., Weisbrod, N., Russak, A., Katz, Y. and D. Kurtzman, D (2018a). Geochemical processes during managed aquifer recharge with desalinated seawater. *Water Resources Research*, 54. <https://doi.org/10.1002/2017WR021798>
- Ganot, Y., Holtzman, R., Weisbrod, N., Bernstein, A., Siebner, H., Katz, Y., and D. Kurtzman (2018b). Managed aquifer recharge with reverse-osmosis desalinated seawater: modeling the spreading in groundwater using stable water isotopes. *Hydrology and Earth System Sciences* 22, 6323-6333/

Sakaguchi-Soder, K.; Jager, J.; Grund, H.; Matthaus, F.; Schuth, C. (2007). Monitoring and evaluation of dechlorination processes using compound-specific chlorine isotope analysis. *Rapid Commun Mass Sp.*, 21 (18), 3077-3084.

Torrento, C.; Palau, J.; Rodriguez-Fernandez, D.; Heckel, B.; Meyer, A.; Domenech, C.; Rosell, M.; Soler, A.; Elsner, M.; Hunkeler, D. (2017). Carbon and Chlorine Isotope Fractionation Patterns Associated with Different Engineered Chloroform Transformation Reactions. *Environ Sci Technol.* 51 (11), 6174-6184.

APPENDICES

Representative groundwater monitoring data, 2015-2019

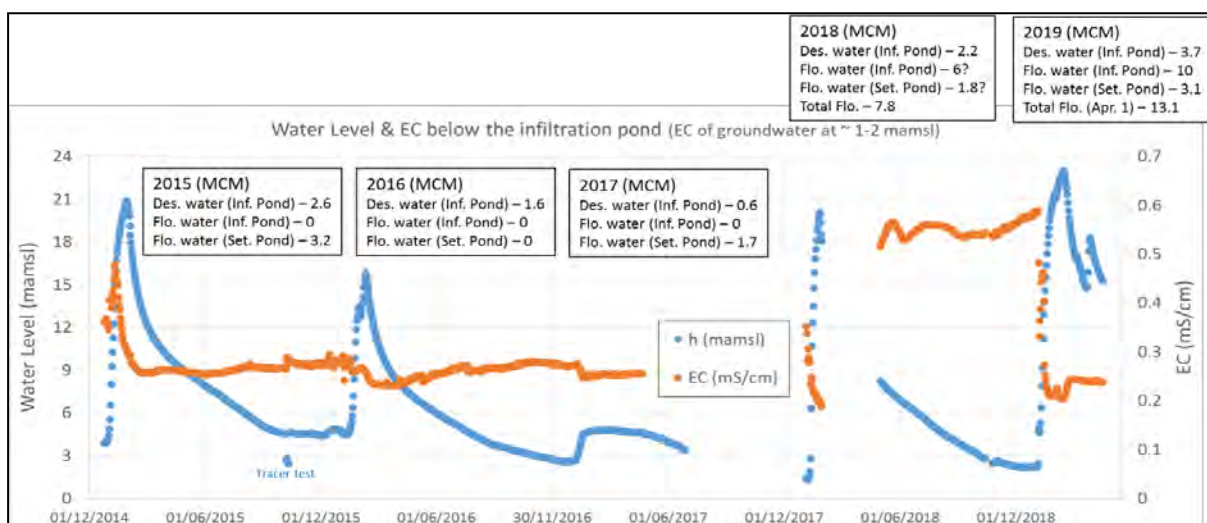


Figure A1. Water level (blue) and EC (orange) at the observation well OA (Ganot et al., 2017). Annual managed aquifer recharge volumes are given for desalinated water (Des.) and flood water (Flo.) at the settling (Set.) and infiltration (Inf.) ponds.



Figure A2. Deuterium (left) and Mg^{2+} (right) in wells surrounding the southern infiltration pond. Red-green-blue refers to the vicinity of the well and downgradient from the infiltration pond. Deuterium data presents a clear enrichment trend downstream to the infiltration pond following increasing mixing of desalinated water with local groundwater. Mg^{2+} concentrations present as well a mixing trend, but with lower consistency than deuterium. The lower consistency is expected as Mg^{2+} is not conservative in groundwater.

TRacking Effects of Environmental Organic Micro-Pollutants in the Subsurface

Carolin RIEGRAF¹, Liat MOSCOVICI², Dror SHAKIBAI², Nidaa ABU RMAILAH², Hadas ATTIAS², Georg REIFFERSCHEID¹, Shimshon BELKIN² and Sebastian BUCHINGER^{1*}

¹ Federal Institute of Hydrology (BfG), Department Biochemistry, Ecotoxicology, Am Mainzer Tor 1, 56068 Koblenz, Germany

² Hebrew University, Institute of Life Sciences, Department of Plant and Environmental Sciences, Jerusalem 91904, Israel

*Corresponding author's e-mail: Buchinger@bafg.de

ABSTRACT

The combination of classic *in vitro* bioassays with high-performance thin-layer chromatography (HPTLC) is a promising technique to link chemical analysis of contaminants directly to their potential adverse biological effects. This effect-directed analysis (EDA) enables the assessment and comparison of the bioactive composition of samples by a generation of activity profiles even in complex matrices. Based on previous findings demonstrating the combination of HPTLC with the yeast estrogen screen (p-YES), we successfully developed a comparable approach for *inter alia* genotoxicity (planar *recA*) and androgenicity (p-YAS). The application of the developed methodology to environmental samples such as wastewater treatment plants, landfills, aquifers, soil retention filters or surface water samples was successfully demonstrated. Furthermore, a set of advanced yeast-based sensor strains for estrogenic and androgenic effects were designed for the multiparallel effect detection within one assay by making use of different fluorescent proteins as reporting elements. We anticipate our methodology to substantially broaden the spectrum of specific endpoints combined with HPTLC for an efficient and robust screening of environmental samples to track effects of micro-pollutants in the environment and to guide a subsequent in-depth EDA.

KEYWORDS

Organic micro-pollutants; genotoxicity; endocrine effects; thin-layer chromatography; effect directed analysis

INTRODUCTION

Serious concerns have been raised about the vast number of micro-pollutants in the environment and their potential adverse effects on environmental and human health (Pignatello et al. 2010, Zoeller et al. 2014, Kabir et al. 2015). These micro-pollutants continuously enter the aquatic environment via diverse sources e.g. wastewater treatment plant (WWTP) effluents, landfill leachates, waste disposal or agricultural activity, and can be identified in surface waters, soil and ground water (Sumpter 2005, Pignatello et al. 2010, Hernández et al. 2015). In case of a targeted chemical analysis, target pollutants are characterized qualitatively and quantitatively, but no information about the overall biological activity of the sample is provided, because unknown compounds with biological activity remain undetected. However, detected biological activity by means of bioassays alone may not be directly linked to the identification of the responsible substance. To combine the advantages of chemical analysis and bioassays, an effect-directed analysis (EDA) can be pursued by directly linking chemical analysis of contaminants to their potential adverse biological effects (Brack 2003, Brack et al. 2007, Weller 2012). The basic principle of EDA is the separation of a compound mixture into different fractions followed by a subsequent analysis of the fractions for biological activity. The methods for sample fractionation are commonly based on HPLC. As reported by Weller, high-performance thin-

layer chromatography (HPTLC) can serve as a complementary separation technique to HPLC because of its higher biocompatibility (Reich and Schibli 2004, Weller 2012). Several studies demonstrated the direct coupling of HPTLC with bioassays for the detection of acute toxic effects (Hamburger and Cordell 1987, Weins and Jork 1996), acetylcholinesterase-inhibition (Weins and Jork 1996) or the detection of antibiotic activity (Herbst 1980). The spectrum of biological endpoints which can be detected directly on the surface of a HPTLC-plate was broadened by the direct coupling of HPTLC with a specific reporter gene based bioassay for the detection of estrogenic activity (planar YES, p-YES) in environmental samples and personal care products (Buchinger et al. 2013, Schönborn and Grimmer 2013). Based on this background, project "TREES" aims to develop an innovative technological platform for monitoring organic micro-pollutants in the environment based on the assessment of their biological effects. We propose a combination of planar chromatography, mass spectrometry and whole cell biosensors for multidimensional detection and tracking of organic micro-pollutants and their transformation products after extraction and pre-concentration from the water phase.

METHODS

Figure 1 illustrates the methodology to track bioactive organic micro-pollutants by combining different bioassays with HPTLC and the application to environmental samples. In general, organic micro-pollutants and possibly their transformation products are extracted and enriched by solid phase extraction (SPE) from environmental samples. After the chromatographic separation of a sample by HPTLC, organic micro-pollutants that might cause adverse biological effects can be visualized by the bioassay. Whole-cell sensors (e.g. genetically engineered *Saccharomyces cerevisiae* or *E. coli*) are exposed directly on the surface of the HPTLC-plate to the separated compounds for the effect-based detection (Buchinger et al. 2013, Schönborn and Grimmer 2013).

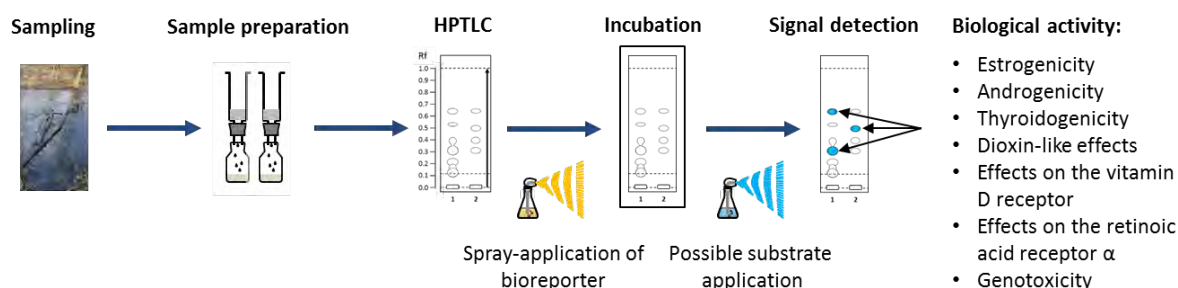


Figure 1: Scheme of the work flow for the combination of bioassays with HPTLC.

The bioassays used in TREES are primarily based on the principle of a reporter gene assay using specifically tailored whole-cell sensor strains (bioreporters). With a reporter gene assay the activation of a target promoter (sensing element) can be externally detected and quantified via a fused reporting element, e.g. an enzyme or a fluorescent protein. In case of genotoxicity, the applied bioreporters are based on a gene promoter from the *E. coli* SOS DNA repair system fused to the *Photorhabdus luminescens luxCDABE* gene cassette, which mark the presence of potentially DNA damaging sample components by increased luminescence (Shakibai et al. 2019). Agonists of diverse nuclear receptors such as estrogen receptor, androgen receptor, thyroid receptor or the aryl hydrocarbon receptor are detected by yeast-based reporter gene systems (Riegraf et al. 2019). For a multiparallel detection of various endocrine and endocrine-like compounds, the respective hormone receptor element sequence was fused in this study to a reporter element that allows a differential signal specific for a given adverse effect. Three fluorescent proteins optimized for yeast cells expression were selected for the imaging combination of the different endocrine endpoints, namely enhanced green fluorescent protein (EGFP), red fluorescent protein (Ruby) and blue fluorescent protein (BFP). The physical removal of separated compounds from the HPTLC plates and their identification using high-performance liquid chromatography coupled with mass spectrometry (HPLC-MS) is currently under development (Klingelhofer and Morlock 2014).

RESULTS AND DISCUSSION

As described, bioassays can provide valuable complementary information to chemical analysis regarding the detection of unknown substances with unwanted biological activity. The application of the optimized bioassays in combination with HPTLC to analyse different environmental samples is addressed in the following section.

Example 1 – Soil retention filter

In case of heavy rainfall events, soil retention filters are used to treat increased amounts of wastewater via a soil passage to avoid the release of untreated wastewater to the receiving waters. It is of interest to what extent biologically active micro-pollutants are retained by the soil retention filters or may even break through at very high volumes of additional wastewater. Influent and effluent samples were taken from a soil retention filter after a heavy rainfall event.

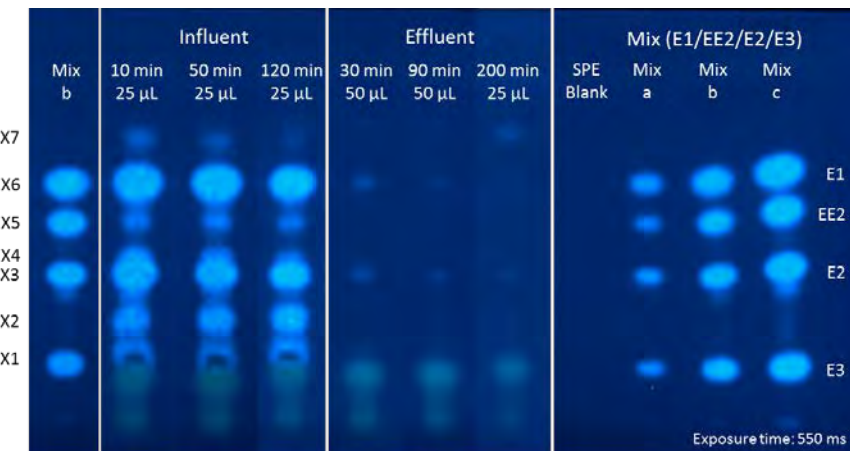


Figure 2: Analysis of estrogenic activity in 500-fold enriched influent and effluent extracts of a soil retention filter in combination with HPTLC assessed with the p-YES. The sampling time points and application volumes are indicated in the figure. A SPE blank served as blank. An estrogen mix consisting of estrone (E1; a: 10, b: 50 and c: 100 pg), 17 β -estradiol (E2; 1, 5 and 10 pg), 17 α -ethinylestradiol (EE2; 1, 5 and 10 pg) and estriol (E3; 0.1, 0.5 and 1 ng) were used as reference compounds. A two-step chromatographic development with 1.) 100% methanol till 20 mm, 2.) chloroform : ethylacetate : petroleum fraction 55:20:25 (v/v/v) till 90 mm was performed. The image shows the signal detection with fluorescence-imaging at an excitation wavelength of 366 nm after an exposure time of 3 h at 30°C.

The time interval of influent sample collection was 10 min, effluent samples were mixed samples collected over 30 min. The samples were investigated for various adverse effects after enrichment. Figure 2 shows exemplarily the estrogenic activity profiles of three selected influent and effluent soil retention filter extracts. Seven zones showing estrogenic activity can be detected. These signals are quantified in terms of a biological equivalent concentration (BEQ) as ng estradiol-equivalents per litre based on a calibration using estrogenic model compounds. By comparing influent and effluent extracts, a decrease in the estrogenic potential can be observed. The elimination of the detected activity zones X1, X2, X4 and X5 was about 100%, X3 was eliminated by 99.3% and X6 by 99.7%. Interestingly, X7 showed again an increased activity in the effluent collected after 200 min. An explanation might be a potential breakthrough of this substance at this time point indicating an exhausted filter capacity for this compound.

Example 2 - Detection of genotoxic effects in wastewater treatment samples

Figure 3 shows the detection of genotoxicity in extracts of influent and effluent samples taken from various municipal WWTPs. Four of six WWTP effluents showed a higher genotoxic potential compared to their influents. As different sample enrichments are compensated by the application volumes, signal intensities of influent and effluent samples are directly comparable. A possible explanation is the formation of transformation products with a higher genotoxic potential during the WWTP process. It can be expected that the genotoxic effects in the samples are caused by different compounds – this hypothesis can be tested by using varying mobile phases for the HPTLC. The identification of individual components in the extracted signal is in progress but even without a definite compound identification, these results provide important information about the efficiency of the wastewater treatment.

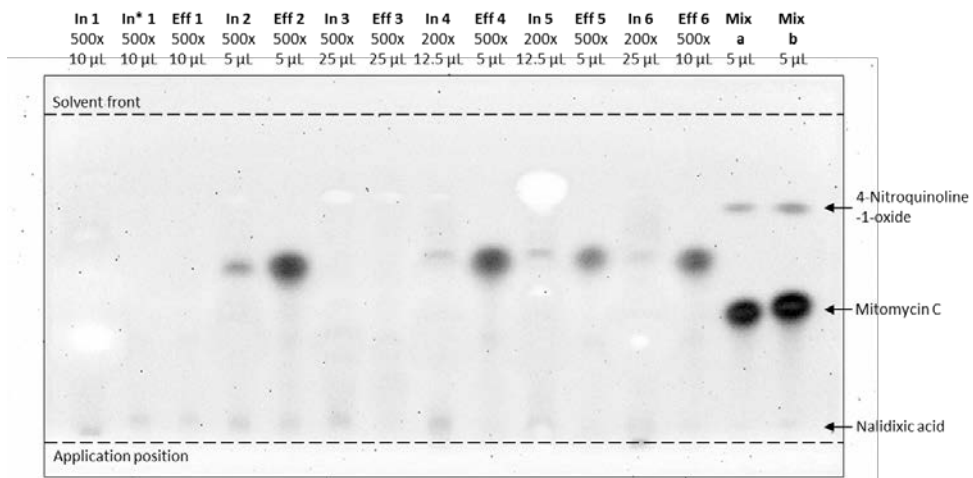


Figure 3: Detection of SOS-inducing components in HPTLC separated influent and effluent sample extracts from municipal WWTPs. The figure shows the luminescence (negative mode) induced by the genotoxic sample components following a 120 min incubation of the HPTLC plate with a bioluminescent *E.coli* bioreporter harbouring a plasmid-borne *recA::luxCDABE* fusion. Influent and effluent samples were enriched by SPE and applied in different volumes as indicated in the figure. Nalidixic acid, mitomycin C and 4-nitroquinoline-1-oxide (each a: 6.25 ng, b: 12.5 ng) were applied as reference compound mix in the two right-hand lanes.

Example 3 - Multiparallel endocrine effect detection

The application of different fluorescent proteins as reporter genes allows a simultaneous detection of different ecotoxicological effects by using several reporter elements. We have constructed different reporter strains for the detection of androgenic and estrogenic activity. A simultaneous detection of multiple signals was successfully performed for both androgenicity and estrogenicity by applying a mixture of yeast strains equipped with different reporter proteins. The change of the excitation wavelength for scanning allows the distinction of the different activities in the same test. Figure 4 shows the parallel detection of estrogenic and androgenic fractions in two different WWTP effluent extracts using p-YES-Ruby and p-YAS-BFP. A quantification of the effects can be made with the TLC-Scanner with a more optimized setting of the excitation wavelengths individually for the red (Ruby) and blue (BFP) fluorescent proteins (Figure 4).

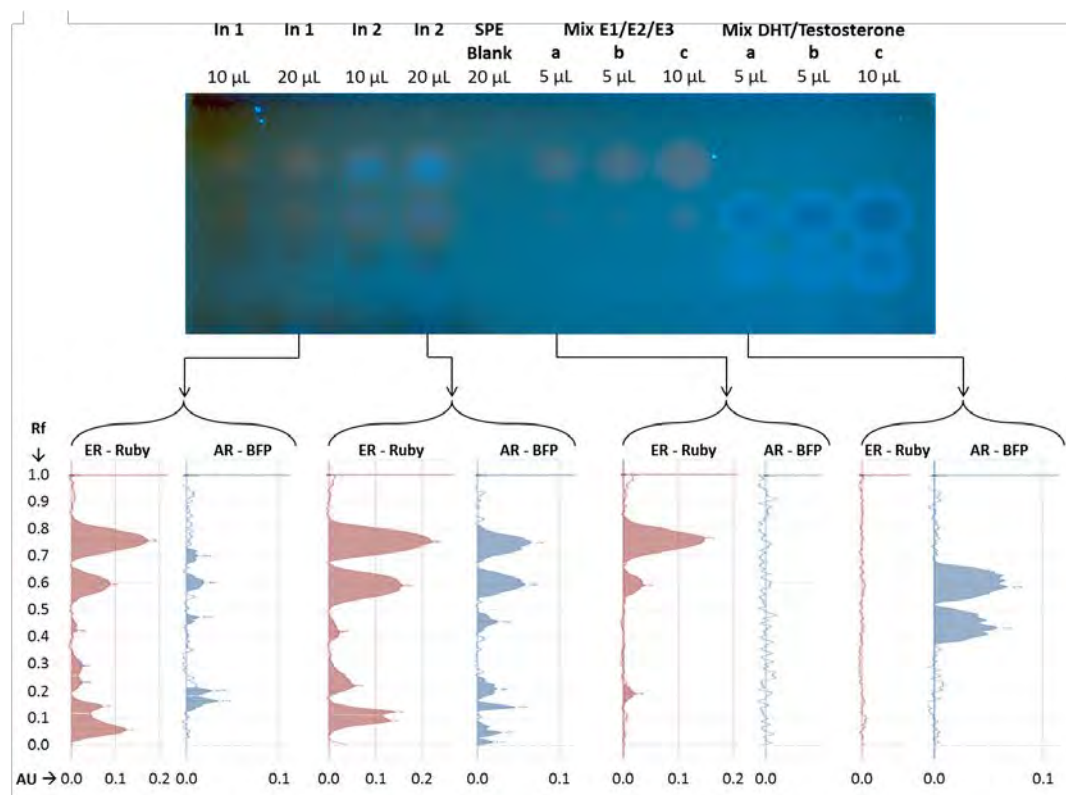


Figure 4: Multi-effect detection in two different WWTP-influent extracts by a parallel exposure of two yeast bioreporter strains (YES-Ruby and YAS-BFP) for a simultaneous detection of estrogenic and androgenic effects. An estrogen mix consisting of E1 (a: 0.1, b: 0.2 and c: 0.4 ng), E2 (10, 20 and 40 pg) and E3 (1, 2 and 4 ng) as well as an androgen mix consisting of dihydrotestosterone (DHT; a: 10, b: 25 and c: 50 ng) and testosterone (10, 25 and 50 ng) were used for calibration purposes. A two-step chromatographic development with 1.) 100% methanol till 20 mm, 2.) chloroform : ethyl acetate : petroleum fraction 55:20:25 (v/v/v) till 90 mm was performed. The image shows the signal detection with fluorescence-imaging at an excitation wavelength of 366 nm after an exposure time of 20 h at 30°C. The graphs show the corresponding scans of the signals for the Ruby- and the BFP-signals.

CONCLUSIONS

The presented data demonstrate the potential of the proposed direct combination of HPTLC and specific bioassays for the detection of adverse effects caused by anthropogenic micro-pollutants in the environment. Various successful applications of the planar bioassays for the detection of estrogenicity, androgenicity and genotoxicity in environmental samples were shown. Furthermore, a proof-of-concept of a multiparallel effect detection was demonstrated. The final steps in the project will include the further method development for the chemical analysis of bioactive compounds from the surface of the HPTLC-plates.

ACKNOWLEDGEMENT

This work was generously supported by the Federal Ministry of Education and Research (BMBF), Karlsruhe Project Management Agency, Germany (Grant No. 02WIL1387) and the Ministry of Science, Technology and Space (MOST), Israel (Grant No. WT1402/2560) in the framework of the German-Israeli Cooperation in Water Technology Research. The authors would like to thank Marina Ohlig, Ramona Pfänder and Gudrun Groß for their excellent technical assistance.

REFERENCES

- Brack, W. (2003). Effect-directed analysis: a promising tool for the identification of organic toxicants in complex mixtures? *Analytical and bioanalytical chemistry* 377(3): 397-407.
- Brack, W., Klamer, H. J., Lopez de Alda, M. and Barcelo D. (2007). Effect-directed analysis of key toxicants in European river basins a review. *Environ Sci Pollut Res Int* 14(1): 30-38.
- Buchinger, S., Spira, D., Bröder, K., Schlüsener, M., Ternes, T., & Reifferscheid, G. (2013). Direct coupling of thin-layer chromatography with a bioassay for the detection of estrogenic compounds: applications for effect-directed analysis. *Analytical chemistry*, 85(15), 7248-7256.
- Hamburger, M. O., & Cordell, G. A. (1987). A direct bioautographic TLC assay for compounds possessing antibacterial activity. *Journal of Natural Products*, 50(1), 19-22.
- Herbst, D. V. (1980). Applications of TLC and bioautography to detect contaminated antibiotic residues: tetracycline identification scheme. *J Pharm Sci* 69(5): 616-618.
- Hernández, F., Ibáñez, M., Portolés, T., Cervera, M. I., Sancho, J. V., & López, F. J. (2015). Advancing towards universal screening for organic pollutants in waters. *Journal of hazardous materials*, 282, 86-95.
- Kabir, E. R., Rahman, M. S., & Rahman, I. (2015). A review on endocrine disruptors and their possible impacts on human health. *Environmental toxicology and pharmacology*, 40(1), 241-258.
- Klingelhofer, I. and Morlock, G. E. (2014). Sharp-bounded zones link to the effect in planar chromatography-bioassay-mass spectrometry. *J Chromatogr A* 1360: 288-295.
- Pignatello, J. J., Katz, B. G., & Li, H. (2010). Sources, interactions, and ecological impacts of organic contaminants in water, soil, and sediment: an introduction to the special series. *Journal of environmental quality*, 39(4), 1133-1138.
- Reich, E. and Schibli, A. (2004). A standardized approach to modern high-performance thin-layer chromatography (HPTLC). *Jpc-Journal of Planar Chromatography-Modern Tlc* 17(6): 438-443.
- Riegraf, C., Reifferscheid, G., Belkin, S., Moscovici, L., Shakibai, D., Hollert, H., Buchinger, S. (2019). Combination of yeast-based in vitro screens with HPTLC as a novel tool for the detection of hormonal and dioxin-like compounds. *Analytica Chimica Acta* (submitted).
- Schönborn, A. and Grimmer, A. (2013). Coupling sample preparation with effect-directed analysis of estrogenic activity-Proposal for a new rapid screening concept for water samples. *JPC-Journal of Planar Chromatography-Modern TLC* 26(5): 402-408.
- Shakibai, D., Riegraf, C., Moscovici, L., Reifferscheid, G., Buchinger, S., & Belkin, S. (2019). Coupling high-performance thin-layer chromatography with bacterial genotoxicity bioreporters. *Environmental science & technology*.
- Sumpter, J. P. (2005). Endocrine disrupters in the aquatic environment: an overview. *CLEAN–Soil, Air, Water* 33(1): 9-16.
- Weins, C. and Jork, H. (1996). Toxicological evaluation of harmful substances by in situ enzymatic and biological detection in high-performance thin-layer chromatography. *J Chromatogr A* 750(1-2): 403-407.
- Weller, M. G. (2012). A unifying review of bioassay-guided fractionation, effect-directed analysis and related techniques. *Sensors* 12(7): 9181-9209.
- Zoeller, R. T., Å. Bergman, G. Becher, P. Bjerregaard, R. Bornman, I. Brandt, T. Iguchi, S. Jobling, K. A. Kidd, A. Kortenkamp, N. E. Skakkebaek, J. Toppari and L. N. Vandenberg (2014). A path forward in the debate over health impacts of endocrine disrupting chemicals. *J Environmental Health* 13(1): 118.

Removal of Inorganic Contaminants Form Aqueous Solutions by Novel Hybrid Adsorption/Filtration Processes

Inga HILBRANDT^{1*}, Hilla SHEMER^{2*}, Aki S. RUHL^{1,3}, Martin JEKEL¹, Raphael SEMIAT²

¹ Technische Universität Berlin, Chair of Water Quality Control, Str. des 17 Juni 135, 10623 Berlin, Germany

² Rabin Desalination Laboratory, Technion - Israel Institute of Technology, Haifa 3200003, Israel

^{1,3}German Environment Agency (UBA), Schichauweg 58, 12307 Berlin, Germany

*Corresponding author's e-mail: Inga.Hilbrandt@tu-berlin.de; shilla@technion.ac.il

ABSTRACT

The general objective of the research is to develop a hybrid adsorption/filtration processes for the removal of inorganic contaminants (phosphate, arsenate, chromium, silica and vanadate) from aqueous solutions. Two iron oxide/hydroxide adsorbents are studied: micro-scale granular ferric hydroxide (μ GFH) and iron oxyhydroxide agglomerates (IOAs). Initially, the particles were comprehensively characterized and adsorption mechanisms were proposed. The micro-scale size of the adsorbents hindrance their application in continues flow systems. Therefore, varying configuration, including fixed-bed filter, stirred tank reactor coupled with ultrafiltration, fluidized bed reactor, and submerged membrane reactor, are studied.

The results, discussed in this paper, focussed on phosphate adsorption in a reactor with submerged ultrafiltration membrane. The performance of the system was evaluated for the two adsorbents at varying phosphate concentrations, residence times and concentrations of accompanying ions. Both the mico-sized iron adsorbents were shown to be suitable for phosphate removal from secondary effluent. The submerged membrane reactor achieved a complete holdback of the μ GFH/IOAs without fouling of the membrane. It was shown that this configuration can be well adjusted according to water composition, initial pollutant concentrations and desired removal of the contaminants.

KEYWORDS

Adsorption; Micro ferric hydroxide; Iron oxide; Iron hydroxide; Ultrafiltration; Fixed-bed filtration

INTRODUCTION

Iron oxides/hydroxides are established adsorbents for the removal of inorganic contaminants from polluted water. Iron is one of the most abundant environmental minerals hence, environmentally benign, chemically stable over a wide pH, and cost effective. Granular ferric hydroxide (GFH) is an established adsorbent in water purification applications (1). During the production process of GFH the fine fraction, with particle sizes below 0.3 mm (μ GFH), is separated out and disposed of. This is because μ GFH causes pressure losses in conventional GFH fixed-bed filters. For the predicted advantages of the ferric hydroxide fine fraction and to avoid disposal of valuable resources, an easy-to-use and efficient application for μ GFH is sought after.

In acidic solutions, iron minerals exist as nano-particles and demonstrate high removal of inorganic contaminants. Yet, separating the nano-sorbents from solution remains a significant challenge limiting scale-up of the technique (2). To achieve facile solid/liquid separation, agglomerates of self-assembled iron nano-particles, at elevated pH, are utilized (3). The hierarchically structured agglomerates composed of nano-particles preserve the large surface area and high surface reactivity (4).

In most cases, iron oxides/hydroxides present slow adsorption kinetics owing to diffusion resistance and their separation from aqueous solutions after adsorption is difficult (5). Enhanced

adsorption may be accomplished by reducing the iron particles size thereby increasing the surface area. Yet, small sized particles are not easily separated and therefore are difficult to use in continues flow systems. The general objective of this research is the development of hybrid adsorption/filtration processes for the removal of inorganic pollutants from aqueous solutions. The Israeli partner focusses on iron (oxy)hydroxide agglomerates (IOAs) adsorbent and the German partner concentrates on micro-scale granular ferric hydroxide.

Throughout the joint project, both particles types were thoroughly characterized (6, 7), adsorption mechanisms were proposed (8) and competitive adsorption was modelled (9). Removal of chromium, phosphate, arsenate, vanadate and silica by adsorption in fixed-bed filter (7, 10), stirred tank reactor coupled with ultrafiltration (UF) (11), fluidized bed reactor (in preparation), and submerged membrane reactor (12, 13) were studied. In the latter configuration, a comprehensive comparison between the particles' structure, properties and adsorption capacities was conducted, as described in details herein.

METHODS

Adsorbents

μGFH. Conventional GFH (GEH Wasserchemie, Germany) consists of akaganeite, ferrihydrite and other iron oxides. Further characterisation can be found in (7).

IOAs. Ferric chloride ($\text{FeCl}_3 \cdot 6\text{H}_2\text{O}$) was hydrolyzed in double deionized water to form nano-sized iron oxy/hydroxide, after which agglomerates were formed by elevating the $\text{pH} > 4$ using NaOH. A 120 h aging time for IOAs was required before use. Full characterization of the particles is given elsewhere (6).

Isotherm studies

Adsorption isotherms of *μGFH* and IOAs were recorded as described in (10, 13, 6).

Submerged membrane adsorption reactor

An acrylic glass reactor ($34 \times 21 \times 2$ cm) was used with a submerged low-pressure ultrafiltration membrane (AMT-SUAIR-200 K, MemTech Company Israel). The membrane is characterized with a cutoff of 200 kD (40 nm) and a surface area of 0.05 m^2 . The adsorbents were added at concentrations of 0.14-1.20 g/L Fe at the beginning of the experiment. To guarantee optimal mixing air was supplied from the bottom of the reactor at an average flow rate of 1.85 L/min. The submerged membrane was operated in dead-end mode. Flow rates of 1.1, 2.1 and 4.2 L/h resulted in residence times of 60, 30 and 15 min in the reactor. Permeate was pumped from the reactor using a second pump with identical flow rates and at specific fluxes of 16, 43 and 90 L/m² h. The pressure drop of the membrane, measured with a piezo-resistive pressure transmitter, was 20 mbar.

Experiments were initially conducted in deionized water dosed with phosphate ($C_0=2.0, 4.5$ and 10.0 mg/L P) after which artificial secondary effluent, simulating effluent from the Nir-Etzion (Israel) domestic wastewater treatment plant was tested. Excellent reproducibility was achieved in duplicate experiments and control experiments confirmed negligible adsorption of phosphate to the membrane and the reactor.

Regeneration

μGFH. For regeneration the adsorbent was filled in a column (2.4×20 cm) and washed downstream with 1M NaOH. A total of 8 bed volumes (BV) was used at a flow rate of 5 BV/h. Samples were taken at the effluent. The regeneration solution was flocculated with CaCl_2 and MgCl_2 (ratio 2:1) to recover phosphate and reuse the NaOH.

IOAs. At the end of the adsorption, the IOAs suspension was settled for 1 h after which the supernatant was removed and the pH of the sediment was adjusted to 13.5 using NaOH. The desorption (i.e., regeneration) efficiency was calculated as the ratio between the amount of contaminant ions desorbed and the amount of ions adsorbed.

Analytical methods

Iron and phosphate concentrations were analysed with a spectrophotometer (Hach DR2008) using FerroVer and PhosVer3 reagents (all purchased from Hach, Germany). Detection limits for the methods are 0.02 mg/L Fe and 0.01 mg/L PO₄³⁻, respectively.

Results and Discussion

Adsorption capacities

The total adsorption capacity of IOAs was found to be 30-50% higher compared to that of μGFH (49 and 29 mg P/g Fe for pH 7). This is explained by the differences in the specific surface area (2,500 compared to 300 m²/g for IOAs and μGFH) and the pH_{PZC} of the particles. At pH values below the pH_{PZC} the surface of the particles is positively charged, increasing the adsorption of the negatively charged phosphate species. The pH_{PZC} of IOAs is around 9.0 as compared to 7.5 of the μGFH.

Membrane adsorption reactor

The membrane provided a physical barrier to prevent the adsorbents from passing on to the product water. Membrane fouling was not observed at the studied adsorbent concentrations and with the synthetic model solution free of effluent organic matter and suspended solids. Thus, membrane backwashing was not required during the adsorption cycle.

Influence of residence time. While a contact time of 2h for IOAs and 6h for μGFH was needed to reach equilibrium in batch experiments, shorter residence times are favourable for reactors to increase the throughput per day. The results of the membrane reactor (1a) show a decrease in loadings of approx. 6 mg/g for both adsorbents when reducing the residence time from 30 to 15 min. With further increase from 30 to 60 min, no significant changes in loadings were observed. Thus, residence times of 30 min was sufficient for phosphate removal in the proposed system. Generally, longer residence times lead to a better performance as there is more time for the reaction to occur, until an optimum is reached.

Influence of adsorbent concentration. Constant phosphate removals of approx. 80 and 70% for IOAs and μGFH independent of adsorbent concentration (0.14-1.2 g/L) were reached in the experiments. Thus, an increase in adsorbent dosage does not lead to increased relative removal.

Decreased capacities were observed with augmentation of the adsorbent dosage, but no differences occurred above 0.25 g/L Fe of IOAs and above 0.60 g/L Fe of μGFH. The decrease in adsorption loadings with the increase in the adsorbent dosage is explained by unsaturated adsorption sites remaining at the end of the adsorption reaction while the number of sites available for adsorption increased. A second explanation refers to a decrease in the number of available adsorption sites due to overlapping between particles and/or aggregation of particles as the concentration of the adsorbent increases.

Water composition. Enhanced phosphate adsorption was observed in artificial secondary effluent (Figure 1b) leading to increases in specific throughput until the 50% breakthrough (effluent concentration 2 mg/L) of 87 and 60% for μGFH and IOAs. Overall, the competitive effects by the anions are over-compensated by the increased adsorption induced by the presence of divalent cations. As calcium and magnesium are positively charged their adsorption to the negatively charged iron hydroxide surface is electrostatically favored (14). Subsequently phosphate adsorption is enhanced and the formation of ternary complexes is possible (15). The anions sulfate (C₀=82.4 mg/L) and bicarbonate (C₀=284.1 mg/L) might compete for adsorption sites. Zelmanov et al. (16) showed no significant effect of sulfate on phosphate removal using fine particulate iron hydroxide. Bicarbonate however acts as a strong competitor in phosphate adsorption onto iron hydroxides (17, 10). As the results show, the proposed hybrid process of adsorption combined with membrane filtration appears feasible for the removal of phosphate from secondary effluent.

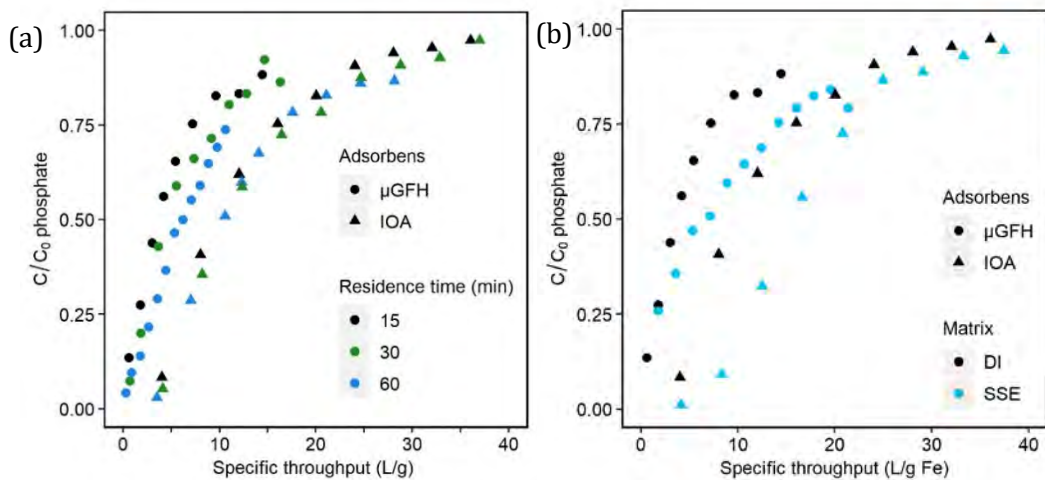


Figure 1: Relative P-breakthroughs for (a) varying residence times and (b) in DI water and artificial secondary effluent (RT=15 min; pH 7.8; $c_0(P)=4.5$ mg/L; $c(Fe,\mu GFH)=0.6$ g/L; $c(Fe,IOA)=0.3$ g/L).

Regeneration

μ GFH. The percentage of desorbed phosphate with increasing NaOH throughput is shown in 2a. After a throughput of 4 BV approx. 60% of phosphate is desorbed and the slope of the desorption curve decreases drastically. Approx. 35 mg P/g Fe were desorbed within 8 BV. In total, 100 L with phosphate polluted water was treated with approx. 6 g Fe (9.4 g μ GFH) and regeneration of the material resulted in 130 mL highly concentrated phosphate solution. Subsequently, phosphate was precipitated using $CaCl_2$ and $MgCl_2$ (2b). Approx. 40 mmol/L flocculent were sufficient for 85% phosphate removal. Thus, making it possible to reuse the NaOH for further desorption cycles.

IOAs. 4 displays the phosphate adsorption capacities in five consecutive adsorption/regeneration cycles. In all cycles 100% regeneration efficiency was obtained. As seen in the Figure, a minute gradual reduction in the adsorption capacity was obtained for the second and third cycles (less than 2% reduction). However, the fourth and fifth cycles showed about 10% reduction compared to the first adsorption cycle (61.0 ± 0.9 mg P/g Fe). Both these re-loading cycles maintained similar adsorption capacities of 56.6 ± 0.5 mg P/g Fe.

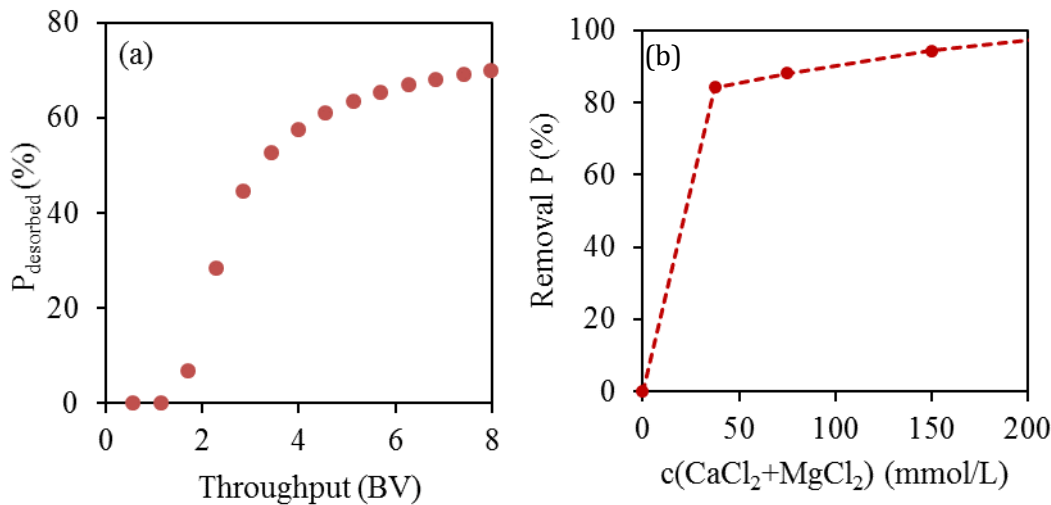


Figure 2: (a) Cumulative desorbed phosphate from μ GFH using 1M NaOH at 5 BV/h and (b) precipitation of phosphate from regeneration solution using $CaCl_2$ and $MgCl_2$ (ratio 2:1)

Techno-economic evaluation entailed synthesis of the IOAs and their regeneration for reuse. This evaluation considers only the chemicals costs (without accounting for the end product water quality, down-stream treatments, and cost of sludge handling and disposal). The market price of the chemical were obtained online (www.alibaba.com, May 2019). It is seen (Figure) that the synthesis of the IOAs cost about five folds more than their regeneration.

The lower cost of IOAs regeneration as compared to their synthesis and the fact that the adsorption capacity was not significantly changed with the adsorption/regeneration cycle number points to the promising potential usage of IOAs adsorbent for phosphate removal from wastewater. Additionally, the pH of desorbing solution (13.5) favors precipitation-recovery of calcium phosphate, possibly applicable as fertilizer.

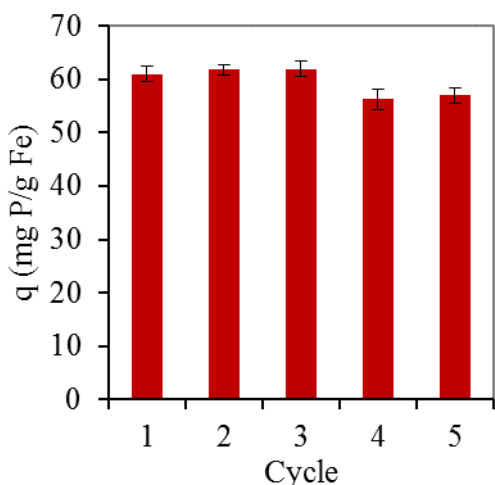


Figure 3: Adsorption capacity during five consecutive adsorption/desorption cycles.

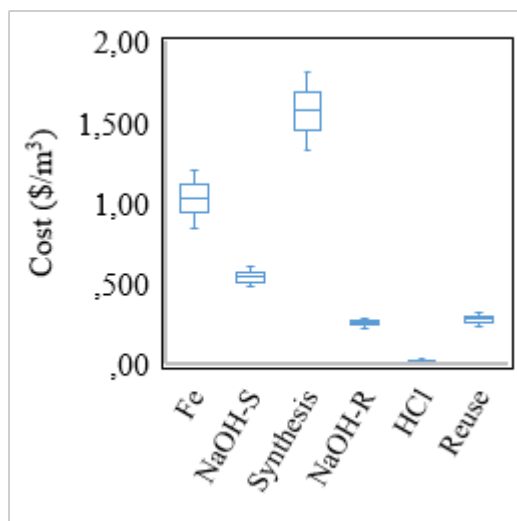


Figure 4: Cost of iron, NaOH and HCl used for synthesis and regeneration of the IOAs.

CONCLUSIONS

- Complete holdback of the adsorbents was achieved without fouling of the membrane.
- Specific throughputs up to 50% breakthrough of phosphate ($C_0=4$ mg/L) were limited to approx. 6 and 15 L/g Fe for μ GFH and IOAs in artificial secondary effluent.
- A residence time of 30 min was sufficient for phosphate adsorption.
- Higher removals (by approx. 50%) was achieved in artificial secondary effluent compared to deionized water.
- The adsorbents can be regenerated using 1M NaOH and the recovered phosphate can possibly be used as fertilizer.

ACKNOWLEDGEMENT

The current research as part of the German-Israeli project AdsFilt (WT1404) is funded by the German Ministry of Education and Research (BMBF) and Israeli Ministry of Science & Technology (MOST) within the framework of the German-Israeli water technology cooperation. We would further like to thank the BMBF-MOST Young Scientist Exchange Program (ID YSEP118).

REFERENCES

1. Driehaus, W.; Jekel, M.; Hildebrandt, U. Granular ferric hydroxide - a new adsorbent for the removal of arsenic from natural water. *J Water Serv. Res. Tec.* **1998**, *47* (1), 30–35.
2. Zach-Maor, A.; Semiat, R.; Shemer, H. Synthesis, performance, and modeling of immobilized nano-sized magnetite layer for phosphate removal. *J. colloid interf. sci.* **2011**, *357* (2), 440-446.
3. Hu, J.S.; Zhong, L.S.; Song, W.G.; Wan, L.J. Synthesis of hierarchically structured metal oxides and their application in heavy metal ion removal. *Adv. Mater.* **2008**, *20* (15), 2977-2982.
4. Zhong, L.S.; Hu, J.S.; Wan, L.J.; Song, W.G. Facile synthesis of nanoporous anatase spheres and their environmental applications. *Chem. commun.* **2008**, *10*, 1184-1186.
5. Zhang, S.; Li, X.Y.; Chen, J.P. An XPS study for mechanisms of arsenate adsorption onto a magnetite-doped activated carbon fiber. *J. colloid Interf. Sci.* **2010**, *343* (1), 232–238.
6. Wei, Z.; Luo, S.; Xiao, R.; Khalfin, R.; Semiat, R. Characterization and quantification of chromate adsorption by layered porous iron oxyhydroxide: An experimental and theoretical study. *J. Hazard. Mater.* **2017**, *338*, 472-481.
7. Hilbrandt, I.; Ruhl, A. S.; Jekel, M. Conditioning fixed-bed filters with fine fractions of granulated iron hydroxide (GFH). *Water* **2018**, *10* (10).

8. Wei, Z.; Semiat, R. Applying a modified Donnan model to describe the surface complexation of chromate to iron oxyhydroxide agglomerates with heteromorphous pores. *J. Colloid Interf. Sci.* **2017**, *506*, 66-75.
9. Hilbrandt, I.; Lehmann, V.; Zietzschmann, F.; Ruhl, A. S.; Jekel, M. Quantification and isotherm modelling of competitive phosphate and silica adsorption onto micro-sized ferric hydroxide. *Chemosphere* **2019**, submitted.
10. Hilbrandt, I.; Ruhl, A. S.; Zietzschmann, F.; Molkenthin, M.; Jekel, M. Competition in chromate adsorption onto micro-sized granular ferric hydroxide. *Chemosphere* **2019**, *218*, 749-757.
11. Shemer, H.; Melki-Dabush, N.; Semiat, R. Removal of silica from brackish water by integrated adsorption/ultrafiltration process. *Environ. Sci. Poll. Res* **2019**, submitted.
12. Shemer, H.; Armush, A.; Semiat, R. Reusability of iron oxyhydroxide agglomerates adsorbent for repetitive phosphate removal. *Colloid. Surf. A: Physicochem. Eng. Asp* **2019**, submitted.
13. Hilbrandt, I.; Shemer, H.; Ruhl, A. S.; Semiat, R.; Jekel, M. Comparing fine particulate iron hydroxide adsorbents for the removal of phosphate in a hybrid adsorption/ ultrafiltration system. *Sep. Purif. Technol.* **2019**, *221*, 23-28.
14. Li, M.; Liu, J.; Xu, Y.; Qian, G. Phosphate adsorption on metal oxides and metal hydroxides: A comparative review. *Environ. Rev.* **2016**, *24* (3), 319-332.
15. Sperlich, A. Dissertation. Phosphate Adsorption onto Granular Ferric Hydroxide (GFH) for Wastewater Reuse; Berlin, Technische Universität, Berlin, 2010.
16. Zelmanov, G.; Semiat, R. The influence of competitive inorganic ions on phosphate removal from water by adsorption on iron (Fe^{+3}) oxide/hydroxide nanoparticles-based agglomerates. *J. Water Pro. Eng.* **2015**, *5*, 143-152.
17. Zachara, J. M.; Girvin, D. C.; Schmidt, R. L.; Resch, C. T. Chromate adsorption on amorphous iron oxyhydroxide in the presence of major groundwater ions. *Environ. Sci. Technol.* **1987**, *21* (6), 589-594.

Overview of New Projects Started in 2019

Correlated projects are framed **bold**, the German partner's projects are *italicized*

	WT1801	Bioaugmentation and Monitoring for Aerobic Chloroethene Biodegradation			Ben Gurion University of the Negev	Prof. Ariel Kushmaro	01.06.19-31.05.22
1	<i>02WIL1520</i>		<i>DVGW-Technologiezentrum Wasser (TZW)</i>	<i>Prof. Dr. Andreas Tiehm</i>			<i>01.06.19-31.05.22</i>
	WT1802	Pathogen detection by plasmonic nanoarray			Technion	Prof. Dr. Yechezkel Kashi	01.06.19-31.05.22
2	<i>02WIL1521</i>		<i>Leibniz-Institut für Photonische Technologien (IPHT)</i>	<i>Apl. Prof. Dr. Wolfgang Fritzsche</i>			<i>01.06.19-31.05.22</i>
	WT1803	Cosmic-Ray Neutron Sensor for quantifying Non-Rainfall Water Inputs (CoNRaWI)			Ben Gurion University of the Negev	Dr. Nurit Agam	01.09.19-31.08.22
3	<i>02WIL1522</i>		<i>Helmholtz Centre for Environmental Research GmbH - UFZ</i>	<i>Dr. Martin Schrön</i>			<i>01.09.19-31.08.22</i>
	WT1804	ISCO3 for GW remediation			Tel Aviv University (TAU)	Ines Zucker	01.06.19-31.05.22
4	<i>02WIL1523</i>		<i>Technische Universität München</i>	<i>Uwe Hübner</i>			<i>01.06.19-31.05.22</i>
	WT1805	PALM-IRRI - Improve date palm irrigation scheduling			Ben Gurion University of the Negev	Prof. Dr. Naftali Lazarovitch	01.06.19-31.05.22
5	<i>02WIL1524</i>		<i>Forschungszentrum Jülich GmbH</i>	<i>Prof. Dr. Johan A. Huisman</i>			<i>01.06.19-31.05.22</i>

Imprint

Edited by

Project Management Agency Karlsruhe (PTKA), Karlsruhe

Layout

Project Management Agency Karlsruhe (PTKA), Karlsruhe

Printed by

Systemedia GmbH, Wurmberg

Photo Credits

Cover: Adobe Stock / deaw59

p. 2, 3: Adobe Stock / Alexey Protasov

p. 28: Dr. Leif Wolf

p. 59: ddpix.de



PTKA
Projektträger Karlsruhe
Karlsruher Institut für Technologie

